

**DESIGN OF MICROSTRIP LINEAR PHASED ARRAY  
ANTENNA USING INTEGRATED ARRAY FEEDER**

BY

**MIR RIYAZ ALI**

A Thesis Presented to the  
DEANSHIP OF GRADUATE STUDIES

**KING FAHD UNIVERSITY OF PETROLEUM & MINERALS**

DHAHRAN, SAUDI ARABIA

In Partial Fulfillment of the  
Requirements for the Degree of

**MASTER OF SCIENCE**

In

**TELECOMMUNICATION ENGINEERING**

**DECEMBER 2005**

KING FAHD UNIVERSITY OF PETROLEUM & MINERALS  
DHAHRAN 31261, SAUDI ARABIA

DEANSHIP OF GRADUATE STUDIES

This thesis, written by MIR RIYAZ ALI  
under the direction of his thesis advisor and approved by his  
thesis committee, has been presented to and accepted by Dean of  
Graduate Studies, in partial fulfillment of the requirements for the  
degree of  
MASTER OF SCIENCE IN TELECOMMUNICATION ENGINEERING.

Thesis Committee

*Sheikh Sharif 1-2-06*

Dr. SHEIKH SHARIF IQBAL (Advisor)

*Mahmoud M. Dawoud 1/2/06*

Dr. MAHMOUD M. DAWOUD (Member)

*Ahmed Yamani 25/02/06*

Dr. AHMED YAMANI (Member)

*Jamil M. Bakhawain*

Dr. JAMIL M. BAKHASHWAIN  
(Department Chairman)

*Mohammed Abdulaziz Al Ohali*

Dr. MOHAMMED ABDULAZIZ AL OHALI  
(Dean of Graduate Studies)

*13/3/2006*

13-3-2006





*DEDICATED TO THE  
TREASURE OF MY LIFE,  
MY MOTHER, FATHER &  
SISTERS*

## ACKNOWLEDGEMENT

*All praises be to **Allah (SWT)** for blessing me with opportunities abound and showering upon me his mercy and guidance all through the life. I pray that He continues the same the rest of my life.*

First and foremost I would like to acknowledge a few persons who have helped me in achieving this goal and coming out joyfully. I would like to thank my supervisor Dr. Sheikh Sharif Iqbal, for guiding me and helping me during the course of this research work. I would also like to thank my committee members Dr. Dawoud & Dr. Yamani whose valuable comments paved way for successful completion of this study.

I would take this opportunity to thank my Chairman Dr. Jamil Bakhshwain for providing me with whatever facility I had utilized for completion of this research. Also I would like to thank my department and all the people who have helped me in one way or other during the research.

All thanks due especially to my family members, my father, mother and my sisters for their prayers and inspiration, which has helped me in becoming what I'm today.

And lastly to all my friends who have been a pillar of support during the arduous times of my research. Some of whose names I would especially like to mention here, Fasiuddin, Amer, Faisal, Baber, Anees, Hameed, Aleem, Mazher, Farooq, Kashif, Abdul Qayyum, Rizwan Maulana, Abbas and the rest of the IndoKFUPM community. It's a bond that I will cherish all through my life.

## TABLE OF CONTENTS

	Page
<b>List of Tables .....</b>	<b>viii</b>
<b>List of Figures.....</b>	<b>ix</b>
<b>Thesis Abstract.....</b>	<b>xii</b>
<b>Thesis Abstract (Arabic) .....</b>	<b>xiii</b>
<b>CHAPTER 1INTRODUCTION .....</b>	<b>1</b>
1.1 THESIS MOTIVATION .....	1
1.2 THESIS OBJECTIVE.....	7
1.3 THESIS OVER VIEW .....	9
<b>CHAPTER 2LITERATURE REVIEW .....</b>	<b>11</b>
2.1. INTRODUCTION .....	11
2.2. MICROSTRIP ANTENNAS .....	12
2.2.1 ADVANTAGES OF MICROSTRIP ANTENNAS.....	18
2.2.2 DISADVANTAGES OF MICROSTRIP ANTENNAS .....	18
2.3. METHODS OF ANALYSIS .....	19
2.3.1 THE TRANSMISSION LINE MODEL .....	19
2.3.2. THE CAVITY MODEL .....	22
2.3.3. FULL WAVE MODEL .....	23
2.4. EXCITATION TECHNIQUES OF MICROSTRIP ANTENNAS.....	24
2.4.1 MICROSTRIP LINE FEED .....	25
2.4.2. COAXIAL FEED.....	26
2.4.3. APERTURE COUPLING.....	27
2.4.4. PROXIMITY COUPLING .....	29
2.5. ANTENNA ARRAY .....	30
2.5.1 ARRAY FACTOR.....	32
2.5.2 MUTUAL COUPLING .....	35
2.6 POWER DIVIDER.....	37
2.7. PHASE SHIFTERS .....	41

<b>CHAPTER 3 DESIGN OF FEED NETWORK FOR ANTENNA ARRAY.....</b>	<b>46</b>
3.1 INTRODUCTION .....	46
3.2 DESIGN OF THE ARRAY FEEDER .....	49
3.2.1. WILKINSON POWER DIVIDER .....	52
3.2.3 DESIGNED POWER DIVIDER FEED NETWORK .....	58
3.3. DESIGN OF PHASE SHIFTER USING FERRITE .....	65
<b>CHAPTER 4 DESIGN OF MICROSTRIP LINEAR PHASED ARRAY ANTENNA .....</b>	<b>78</b>
4.1 INTRODUCTION .....	78
4.2 DESIGN CONSIDERATIONS .....	79
4.2.1 DIMENSIONS OF RADIATING ELEMENTS.....	79
4.2.2 RELATIVE DISPLACEMENT OF RADIATING ELEMENTS ..	83
4.2.3 EXCITATION AMPLITUDE AND PHASE OF ELEMENTS .....	85
4.2.4 RADIATION CHARACTERISTICS .....	90
4.2.5 INTEGRATED ARRAY FEEDER .....	95
4.3 DESIGN OF MICROSTRIPLINE FED LINEAR PHASED ANTENNA ARRAY .....	100
<b>CHAPTER 5 EXPERIMENTAL RESULTS &amp; DISCUSSIONS .....</b>	<b>112</b>
5.1 INTRODUCTION .....	112
5.2. CAD/CAM TOOLS DESCRIPTION .....	112
5.3 ANTENNA MEASUREMENT TOOLS .....	114
5.4 FABRICATION & BIASING TECHNIQUES OF THE DESIGNED ANTENNA ARRAY .....	118
5.5 EXPERIMENTAL RESULTS & ANALYSIS .....	121
<b>CHAPTER 6 CONCLUSION &amp; FUTURE WORK .....</b>	<b>128</b>
6.1 CONCLUSIONS.....	128
6.2 COMPARISON WITH LITERATURE .....	132
6.3 FUTURE RECOMMENDATIONS .....	133
<b>APPENDIX A .....</b>	<b>135</b>
<b>REFERENCE:.....</b>	<b>138</b>
<b>VITAE .....</b>	<b>146</b>

## LIST OF TABLES

TABLE	Page
Table1. 1 Phased Array Antenna Specifications.....	8
Table2. 1 Comparison between microstrip transmission line and microstrip antenna .....	17
Table3. 1 Microstripline widths as calculated for corresponding impedances .....	54
Table4. 1 Dimension of rectangular microstrip patch calculated .....	82
Table4. 2 Power Divider Phase Shifter Parameters .....	96
Table4. 3 Geometrical and material Parameters of Microstrip line fed Antenna Array.....	102
Table4. 4 Antenna Characteristics as obtained from Matlab (Theoretical)	103
Table4. 5 Antenna Characteristics as obtained from Simulation (Practical) .....	108
Table4. 6 Main beam angle scanning at different magnetic bias.....	111
Table5. 1 Main beam scan of the antenna array with different magnetic biases.....	127

## LIST OF FIGURES

Figure	Page
Figure1. 1 Block Diagram of a simple Microstrip Antenna Array [54] .....	2
Figure2. 1 Microstrip rectangular patch antenna .....	13
Figure2. 2 Radiation mechanism associated with microstrip patch.....	14
Figure2. 3 Electric field distribution (side view) .....	14
Figure2. 4 Increase in length of the microstrip patch. ....	15
Figure2. 5 Transmission-line model of rectangular microstrip patch [1] ....	20
Figure2. 6 Rectangular patch represented as a cavity in Cavity model analysis.....	23
Figure2. 7 Microstripline feed .....	26
Figure2. 8 Coaxial probe feed.....	27
Figure2. 9 Aperture coupled microstrip antenna and its equivalent circuit. ....	28
Figure2. 10 Proximity coupled feed.....	30
Figure2. 11 Antenna array configurations [1].....	31
Figure2. 12 Pattern multiplication shown graphically [1] .....	33
Figure2. 13 H-plane arrangements of microstrip patch antennas [1].....	36
Figure2. 14 Block diagram power divider .....	38
Figure2. 15 Wilkinson power divider and it equivalent microstripline implementation. ....	40
Figure2. 16 Magnetic field's rotation in ferrite .....	43
Figure3. 1 Types of feed networks [1].....	48
Figure3. 2 Block diagram of general power divider phase shifter combined network feeding the antenna array .....	49
Figure3. 3 Quarter wave transformer.....	50
Figure3. 4 Equivalent circuit of quarter wave transformer.....	51
Figure3. 5 Typical Microstrip Wilkinson power divider .....	53
Figure3. 6 Microstrip Wilkinson power divider of Antsos, Crist and Sukanto [38].....	55
Figure3. 7 Two port power divider with multisection quarter wave transformer .....	56
Figure3. 8 Design of Wilkinson two way power divider on dielectric.....	59
Figure3. 9 Design of modified Wilkinson two way power divider (top section).....	60
Figure3. 10 S-parameters of two-way Wilkinson power divider (top segment).....	61
Figure3. 11 S-parameters of two-way Wilkinson power divider (bottom segment).....	62

Figure3. 12 Modified Wilkinson four-way power divider network on dielectric.....	63
Figure3. 13 S-parameter response of four-way power divider on dielectric similar to ferrite.....	64
Figure3. 14 Behavior of effective permeability of ferrite media with magnetic bias and frequency.....	67
Figure3. 15 Parallel plate ferrite structure used for derivation of characteristic equation .....	69
Figure3. 16 Theoretical plot of variation of propagation constant $\beta$ with magnetic bias $H_{dc}$ .....	74
Figure3. 17 Four way power divider on ferrite substrate.....	76
Figure3. 18 Variation of propagation constant beta ( $\beta$ ) with magnetic bias for ferrite media .....	77
Figure4. 1 Radiation mechanism associated with microstrip patch [ 1].....	80
Figure4. 2 Radiation pattern of the antenna array for varying distance in terms $\lambda$ between elements, (a) dB scale, (b) normalized .....	84
Figure4. 3 Array factor of 4-element non-uniform Dolph-Tschebysheff array designing.....	88
Figure4. 4 Unequal power divider implemented on ferrite substrate .....	89
Figure4. 5 Rectangular microstrip patch and its orientation with respect to azimuthal & elevation angles.....	91
Figure4. 6 Radiation pattern of single microstrip antenna in dB.....	92
Figure4. 7 Radiation pattern of single microstrip patch in polar plot.....	92
Figure4. 8 H-plane radiation pattern of the single microstrip patch in polar plot .....	93
Figure4. 9 E-plane radiation pattern of the 4-element microstrip linear antenna array.....	94
Figure4. 10 H-plane radiation pattern of the 4-element microstrip linear antenna array.....	94
Figure4. 11 Integrated ferrite based modified Wilkinson power divider/phase shifter.....	96
Figure4. 12 Transmission and reflection S-parameter curves for four port power divider. ....	98
Figure4. 13 Isolation S-parameters for the four port power divider .....	99
Figure4. 14 Reflection S-parameters for the four port power divider .....	100
Figure4. 15 Four-Element microstrip antenna array structure line-fed. ....	101
Figure4. 16 HFSS Schematic of implementation of microstrip line fed patch antenna array.....	104
Figure4. 17 Reflection curve ( $S_{11}$ ) of four element microstrip antenna array .....	106

Figure4. 18 Radiation pattern (E-plane) of the four element antenna array	107
Figure4. 19 Radiation pattern showing the main beam of the antenna scanned for different magnetic biases.	110
Figure5. 1 PCB plotter used to fabricated the designed microstrip array antenna	114
Figure5. 2 Network Analyzer [54]	115
Figure5. 3 Block diagram of the Network Analyzer 8410 (Internal view)	116
Figure5. 4 Feed Network implemented on Ferrite	119
Figure5. 5 Microstrip Patches implemented on Duroid	119
Figure5. 6 Linear Microstrip Antenna array against a metallic coin for comparison	120
Figure5. 7 Reflection $S_{11}$ for practically designed microstrip antenna array	122
Figure5. 8 Comparison of simulated and experimental $S_{11}$ response of antenna array	123
Figure5. 9 Block diagram of Antenna Training and Measuring Systems (ATMS)	124
Figure5. 10 E-plane H-plane of the microstrip antenna array tested experimentally	125
Figure5. 11 Main beam scan of fabricated microstrip antenna array for different magnetic bias	125

## THESIS ABSTRACT

**Name:** MIR RIYAZ ALI

**Title:** DESIGN OF MICROSTRIP LINEAR PHASED ARRAY  
ANTENNA USING INTEGRATED ARRAY FEEDER

**Major Field:** TELECOMMUNICATION ENGINEERING

**Date of Degree:** DECEMBER 2005

Antennas play an integral part in wireless communication system. Microstrip patch antennas are versatile in terms of their geometrical shapes and implementations. Inhibiting characteristics of a single microstrip patch, like low gain and smaller bandwidth, make it more popular for array configuration. The aim of this work is to design and implement a microstrip phased array antenna, printed on a composite ferrite-dielectric substrate. Four rectangular radiating patches on a low dielectric constant substrate are arranged in linear configuration to achieve required radiation properties. The microstrip array feeder network, consisted of integrated power divider and phase shifters, is realized on an externally magnetized ferrite substrate. Tunable progressive phase shift is produced by varying the magnetic bias that changes the permeability of ferrite material, which in turn changes the phase velocity and, hence, the insertion phase of the propagating microwave signal. The four-way power splitter is attained using Wilkinson type power dividers, which improves the isolation and matching of the ports. The antenna array is designed using standard equations and simulated by professional software called, High Frequency Structural Simulator (HFSS). Among many antenna simulators, HFSS is selected as it allowed the inclusion of anisotropic ferrite material in the simulation process. The antenna prototype is printed using the PCB plotter and manually transferred on the composite substrate, which introduced some inaccuracy. Finally, the simulated reflection response and radiation characteristics of the designed antenna array are corroborated using experimental results obtained from the Network Analyzer and the Antenna Transmission & Measurement System, respectively. The designed array exhibited very close radiation response to that of design objective.

## ملخص الرسالة

الاسم: مير رياض على

عنوان الرسالة: تصميم صف خطي من هوائيات الشرائح الصغيرة باستخدام مغذي المصفوفات المتكامل

التخصص: هندسة الاتصالات

تاريخ التخرج: ديسمبر 2005

تلعب الهوائيات دوراً تكاملياً في نظام الاتصالات اللاسلكي. إن الأشكال الهندسية والتطبيقات المتعددة لهوائيات الشرائح الصغيرة تتيح لها الاستخدام في مجالات مختلفة. كما إن الخواص المثبطة لهوائي الشرائح الصغيرة المفرد مثل انخفاض الكسب وصغر سعة الحزمة يزيد من استخدامها على شكل مصفوفات. هدف هذا العمل هو تصميم وتطبيق صف خطي من هوائيات الشرائح الصغيرة مطبوعة على ركيزة مؤلفة من مادة العازل وخام الحديد. يتألف التصميم من أربع هوائيات مربعة مطبوعة على مادة ذات ثابت عزل منخفض بشكل خط عرضي مستقيم للحصول على الخواص الإشعاعية المرغوبة. أما شبكة مغذي المصفوفات فتتكون من مقسم طاقة ومزيج للطور وهي مطبوعة على أرضية تتكون من خام الحديد الممغنط. كذلك من الممكن الحصول على مزيج طور تدريجي بتغيير الانحياز المغناطيسي مما يؤدي إلى تغيير الإنفاذية المغناطيسية لمادة الحديد الخام الذي بدوره يغير سرعة الطور وطور الإدخال لإشارة موجات الميكروويف. وقد تم تصميم مقسم الطاقة رباعي الأبعاد باستخدام مقسم ويلكينسون للطاقة الذي يحسن الفصل والملائمة بين المنافذ.

لقد تم تصميم مصفوفة الهوائيات باستخدام المعادلات النموذجية كما تم محاكاتها باستخدام برنامج متطور يسمى محاكي التصميمات عالية التردد (HFSS). من بين العديد من البرامج التي تستخدم في محاكاة تصاميم الهوائيات، تم اختيار (HFSS) كونه يسمح باستخدام مادة الحديد الخام المتباينة الخواص في عملية المحاكاة. النموذج الأولي للهوائي المصمم تمت طباعته على PCB ومن ثم تم نقله يدوياً إلى الركيزة المشتركة مما أدى إلى شيء بسيط من عدم الدقة.

وختاماً، فإن نتائج المحاكاة من رد الفعل الانعكاسي وخواص الإشعاع قد تم تعزيزها بالنتائج التجريبية التي تم الحصول عليها باستخدام كل من المحلل الشبكي ونظام القياس والإرسال الهوائي. النتائج التي ظهرت من المصفوفة المصممة أظهرت تطابقاً كبيراً مع الهدف العن لهذا التصميم.

# **CHAPTER 1**

## **INTRODUCTION**

According to the IEEE Standard Definitions, the antenna or aerial is defined as “a means of radiating or receiving radio waves” [1]. In other words, antennas act as an interface for electromagnetic energy, propagating between free space and guided medium. Amongst the various types of antennas that include wire antennas, aperture antennas, reflector antennas, lens antennas etc, microstrip patches are one of the most versatile, conformal and easy to fabricate antennas. In this thesis, a microstrip-fed ferrite based patch antenna array with beam steering capability is designed, fabricated and tested.

### **1.1 THESIS MOTIVATION**

In the recent years, there has been rapid growth in wireless communication. With the increasing number of users and limited bandwidth that is available, operators are trying hard to optimize their network for larger capacity and improved quality coverage [1]. This surge has led the field of antenna engineering to constantly evolve and accommodate the need for wideband, low-cost, miniaturized and easily integrated antennas [1]. A

widely used antenna structure with above characteristics is Microstrip antenna. The microstrip patch antennas are associated with several advantages of being low profile, versatile, conformal and low-cost devices. The advantages of microstrip antennas make them suitable for various applications like, vehicle based satellite link antennas [3], global positioning systems (GPS) [4], radar for missiles and telemetry [3] and mobile handheld radios or communication devices [4]. But nonetheless, the microstrip antennas are also associated with some disadvantages, such as narrow bandwidth, low gain and the excitation of surface waves.

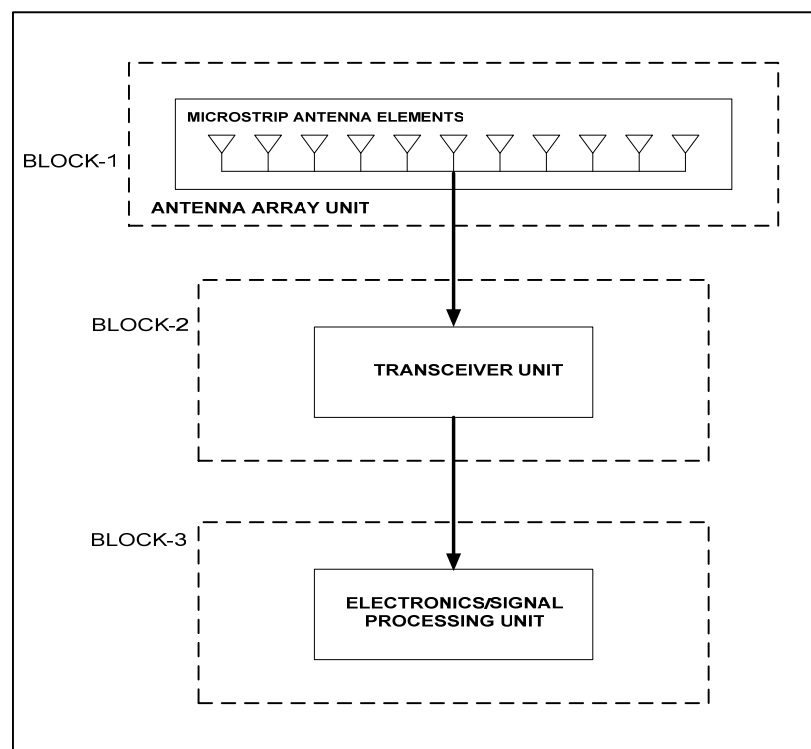


Figure1. 1 Block Diagram of a simple Microstrip Antenna Array [58]

The Figure 1.1 below shows a simple microstrip patch antenna element in array configuration. Over the years, a lot of research has been undertaken to overcome the disadvantages associated with these antennas. Some of the popular techniques proposed by researchers to widen the bandwidth are; increasing the height of antenna substrate [7], using aperture coupling method [7, 8] or using stacked patch structure [8]. Another method of using coplanar parasitic elements around or in line with primary driven element are also mentioned in the literature [9], where a geometry of four parasitic patches around four corners of a single probe fed patch yielded approximately 6 times the bandwidth of a single patch. The second important factor which falls as a disadvantage in the performance of this antenna is the gain. For microstrip patch antennas, gain can be increased by employing thin, low loss and low permittivity substrates [10]. Some researchers used another technique of employing high permittivity superstrate layers for gain enhancement [11], while others [12] used cavity backed approach or by minimizing the surface wave excitation in the substrate. Surface waves can be reduced by employing techniques such as photonic bandgap (PBG) structures, wherein the substrate is loaded so that surface waves does not propagate over a frequency band [10]. So far the most common method of improving the antenna radiating characteristics is

by arranging the radiating elements in one, two or three dimensional arrays configurations.

For the present study, a tunable linear array antenna with phase scanning capability is to be implemented. In the design process of this array the first step is to design the feed network of the antenna (array feeder), which is composed of the power divider and the tunable phase shifter. Power dividers play a very pivotal role in the splitting of microwave signals to feed the radiating elements. The array feeder is implemented using the Wilkinson type power divider because it provides a reduction in reflection of electromagnetic waves from each output arm of the divider network. In its basic form, Wilkinson power divider splits the input signal into two output signals with equal phase and amplitude. This class of dividers uses impedance matching transformers and isolation resistors to improve the transmission, reflection and isolation response of the device. Other types of power dividers found in the literature include the unequal power dividers, the  $90^\circ$  quadrature hybrid power divider, the  $180^\circ$  hybrid power divider, branchline couplers and the magic tees [15]. Each one has its own advantages depending upon the need and application.

Normally phase shifters are the devices in a phased array antenna that allow the radiated beam to be steered in the desired direction. But this beam scanning can be achieved in two ways, mechanically and electronically [14].

Mechanically scanning the main beam in array antennas is very difficult as the whole circuit becomes bulky, large, and hard to manufacture & control [39]. So the concept of electronically steered beams/nulls has evolved. The electronic phase shifters are used to construct the phase array antennas designed for fighter aircraft radars, cellular base stations, wireless and microwave communication devices and anti collision radars [6]. Depending on the manufacturing method, phase shifters can be classified into the following categories; (1) Ferrite based digital or analogue phase shifters, (2) Gallium-Arsenide based digital phase shifters, (3) Micro-electrical mechanical system (MEMS) devices, and (3) Ferroelectric based analog phase shifters [14]. Among analogue phase shift devices, the most popular one is ferrite phase shifter, where magnetic properties of externally biased ferrite material are exploited to achieve the desired phase shifts required by the antenna array. According to Adam *et al.* [54], most ferrite phase shifters uses biasing magnetic fields to change the permeability of the ferrite material, which in turn changes the phase velocity and, hence, the insertion phase of the microwave signal propagating through the phase shifter. Despite this similarity, ferrite phase shifters come in many different designs, and can be grouped based on the following classification: reciprocal versus non reciprocal, driven versus latching and analogue versus digital [54]. In this work, an analogue ferrite based phase shifter will be used. Since the cost of

the phase shifters increases the price tag of the array antenna, low cost and conformal phase shifters are always on demand. In this study, printed circuit phase shifter with ferrite substrate will be used to minimize the associated cost.

Phased arrays have received considerable attention due to their importance in radar and mobile satellite communication systems. These arrays are systems where the spatial distributions of the radiated or received electromagnetic waves are electronically scanned to enhance desired signals and/or suppress interference, noise and jamming signals. Typically, the angular pattern radiated from an array antenna depends on the number, geometrical arrangement and relative signal amplitudes and phases of the array elements. Uniform array antennas are the simplest one-dimensional array antenna, where the signal inputted in each identical element consists of identical amplitude and equal differential phase distribution. There are several methods associated with the design of phase array antenna, such as, the binomial method, the Taylor-Kaiser method, the Dolph-Tschebyscheff method etc. The Taylor-Kaiser produces somewhat wider mainlobe compared to that of Dolph-Tschebyscheff, but it exhibits no control over sidelobe behaviour. The binomial method has the widest mainlobe but no sidelobes at all [16]. But the Dolph-Tschebyscheff radiation response is considered to be optimum in the sense, that, it has the narrowest main beam

width and allows controlling the sidelobe levels. It also has the flexibility of employing equal or unequal power dividers, as an array feeder. In this study, Dolph- Tschebysheff method of designing power dividers will be adopted to construct the phase array antenna. The non-uniform (amplitude and phase) array antennas will be considered first and as predicted if it becomes difficult to fabricate, the uniform (phase only) version of that array will be designed.

Finally, the designed microstrip power divider and the phase shifters will be integrated. This will be done by introducing the ferrite substrate and redesigning the array feeder arms. External biasing magnets will then be used to achieve required tunable insertion phase. The required response of the designed array antenna is summarized in the next section.

## **1.2 THESIS OBJECTIVE**

The objectives for this study are the following:

1. Design a microstrip linear phased antenna array to operate at a center frequency of 10GHz with an impedance bandwidth of 10%.
2. Design a ferrite based array-feeder network with integrated power divider and phase shifters. Use external biasing to control the insertion phase of the phase shifter, required to achieve the desired main-beam squint of the array antenna.

3. Simulate and optimize the designed antenna array using finite element based HFSS software. Fabricate the antenna using PCB plotter. Use the “network analyzer” and the “Antenna Test and Measurement System” to observe the radiation characteristics and the beam scanning properties of the antenna.
4. The antenna design criterion's set as goals for this study are tabulate in table 1.1.

Table1. 1 Phased Array Antenna Specifications

Features	Required Values
Centre Frequency	10GHz
S-Parameters of the Power Divider	Isolation = -20dB Reflection = -20dB Transmission = -6dB
Phase shifter Type	Analogue microstrip ferrite phase shifter
Array Antenna configuration	Linear Array
Microstrip Radiator used	Rectangular Patch
Polarization	Linear
Antenna Impedance Bandwidth	10%
Antenna Gain	15dB
Antenna Half-power beamwidth	30 <sup>0</sup>
Antenna Beam Scan Range (Mag. Bias 0- 300 KA/m)	+/- 35 degrees

## 1.3 THESIS OVER VIEW

Before embarking on the antenna design process, it is essential to have a good theoretical background on the topic. Chapter 2 of this thesis summarizes the reviewed literature, which helped the authors to gain a comprehensive yet thorough background on various components methods use in designing phased array antennas. The process of designing the array antenna started with the array-feeder, used to excite the radiating elements. In Chapter 3, the design of integrated array feeder is describes, where the first part describes the power divider network, second part is dedicated to the phase shifter and the final part discusses the methods used to integrate the power-divider and phase-shifter on a common ferrite substrate. The simulated and optimized frequency responses, related to the power divider and the phase shifter, are also presented in this chapter. Once the fed network is ready, the radiating elements of the array antenna can be selected and arranged to achieve the desired radiation characteristics. Chapter 4 of this thesis discusses all the issues related to the design of the radiating elements and the linear phased array antenna. It also includes the simulated (HFSS) radiation characteristics associated with the designed antenna array. The fabrication process of the array antenna and the equipments/methods used in the experimental procedure are discussed in the early part of Chapter 5. The

experimentally observed results are then presented and analyzed. Comparisons between the experimental and simulated results are also tabulated in this chapter. Finally chapter 6 describes the conclusions drawn from this research work and recommendations on future work to be carried on this subject.

## **CHAPTER 2**

### **LITERATURE REVIEW**

#### **2.1. INTRODUCTION**

The use of microstrip structures to radiate electromagnetic waves was contemplated in the 1950's [2]. The earliest form of planar antennas, integrated with planar transmission line, was developed by Deschamps [17]. Later it was formally introduced by Munson [18] as planar antennas on missiles. By early 1970's, the importance of microstrip radiators was realized when researchers noted that almost half of the power in a microstrip radiator escapes as radiation. Thus, a microstrip radiating patch with considerable radiation loss was defined as microstrip antennas. Later, it was proved that this radiation mechanism was arising from the discontinuities at each end of the microstrip transmission line [5]. At the time of its inception microstrip antennas were associated with many disadvantages, such as low efficiency, lower power, high Q, poor polarization purity, poor scan capability, and very narrow bandwidth. With the evolution of design technology, planar microstrip antennas have achieved higher bandwidth, mechanical robustness and versatility with respect to resonant frequency, improved polarization

pattern and wider impedance bandwidth [5]. Also ample research on this topic has led to the development of microstrip antenna arrays with improved efficiency, directivity and beam scanning capability.

Since printed circuit technology is currently widely used to provide smaller and low profile antennas for personal and mobile communication devices, this research study will embark on designing a microstrip phased array antenna for specified beam scanning purposes. But before these antennas can be designed to meet our desired requirements, the basic theory associated with the technology needs to be understood. The theoretical background associated with the design and analysis of microstrip patch elements/arrays, along with their advantages and disadvantages are briefly discussed in the following section.

## **2.2. MICROSTRIP ANTENNAS**

In its basic form, microstrip antennas are similar to parallel plate capacitors. Both have parallel plates of metal layer and a sandwiched dielectric substrate between them. But in microstrip antenna, one of these metal plates is infinitely extended than the other, to form the ground plane; where as the smaller metal plate is described as radiating patch. Since the size of the patch is often proportional to frequency of the propagating signal, this class of antenna is classified as resonant antennas. This contributes to the

basic shortcoming of the microstrip antennas related with its narrow bandwidth, usually only a few percent [1] of the resonance frequency. So far, several shapes of microstrip patches, such as rectangular, circular, triangular, semicircular, sectoral and annular etc, are successfully used as radiating antenna elements employed in various communication and control devices [1].

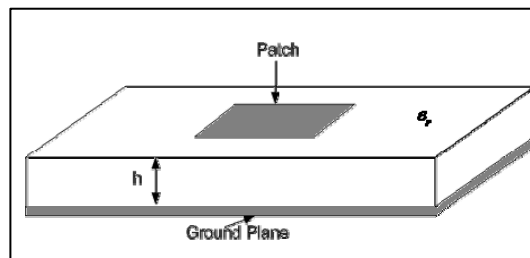


Figure2. 1 Microstrip rectangular patch antenna [1]

Figure2. 1 shows the most basic type of microstrip patch antenna consisting of rectangular radiating elements. When the patch is excited by a feed line, charge is distributed on the underside of the patch and the ground plane. At a particular instant of time the attractive forces between the underside of the patch and the ground plane tend to hold a large amount of charge. And also the repulsive forces push the charges to the edge of the patch, creating a large density of charge at the edges. These are the sources of fringing field. Radiation from the microstrip antenna can occur from the fringing fields between the periphery of the patch and the ground plane [1].

Assuming no variations of the electric field along the width ( $W$ ) and the thickness ( $t$ ) of the microstrip structure, the electric field excited by the patch is shown in Figure2. 3

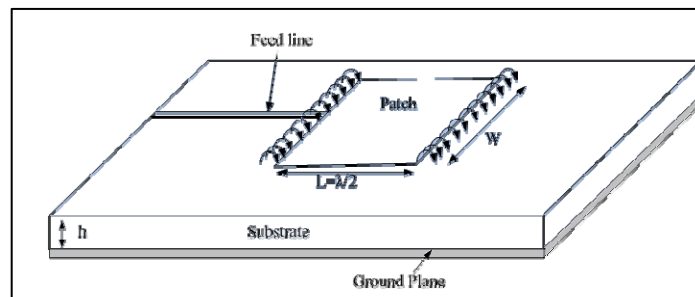


Figure2. 2 Radiation mechanism associated with microstrip patch [ 1]

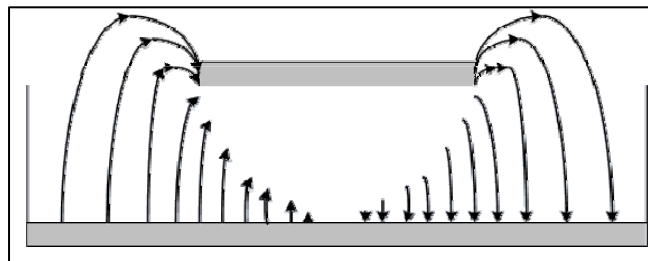


Figure2. 3 Electric field distribution (side view) [ 1]

Radiation is ascribed mostly to the fringing fields at the open circuited edges of the patch length. The fields at the end can be resolved into normal and tangential components with respect to the ground plane. The normal components are  $180^\circ$  out of phase because the patch line is  $\lambda/2$  long; therefore the far field radiation produced by them cancels in the broadside

direction [2]. The tangential components (those parallel to the ground plane) are in phase, and the resulting fields combine to give maximum radiated field normal to the surface of the structure i.e., broadside direction. Therefore, the patch may be represented by two slots  $\lambda/2$  apart as shown in figure below, excited in phase and radiating in the half space above the ground plane.

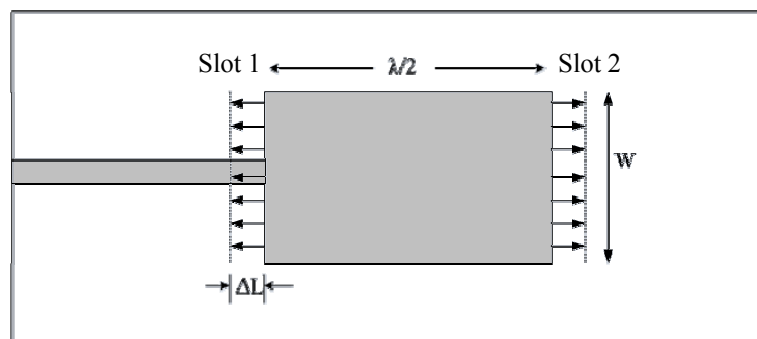


Figure2. 4 Increase in length of the microstrip patch [ 1]

Typically, to excite the fundamental TEM mode, the length  $L$  of the rectangular patch remains slightly smaller than  $\lambda/2$ , where  $\lambda$  is the wavelength in the effective dielectric medium [3]. In terms of free space wavelength ( $\lambda_0$ ),  $\lambda$  is expressed by [3];

$$\lambda = \frac{\lambda_0}{\sqrt{\epsilon_{eff}}} \quad (2.1)$$

Where  $\epsilon_{eff}$  is the effective dielectric constant of a microstrip line and is given as

$$\epsilon_{eff} = \frac{\epsilon_r + 1}{2} + \frac{\epsilon_r - 1}{2} \left[ 1 + 12 \frac{h}{W} \right]^{-1/2} \quad (2.2)$$

The value of  $\epsilon_{eff}$  stays between 1 (dielectric constant of air) and the dielectric constant of the substrate,  $\epsilon_r$ , because the electromagnetic fields excited by the microstrip resides partially in the air and partially in the substrate. However, to enhance the electromagnetic (EM) fields in the air, which account for radiation, the width ( $W$ ) of the patch needs to be increased. Radiating EM fields can also be enhanced by decreasing the  $\epsilon_r$  or by increasing the substrate thickness ( $h$ ). It is of note that, since ' $W$ ' and ' $h$ ' are constrained by the input-impedance and unwanted-surface-waves respectively, a compromise is required while selecting antenna dimensions. Since microstrip patches are often feed or integrated with microstrip transmission-lines or circuits, the design requirement of these devices are also important. At microwave frequency band, typical comparison of microstrip antenna with that of microwave transmission-line is given in Table 2.1.

Table2. 1 Comparison between microstrip transmission line and microstrip antenna

	<b>Microstrip transmission-line</b>	<b>Microstrip Antenna</b>
<b><i>h</i></b>	Thin	Thick
<b><math>\epsilon_r</math></b>	High	Low
<b><i>W</i></b>	Small	Large
	Maximum propagation	Maximized radiation

For broadside radiation, microstrip antenna array are designed to produce the main beam of the antenna normal to the patch plane. The far field component can be written as

$$\left. \begin{aligned} E_\theta &= E_0 \cos \phi f(\theta, \phi) \\ E_\phi &= -E_0 \cos \theta \sin \phi f(\theta, \phi) \end{aligned} \right\} \quad (2.3)$$

Where

$$f(\theta, \phi) = \frac{\sin \left[ \frac{\beta W}{2} \sin \theta \sin \phi \right]}{\frac{\beta W}{2} \sin \theta \sin \phi} \cos \left( \frac{\beta W}{2} \sin \theta \cos \phi \right) \quad (2.4)$$

Although microstrip antennas have come a long way in past two decades, the disadvantages associated with it is still an area of exploration. The advantages and disadvantages of these antennas are summarized below as,

### **2.2.1 ADVANTAGES OF MICROSTRIP ANTENNAS**

- They are light in weight and low profile.
- They can be made conformal to the host surface.
- Their ease of mass production using printed circuit technology leads to a low fabrication cost
- They are easier to integrate with other microstrip circuits [7].
- They support both linear polarization and circular polarization [7].
- They can be realized in a very compact form, desirable for personal and mobile communication hand held devices.
- They allow for dual and triple band operations [6].

### **2.2.2 DISADVANTAGES OF MICROSTRIP ANTENNAS**

- Narrow bandwidth [1, 2, 6].
- Lower power gain [6].
- Lower power handling capability [19].
- Polarization impurity
- Surface wave [4]

## **2.3. METHODS OF ANALYSIS**

The general structure of a microstrip antenna is that of two dimensional radiating patches on a thin dielectric substrate and therefore may be categorized as two-dimensional planar component for analysis purposes. There are many methods of analysis for microstrip antennas. The most popular methods are based on the transmission line model, cavity model and full-wave analysis. In this work transmission line model is used to calculate the dimensions and input impedance associated with the radiating patches. But the simulating software, HFSS, used in this study uses finite element method to carry out the full wave analysis of the designed structure. Brief descriptions of these methods are as follows:

### **2.3.1 THE TRANSMISSION LINE MODEL**

Although the transmission line model yields less accurate results, it is a very simple model and provides a good physical insight of the basic antenna performance. In this model, the microstrip patch element is viewed as a transmission line resonator with the field only varying along the length (no transverse field variations), and the radiation occurs mainly from the fringing fields at the open circuited ends. The patch is represented by two slots that are spaced by length of resonator. This model was originally developed for rectangular patches but has been extended for generalized

patch shapes. Many variations of this model have been used to analyze the microstrip antenna [20], since the normal analysis was derived for rectangular patch, some authors [21] have modified it to suite to other patch shapes like rectangular, and others have modified it to suite to triangular patch shapes [22].

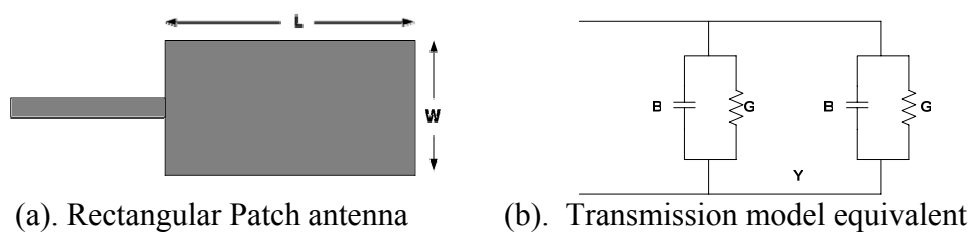


Figure2. 5 Transmission-line model of rectangular microstrip patch [ 1]

Figure2. 5 shows a typical rectangular patch antenna and its equivalent circuit using transmission-line model. Each radiating slots corresponding to the edges of the patch is represented by parallel equivalent admittance,  $Y$ , which is given by

$$Y = G + jB \quad (2. 5)$$

where  $G$  and  $B$  represents the conductance and the susceptance produced by the slot or the radiating edge of the microstrip patch. These conductance and susceptance are typically expressed as [1],

$$G = \frac{W}{120\lambda_0} \left[ 1 - \frac{1}{24} (\kappa_0 h)^2 \right] \quad \frac{h}{\lambda_0} < \frac{1}{10} \quad (2.6)$$

$$B = \frac{W}{120\lambda_0} \left[ 1 - 0.636 \ln(\kappa_0 h) \right] \quad \frac{h}{\lambda_0} < \frac{1}{10} \quad (2.7)$$

where  $W$  is the width of the microstrip patch and  $h$  is the height of the substrate,  $\lambda_0$  is the free-space wavelength of the propagating electromagnetic wave. Thus the resonant input impedance can be given as,

$$R_m(y=0) = \frac{1}{2(G_1 + G_{12})} \quad (2.8)$$

Where  $G_{12}$  is the mutual conductance between the slots which are representative of patch edges and is given by,

$$G_{12} = \frac{1}{120\pi^2} \int_0^\pi \left[ \frac{\sin\left(\frac{k_0 W}{2} \cos\theta\right)}{\cos\theta} \right]^2 J_0(k_0 L \sin\theta) \sin^3\theta d\theta \quad (2.9)$$

Where  $J_0$  is the Bessel function of the first kind and order zero.

Also the resonant frequency of the microstrip patch for the dominant mode  $TM_{010}$  is given as,

$$(f_r)_{010} = \frac{1}{2L_{eff} \sqrt{\epsilon_{reff}} \sqrt{\mu_0 \epsilon_0}} = \frac{1}{2(L + 2\Delta L) \sqrt{\epsilon_{reff}} \sqrt{\mu_0 \epsilon_0}} \quad (2.10)$$

Where  $\Delta L$ , is the increase in patch length because of fringing. Although the transmission line model is easy to use, many patch configurations cannot be

analyzed using this model due to its inability to consider the field variation orthogonal to the direction of propagation. In this study, this model is used to calculate the patch dimensions and input impedance.

### **2.3.2. THE CAVITY MODEL**

Cavity model is more complex than transmission line model and provides more accurate results. In this model the region between the patch and the ground plane is treated as a cavity, which is surrounded by magnetic walls around the periphery and by electric walls from the top and bottom sides. Since thin substrates are used, the field inside the cavity is assumed to be uniform along the thickness of the substrate [1]. In cavity model, the analysis is made simple, by expressing the electromagnetic fields within the patch substrate, as a summation of the various resonant modes of the two dimensional radiator (i.e., the patch in this case). Since the normal substrates that are used to produce the microstrip patch antennas are thin, the usual assumption is that the field inside the cavity is uniform along the thickness of the substrate [23].

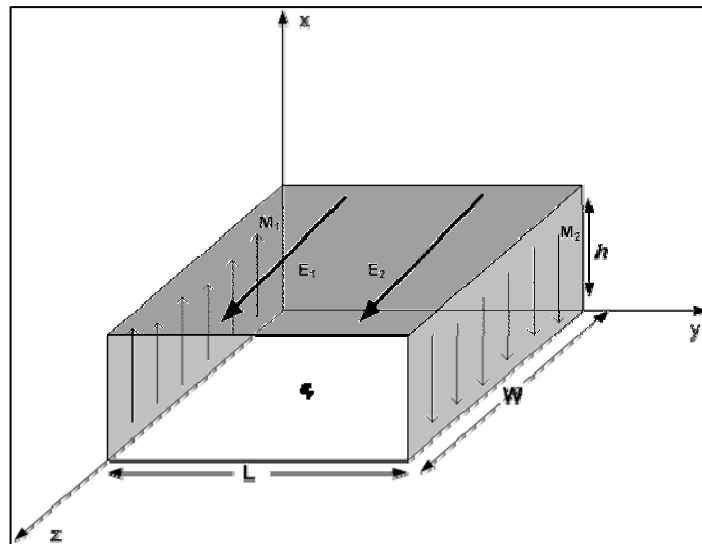


Figure2. 6 Rectangular patch represented as a cavity in Cavity model analysis [ 1]

The cavity model makes the following assumptions [ 5]:

- Since the substrate is assumed thin, fields in the cavity do not vary with z-axis.
- Tangential component of the magnetic field is negligible at the edge of patch.
- The existence of a fringing field can be accounted for by slightly extending the edges of the patches.

### **2.3.3. FULL WAVE MODEL**

Full wave models are very versatile and can provide very accurate results. Method of Moments [24], the Finite Difference Time Domain method [28], the Finite element method (FEM) [25] all belong to this

category, they are suitable for volumetric configurations. The Finite Element Method (FEM) is more popular amongst these methods and in this method the region of interest is divided into any number of finite surfaces or volume elements depending upon the planar or volumetric structures to be analyzed. These discretized units, generally referred to as finite elements, are well defined geometrical shapes, such as triangular elements for planar configurations and tetrahedral and prismatic elements for three dimensional configurations [23]. The software used in this study, called High Frequency Simulation Software (Ansoft HFSS v9), is a FEM based.

## **2.4. EXCITATION TECHNIQUES OF MICROSTRIP ANTENNAS**

The microstrip antennas can be excited or fed directly either by coaxial probe or by a microstrip line. It can also be excited indirectly using electromagnetic coupling (proximity) or by aperture coupling method, in which there are no direct metallic contact between the feed line and the patch. Since feeding technique influences the input impedance, it is often exploited for matching purposes. Also as the antenna efficiency depends on the transfer of power to the radiating element, feeding technique plays a vital

role in the design process. The four most popular feeding techniques are discussed below.

### **2.4.1 MICROSTRIP LINE FEED**

Microstrip line feed patch antennas are easy to fabricate as both the feed line and the radiating elements are printed on the same substrate. The impedance matching associated with this class of antennas are also simpler compared to other methods. Although these antennas have low spurious radiation, often the radiation from the feed line increases the cross polarization level. Also, the thick substrate associated with these antennas (for bandwidth improvement) introduces surface waves that deteriorate the antenna performance. In millimeter-wave range, the size of the feed line is comparable to the patch size, leading to increased undesired radiation. Typically, the patches are feed from its edge and the edge impedance should be matched with the impedance of the feed line for maximum power transfer. Since the input impedance of the patch gradually decreases from maximum at the edge (150 to 300  $\Omega$ ) to minimum at the center, insets are often used to connect the feed line to a relatively low impedance spot of the patch. This popular technique is shown in Figure2. 7. The input impedance related to the length of the inset is given by,

$$R_{in}(y = y_0) = \frac{1}{2(G_1 + G_{12})} \cos^2\left(\frac{\pi}{L} y_0\right) \quad (2.11)$$

where  $y_0$  is the inset length from slot at the feeding edge of patch,  $L$  is the length of the patch,  $G_1$  and  $G_{12}$  are self and mutual conductance's expressed in section 2.2.1

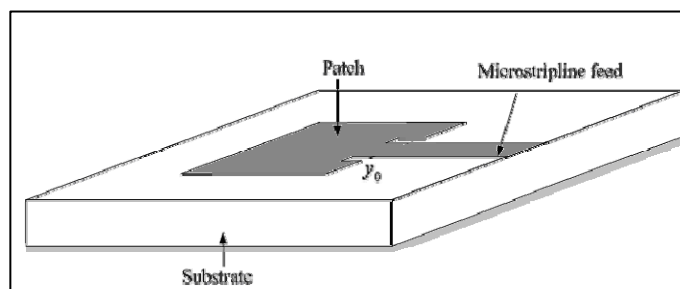


Figure2. 7 Microstripline feed

Other methods of impedance matching between the feed line and radiating patch is achieved by introducing a single or multi-section quarter-wave-transformers. In this study, optimized insets are introduced to match the rectangular radiating elements with microstrip feed lines.

#### **2.4.2. COAXIAL FEED**

The coaxial or probe feed arrangement is one in which the center conductor of the coaxial connector is soldered to the patch. The main advantage of this feed is that it can be placed at any desired location inside

the patch to match its input impedance; other advantages are that it can be easily fabricated and has low spurious radiation [1]. The main disadvantage of a coaxial feed antenna is the requirement of drilling a hole in the substrate to reach the bottom part of the patch. Other disadvantages include narrow bandwidth, difficult to theoretically model, and its asymmetrical non planar configuration.

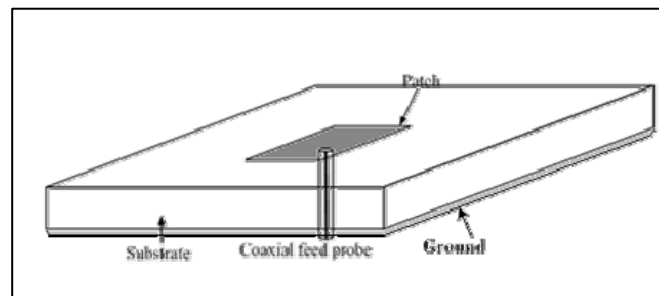


Figure2. 8 Coaxial probe feed

### **2.4.3. APERTURE COUPLING**

This is a method of indirectly exciting the patch, where the electromagnetic fields are coupled from the microstrip feed line to the radiating patch through an electrically small aperture or slot, cut in the ground plane. Figure2. 9 illustrates such an aperture coupled microstrip rectangular antenna. The coupling aperture is usually centered under the patch, leading to lower cross polarization due to symmetry of the configuration. The shape, size, and location of the aperture decide the

amount of coupling from the feed line to the patch [3], this can lead to improved bandwidth as shown by some authors [26 and 27]. The slot aperture can be either resonant or non resonant [28]. The resonant slot provides another resonance in addition to the patch resonance thereby increasing the bandwidth, but at the expense of back radiation. Therefore, the slot should not resonate within the operating frequency band of the antenna.

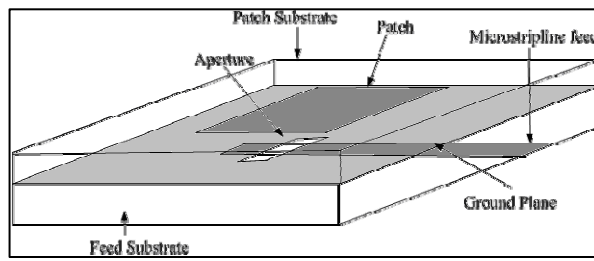


Figure2. 9 Aperture coupled microstrip antenna and its equivalent circuit

The advantage of this feeding technique is that the radiator is shielded from the feed structure by the ground plane. Another important advantage is the freedom of selecting two different substrates; one for the feed line and another for the radiating patch. Since both substrates can be optimized simultaneously, the need for a compromise between radiation and propagation requirements can be avoided. This flexibility in choosing the appropriate substrates also minimizes unwanted surface waves, spurious coupling between antenna elements and thereby increasing the efficiency as

well as the bandwidth of the antenna. However, the fabricating process of this class of antenna is difficult and can easily deteriorate the performance due to small errors in the alignment of the different layers. In this study an aperture coupled stacked patch antenna is also designed for beam scanning purposes.

#### **2.4.4. PROXIMITY COUPLING**

This is another coupling method which does not involve the direct contact of the feed line. But unlike aperture coupling, this method uses electromagnetic coupling between the feed line and the radiating patches, printed on separate substrates [1]. Figure 2.10 shows proximity coupled rectangular patch antenna. Typically, the bottom feeder substrate is thin and made of high dielectric constant, whereas the top patch substrate is thick and made of low dielectric constant. The advantage of this coupling is that it yields the largest bandwidth compared to other coupling methods; it is somewhat easy to model and has low spurious radiation. Some authors have shown the improvement in bandwidth [29]. The disadvantage is that it is more difficult to fabricate.

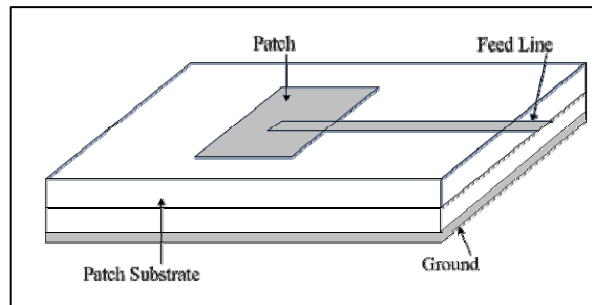


Figure2. 10 Proximity coupled feed.

## 2.5. ANTENNA ARRAY

Typically the array arrangements of microstrip antennas are used to improve the efficiency, directivity and gain for the radiating system. That is because the radiation from the single antenna element is often very wide in pattern with large beam angles. This is not good for point to point communications, which requires antennas that are more directive in nature. Also a single radiating element often generates radiation patterns with unacceptable bandwidth, efficiency, and gain parameters. All these and more make the utilization of a single element antenna not recommendable. The implementation of antennas in array configuration overcomes these drawbacks. In this section the concept of arrays is briefly described.

Antenna arrays are basically a collection of radiating elements, geometrically arranged in a specific manner, to generate the required radiation pattern. Each antenna in the array is called as an element, and it can be anything from simple dipole antenna, monopole antennas, horn antennas,

or as in this case microstrip patches. These antenna arrays are classified into linear arrays, circular arrays, planar arrays or 3-dimensional arrays depending on the positioning of the antenna elements

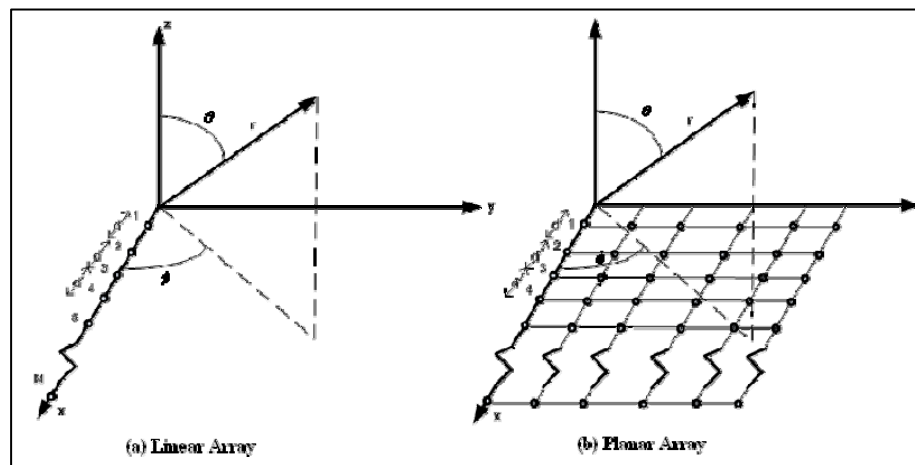


Figure2. 11 Antenna array configurations [ 1]

Figure2. 11 illustrates the linear and planar arrangements of antenna array. The two basic types of antenna array are: uniform and non-uniform. Uniform arrays are the simplest one-dimensional array antenna, where the signal inputted in each identical element consists of identical amplitude and equal differential phase distribution. This class of array has the narrowest main-lobe and considerable amount of sidelobes. On the other hand, non-uniform array antenna with unequal amplitude distribution yields a more controlled side-lobe level. The phased array is a special type of antenna array, where the spatial distributions of the radiated fields are electronically scanned to

enhance the desired signal, by introducing differential phase (and/or magnitude) in the input signal of the radiating elements. Phased-array antennas have been developed mainly for radar applications but are being used more now for space-based communications applications because of their advantages in scanning, re-configurability, weight, and power [30]. Also because of the development in the integration technology of small microwave circuits, has led the deployment of these antennas in ground, ship, air and space communication [30]. Also they find application in other areas apart from communication, like the non destructive testing (NDT) etc.

In phased array antenna, several types of phase shifters are used to control the phases of the antenna elements to achieve beam steering. In this study we will use planar microstrip ferrite phase shifters with external biasing, where variable phase shift is obtained by changing the magnitude of the biasing field. A detail description of a linear microstrip phased array antenna, designed in this study, is presented in chapter 4.

### **2.5.1 ARRAY FACTOR**

The total field of an antenna array can be calculated by pattern multiplication [1].

$$E (\text{total}) = [E (\text{single element at reference point})] \times [\text{array factor}]$$

This is equal to the field of a single element multiplied by the factor, called array factor [1], as shown in figure 12. The array factor is a function of array geometry and the excitation phase

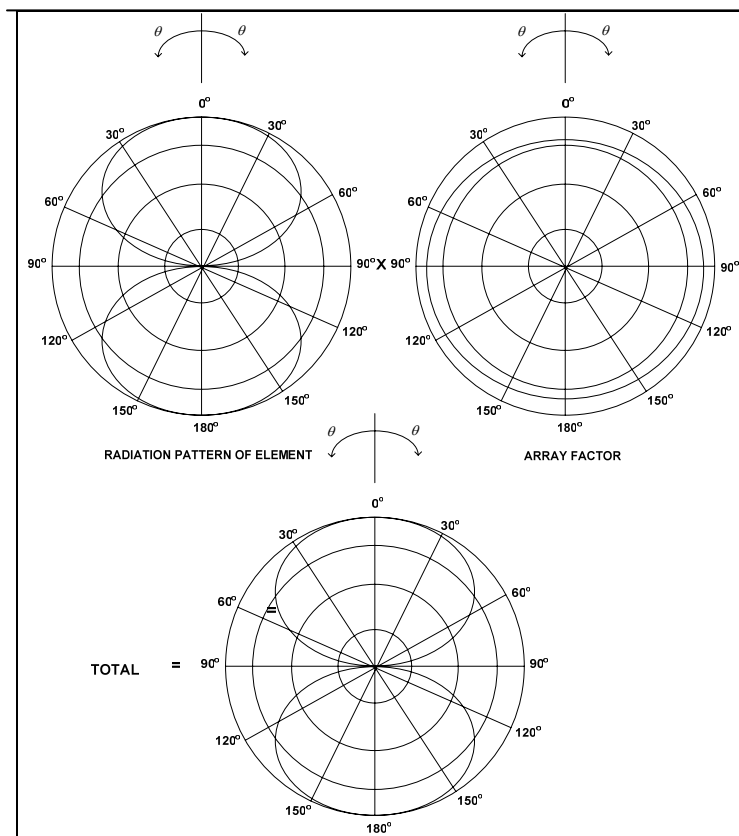


Figure2. 12 Pattern multiplication shown graphically [1]

By varying the separation between the array elements and introducing the progressive phase shift ( $\beta$ ), the radiation pattern of the antenna array can be controlled. This type of control is normally referred to as phase scan or beam steering of the antenna array. The arrays are of uniform type, if the elements

are fed with microwave signal with same magnitude (current amplitudes), and same progressive phase difference ( $\beta$ ). But they are called non-uniform, if the elements are fed with signals of different magnitude and same or different  $\beta$  [1]. The array factor for any N-element array is given by the following equation [1],

$$AF = \sum_{n=1}^N a_n e^{j(n-1)\psi} \quad (2.12)$$

$$\text{Where } \psi = kd \cos \theta + \beta = \frac{2\pi d}{\lambda} \cos \theta + \beta \quad (2.13)$$

$k$  is the wave number given by  $2\pi/\lambda$ ,

$d$  is the distance between the elements,

$\theta$  is the angle of the main beam of antenna array,

$\beta$  is the progressive phase shift between individual elements and

$a_n$  is the amplitude of individual elements

For a uniform array the amplitudes are taken unity and all the  $a_n = 1$ . In the literature, several methods are proposed for calculating the array factors. Some of the widely used techniques are Binomial method, Dolph-Tschebysheff method, Taylor-Kaiser method and Schelkunoff method. Each designing method has its own advantages and drawbacks. In the binomial

method, as the half power beam-width increases the directivity decreases, and for the design of large arrays, larger amplitude ratio of sources is required. On the other hand, the Dolph-Tschebysheff method has the flexibility of choosing the main lobe to side lobe ratio and all its side lobes are of same amplitude, unlike uniform distribution. Also this method provides optimum beam width for a specified side lobe level reduction. In this thesis, a uniform phase array antenna and a non-uniform array antenna using Dolph-Tschebysheff method is designed and investigated.

### **2.5.2 MUTUAL COUPLING**

When two or more radiating patches are near each other, they interfere with each other depending on; radiation characteristic of each, relative separation between them and relative orientation of each antenna. This interference of energy is known as mutual coupling. Due to the significant contribution of this factor in the antenna performance, it must be included in the design process. Although mutual coupling is difficult to predict analytically, but using full-wave analysis, adopted by the software (HFSS) used in this study, it can be easily incorporated in the array design. As an example, for the two rectangular patches in Figure 2.13, the coupling for two side-by-side elements is a function of relative alignment. When the

elements are positioned collinearly along the E-plane, even for a small separation, the elements exhibit isolation. Whereas, when they are positioned collinearly in the H-plane, the separation has to be large. The figure below shows the positioning of the patches.

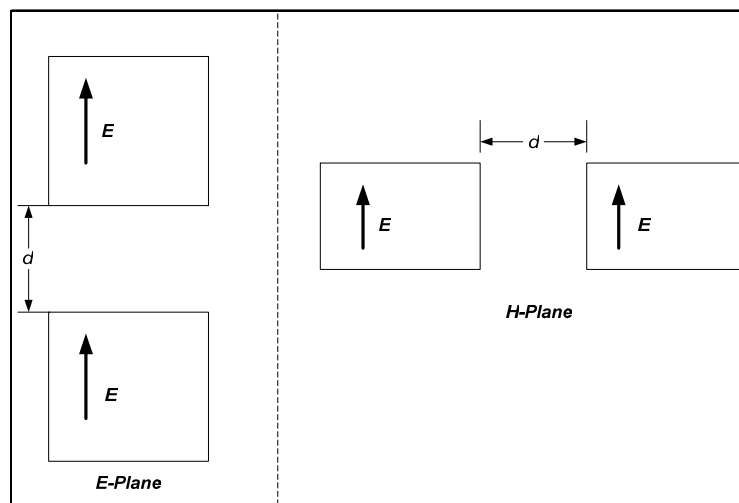


Figure2. 13 H-plane arrangements of microstrip patch antennas [ 1 ]

Mutual coupling is primarily attributed to the fields that exist along the air-dielectric interface. So by selecting the correct distance, these fields can be decomposed to constructive space waves or destructive surface waves. The spacing at which one plane coupling overtakes the other one also depends on the electrical properties and the geometrical dimensions of the microstrip antenna.

Since the design of a linear phased array antenna is carried out here using simulating software HFSS, mutual coupling factors are optimized using the software.

In phased array antenna, several types of array feeders and phase shifters can be used to electronically steer the beam of the array antenna. In order to select the suitable power divider and phase shifter for our designed array antenna, basic knowledge about these devices are essential. In the following section, the theoretical background about these essential components array antenna is briefly described.

## **2.6 POWER DIVIDER**

The design process of the antenna array requires the dimensions of associated array feeder. Array feeder is a power divider network that provides required transmission, reflection and isolation properties. In this study, the four-way power divider network is designed using microstrip transmission line that supports quasi-TEM mode of propagation. In the literature, various types of microstrip power dividers have been employed in the feeding of the microstrip antennas. The most popular ones being the quadrature hybrid, annular or ring, Wilkinson and Y-junction power divider. By definition, a -3dB power divider is ideally a passive lossless reciprocal three port device that divides power equally in magnitude and phase.

Figure2. 14 shows a three port lossless and reciprocal power divider with all matched ports.

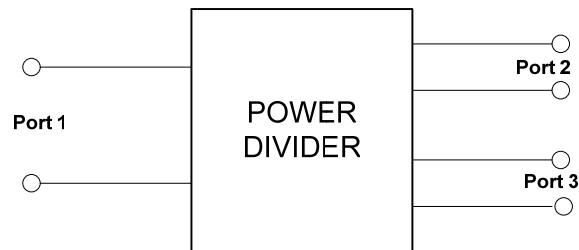


Figure2. 14 Block diagram power divider

The general expression of the S-parameter matrix related this device is:

$$[S] = \begin{pmatrix} S_{11} & S_{12} & S_{13} \\ S_{21} & S_{22} & S_{23} \\ S_{31} & S_{32} & S_{33} \end{pmatrix} \quad (2. 14)$$

Since all the three ports of this power divider are matched,  $S_{ii} = 0$ , and the network is nonreciprocal,  $S_{ij} = S_{ji}$ , the modified S-matrix can be written as,

$$[S] = \begin{pmatrix} 0 & S_{12} & S_{13} \\ S_{12} & 0 & S_{23} \\ S_{13} & S_{23} & 0 \end{pmatrix} \quad (2. 15)$$

Also as the network is lossless then this matrix should be unitary and yields,

$$|S_{12}|^2 + |S_{13}|^2 = 1 \quad S_{13}S_{23}^* = 0$$

$$|S_{12}|^2 + |S_{23}|^2 = 1 \quad S_{12}S_{13}^* = 0$$

$$|S_{13}|^2 + |S_{23}|^2 = 1 \quad S_{12}S_{23}^* = 0$$

Considering the above equations we see that the second column must have atleast two out of three S parameters to be equal to zero. But if two of them were zero then one of the equations in the first column will be violated. Thus, we can conclude that it is impossible to satisfy all the three criteria of any power divider, such as, lossless, matched and reciprocal. Since relaxing anyone of these constraints makes the other two achievable.

In this study, we will start with the design process of a four way array feeder network using Wilkinson type of power divider. Thus, a brief introduction of this type of power divider is presented here. The Wilkinson power divider, invented around 1960, splits the signal in two equal amplitude equal phase output signals [18]. Wilkinson relied on quarter wave transformers to match the split ports to common port. Since a lossless reciprocal three port network cannot have all ports simultaneously matched, Wilkinson introduced a resistor for the purpose of matching. Apart from matching, the resistor also improved the isolation between the output ports. Figure 2.15 show the equivalent circuit and the microstrip implementation of a Wilkinson two-way power divider. The impedances required for the quarter wave transformer and the isolating resistor are also shown in this figure.

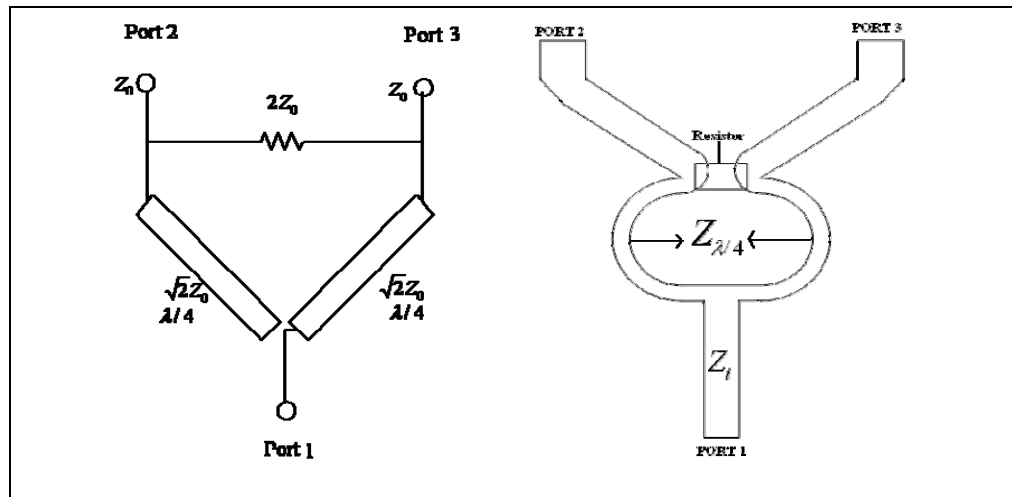


Figure2. 15 Wilkinson power divider and it equivalent microstripline implementation.

Many authors like Lee et al [37] proposed formulae for implementing a multi section power divider by modifying the Wilkinson's design to increase the device bandwidth. Others [38] proposed a 9-way power divider consisting of 3-way power dividers in 2 stages to, further improve the bandwidth. Antsos et al [38] implemented a 14-way power divider in the K-band, based on the novel technique of improving the Wilkinson's design.

Apart from the number of ports, keeping the ports constant and dividing the power unequally also has been done by some authors. Like Antsos et al [38] have designed an unequal power divider based on different impedances employed for different arms of the power divider.

## 2.7. PHASE SHIFTERS

Phase shifters are components of an electronically scanned array that steers the antenna beam in the desired direction without physically re-positioning the antenna. By definition, phase shifters are two ports network where output signal may adjust to have some desired phase relationship to the input signal by using a control signal. The most common phase shifters are classified in two categories [39]:

(a) Analogue phase shifters, in which differential phase shift is varied in continuous manner using a control signal (such as external biasing field, etc).

This class of phase shifter is mostly based on ferrite material.

(b) Digital Phase shifters, in which differential phase shift can be changed by only a few predetermined phase shift values, such as  $45^\circ$ ,  $90^\circ$ ,  $180^\circ$  etc.

These phase shifters are typically designed using ferrite and semiconductor materials. Some of the widely used semiconductor phase shifters are; switched line, loaded line, etc. Recently two other type of planar phase shifters are also widely used, such as, micro-electrical mechanical system (MEMS) devices, and ferroelectric based analog phase shifters [39]. In ferroelectric based phase shifters the voltage of the microstrip is changed continuously to achieve differential phase shift.

In this thesis, ferrite phase shifters are used to design a linear array

antenna. According to Adam *et al.*[40], ferrite phase shifters use biasing magnetic fields to change the permeability of the ferrite material, which in turn changes the phase velocity and, hence, the insertion phase of the microwave signal propagating through the phase shifter [40]. Despite this similarity, ferrite phase shifters come in many different designs, and can be grouped based on the following classification: reciprocal versus non reciprocal and driven versus latched [39]. In all the above designs, the phase shifters are made of waveguide structures that are only a fraction of the operating wavelength, and require a costly and difficult manufacturing process. Consequently, phase shifters utilizing printed transmission lines or microstrip lines pose a good low-cost alternative.

Before ferrite based phase shifters can be implemented successfully, knowledge about the material properties of ferrite is essential [40 and 39]. The behavior of ferrite material used in this study to obtain the differential phase shift can be explained in terms of: *Faraday Rotation* [40]—the rotation of the plane of polarization as electromagnetic wave propagates through a magnetized ferrite [40 and 39].

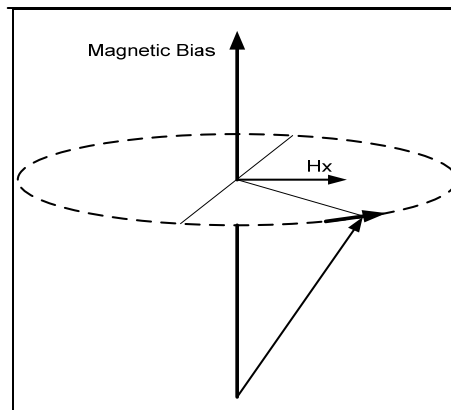


Figure2. 16 Magnetic field's rotation in ferrite

Under the influence of static ( $H_{dc}$ ) and time varying ( $h$ ) magnetic fields, a gyromagnetic medium such as ferrite would behave anisotropically, as shown in Figure2. 16

As a result the ferromagnetic materials are associated with tensor permeability and scalar permittivity. Thus for an external biasing field,  $H_{dc}$ , if the internal intensity of magnetization is given by  $M$ , then we can say that,

$$B = \mu_0 H_{dc} + M \quad (2.16)$$

Also the tensor permeability of a magnetized ferrite material is given by [20],

$$\mu_r = \begin{pmatrix} \mu & -j\kappa & 0 \\ j\kappa & \mu & 0 \\ 0 & 0 & \mu_0 \end{pmatrix} \quad (2.17)$$

where, 
$$\mu = \mu_0 \left( 1 + \frac{\omega_0 \omega_m}{\omega_0^2 - \omega^2} \right) ; \quad \kappa = \mu_0 \frac{\omega_m \omega}{\omega_m^2 - \omega^2}$$

The angular frequencies ( $\omega_0$  and  $\omega_m$ ) are defined in terms of external biasing field ( $H_{dc}$ ), gyromagnetic ratio ( $\gamma$ ), Saturation magnetization ( $M$ ) and demagnetization factor ( $N$ ) as;  $\omega_0 = 2\pi\gamma(H_{dc} - N_z M)$  and  $\omega_m = 2\pi\gamma M$ . The effective permeability of the ferrite medium or substrate can be then given as;

$$\mu_{eff} = \frac{\mu^2 - \kappa^2}{\mu} \quad (2.18)$$

Thus, ferrites allow electromagnetic wave to penetrate, thereby permitting an interaction between the wave and magnetization within the ferrite. This interaction can be controlled by varying externally applied biasing DC magnetic field and has been used to produce a variety of useful phase shift and control devices [41]. When the bias field was varied near the resonance region of the ferrite, then any slight changes in the bias field result in considerable changes in the phase constant  $\beta$ . Batchelor, Langley et al [42]

used this phenomenon to design and simulate a 2-element array of circular patches on the ferrite-alumina composite substrate. They achieved scan angles of up to  $30^0$  and later produced a binomially fed array of three elements and produced higher scan angle.

At present, although ferrites are widely used as load isolators, variable attenuators, modulators, and switches in microwave systems, the most common application of ferrites are to achieve variable phase shifts in electronically steerable phased-array antennas, deployed in aircraft/missile radars, cellular base stations, wireless, microwave and satellite communication devices, anti collision radars etc. In this thesis, we will use externally magnetized microstrip ferrite phase shifters to achieve the required beam steering properties of a linear phased array antenna.

After extensive literature review and study the research was carried out in specific tasks of designing the power divider first, then implementing the phase shifter and finally incorporating the whole feed network into complete antenna array by introducing the patches. The following chapters describe the designing and implementation of this study.

## **CHAPTER 3**

### **DESIGN OF FEED NETWORK FOR ANTENNA ARRAY**

#### **3.1 INTRODUCTION**

For an antenna array, microwave signal divider or feed network is often used to regulate the amplitude and phase feed requirements of the radiating elements (patches) to control the beam scanning properties. Thus selecting, optimizing and implementing the feed network forms a critical part of the antenna array design. Amongst the most common and well-known feeding techniques, the corporate feeding is widely used in scanning phased, multi-beam or shaped-beam arrays. A few other type of feeding techniques are series feed, space feed, and hybrid feed. The following section briefly introduces the common feed networks, shown in Figure 3.1.

- i. Corporate feed network is versatile and allow more control over the feed of each element (amplitude and phase). The distance between the patches and the microwave feed point of the array, are kept equal for equal phase patch excitations. The magnitude of the signal delivered to each patch is varied (if required) by using uneven power dividing arrangements. The combined effect of placing microstrip feeder lines in parallel with each other reduces the effective

resistance and involves the use of quarter wave transformers to match the individual sections to a  $50\Omega$  line source. Also the widths of feed lines can be varied to achieve different magnitudes of power division as shown in Figure 3.1(a).

- ii. Series feed network is more complex, although it uses up less space and is commonly used in arrays with a fixed beam. In this class of feeder, as the wave travels through the microstrip line, it is attenuated because of power radiated from each element of the array. These losses are to be accounted for when determining the element excitations. The connecting transmission line lengths and mutual coupling effects determine the phase of each element.
- iii. The advantages of the space feed are the associated low loss, reduced weight and size of the feed network. With this type of design, a primary antenna is connected to a transmitter and excites several pickup antennas that are connected to the secondary elements that form the array. The amplitude distribution of the array is determined by the primary antenna pattern and the pickup antenna placement. The different path lengths to each pickup antenna determine the phase. These can also be compensated with phase shifters on the radiating elements to enable beam scanning.

- iv. A hybrid feeder incorporates a combination of series and corporate designs. Hybrid feeds are more used for 'n x m' array antennas.

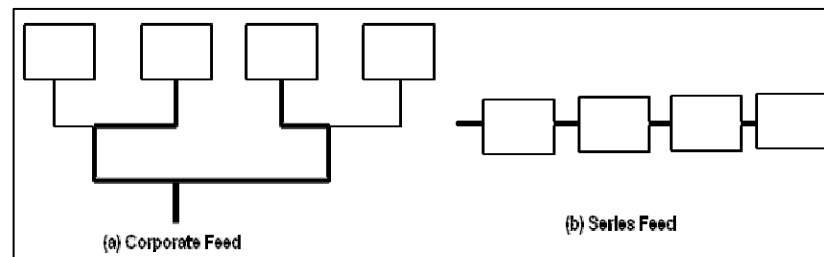


Figure3. 1Types of feed networks [ 1]

In this study, corporate feed network is used to construct a beam scanning linear phase array antenna. The feed network is designed to combine the Wilkinson power divider with the microstrip-line ferrite phase shifter, to achieve the tunable progressive phase shift required for the beam steering purposes. A general block diagram of the array antenna is shown in Figure 3.2, where the power divider and the phase shifter network are implemented on the same microstrip substrate. The design parameters of the related Wilkinson power divider and the ferrite phase shifters are calculated in the following section.

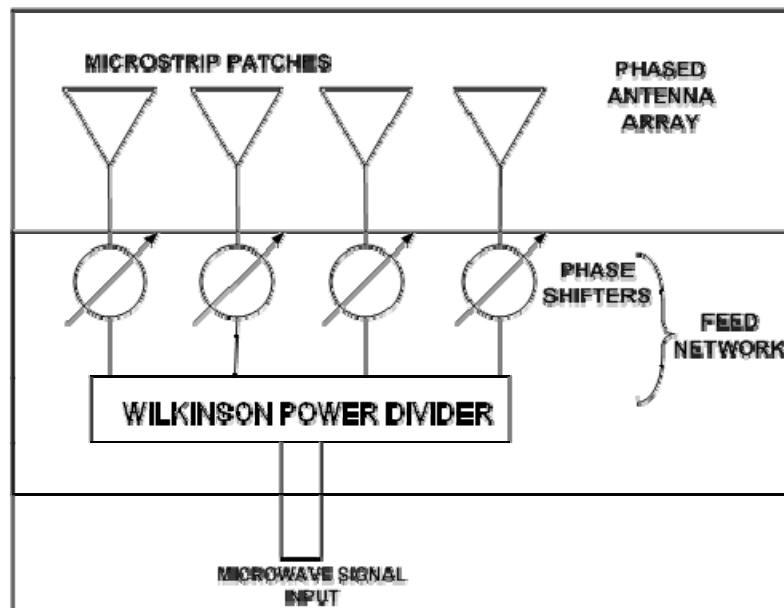


Figure3. 2 Block diagram of general power divider phase shifter combined network feeding the antenna array

### 3.2 DESIGN OF THE ARRAY FEEDER

In power division, an input signal is divided in to two (or more) signals of equal (or different) amplitudes and phases. The simplest type of power divider is a Y-junction with one input and two outputs and is discussed in Chapter 2.5. In this section, a corporate array feed using a Y-junction Wilkinson power divider is designed and optimized to improve the impedance bandwidth.

In microstrip power dividers, discontinuities caused by an abrupt change in the microstrip geometry play an important role. The

discontinuities, such as open ends and sharp bends of microstrip lines, alters the electric and magnetic field distributions and affects the capacitive and inductive behavior of the device. And so, the capacitive, inductive and frequency dependent characteristic of the discontinuities, modeled by Stouten [43], Gopinath [44] and Menzel [45] respectively, needs to be included in the design process of the array feeder network.

Another important aspect of the design process is to introduce proper impedance matching to ensure maximum power transfer. Typically, quarter wave ( $\lambda/4$ ) transformers, shown in Figure 3.3 are employed for this purpose.

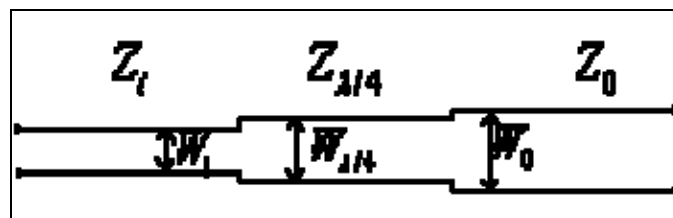


Figure3. 3 Quarter wave transformer

Using this method, smooth transition of power can be achieved between two transmission lines with different impedances [6]. But since the matching section is quarter wave long only for the design frequency,  $\lambda/4$  transformers are associated with low impedance bandwidth. The equation to

determine the impedance of a quarter wave transformer is given in the following expression:

$$Z_{\lambda/4} = \sqrt{Z_0 Z_i} \quad (3.1)$$

The equivalent circuit for a quarter wave transformer and the associated expressions of the series inductance and parallel capacitance are given below:

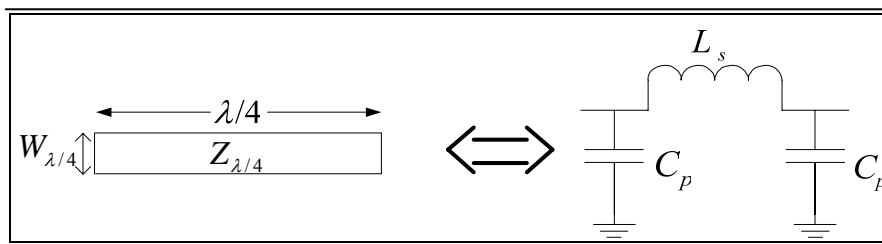


Figure3. 4 Equivalent circuit of quarter wave transformer

The element values are given by the following equations,

$$L_s = \frac{Z_0}{2 * \pi * f_0} \quad (3.2)$$

$$C_p = \frac{1}{2 * \pi * f_0 * Z_0} \quad (3.3)$$

Where  $Z_0$  is the characteristic impedance of the  $\lambda/4$  transformer and  $f_0$  is the frequency of operation.

### **3.2.1. WILKINSON POWER DIVIDER**

Wilkinson power divider can be used for both equal and unequal power division. The basic theory and operating principle associated with Wilkinson power divider is presented in previous chapter (section 2.5). The main advantages of Wilkinson power divider is its ability to isolate the output ports and minimize the mutual affect due to mismatched terminations. But this power divider also has some limitations. The design process of the microstrip array feeder, using Wilkinson power divider, is presented in this chapter. The limitations associated with this class of divider network and methods proposed to overcome them are also discussed.

A typical Wilkinson power divider is shown if Figure3. 5 . If the ports are assumed to be connected with  $50\Omega$  source (port 1) and loads (ports 2 & 3), the design process explained in section 2.5 requires  $Z_1 = 50\Omega$ ,  $Z_2 = 70.7\Omega$  and  $R=100\Omega$ . To implement the designed power divider using microstrip technology, a suitable substrate material is selected that can be easily integrated with the microstrip ferrite phase shifters

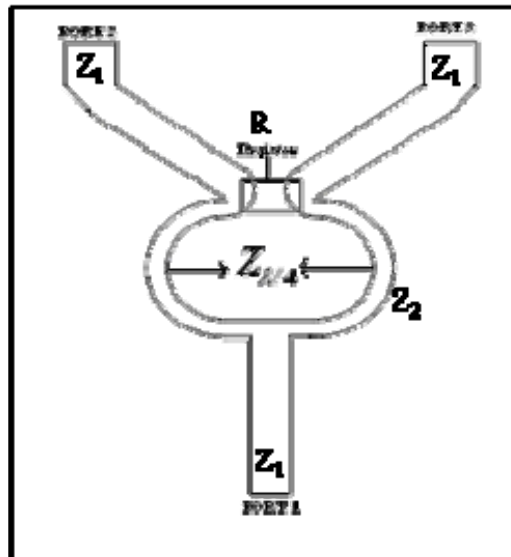


Figure3. 5 Typical Microstrip Wilkinson power divider

Since the ferrite material selected for the phase shifter has a dielectric constant of  $\epsilon_{r,ferrite}=14$  (see section 3.3), the similar dielectric with  $\epsilon_r=14$  is used for this circuit. The characteristic impedances related the microstrip lines required for this design process are then calculated using the following formulas [6]:

$$\frac{w}{h} = \left[ \frac{e^H}{8} - \frac{1}{4e^H} \right]^{-1} \quad (3.4)$$

$$\text{where, } H = \frac{Z_0 \sqrt{2(\epsilon_{reff} + 1)}}{119.9} + \frac{(\epsilon_{reff} - 1)}{2(\epsilon_{reff} + 1)} \left[ \ln \frac{\pi}{2} + \frac{1}{\epsilon_{reff}} \ln \frac{4}{\pi} \right] \quad (3.5)$$

$$\text{And } \epsilon_{\text{reff}} = \frac{\epsilon_r}{0.96 + \epsilon_r (0.109 - 0.004\epsilon_r) [\log(10 + Z_0) - 1]} \quad (3.6)$$

Note that instead of the substrate dielectric constant ( $\epsilon_r$ ) the effective value of the dielectric constant ( $\epsilon_{\text{reff}}$ ) is used. The calculated values of the widths, tabulated below, are used for the initial design of the Wilkinson power divider.

Table3. 1 Microstripline widths as calculated for corresponding impedances

	<b>Impedance</b>	<b>Magnitude</b>	<b>Width in mm</b>
1	$Z_1$	$50\Omega$	0.7
2	$Z_2 (Z_{\lambda/4})$	$70.7\Omega$	0.33

### **3.2.2. MODIFIED WILKINSON POWER DIVIDER:**

The major limitations observed in above design are: (a) strong coupling between the  $\lambda/4$  transformers and the output arms of the divider, (b) the optimum placement of the isolating resistor, (c) the difficulty of implementing  $\lambda/4$  transformers for higher frequency structures and (d) low impedance bandwidth.

In order to improve the first three limitations, a novel power divider proposed by Antsos, Crist and Sukamto [38] as shown in Figure3. 6, where a

$3\lambda/4$  transformer is used instead of the  $\lambda/4$  transformer with an additional  $100\Omega$  line of  $\lambda/2$  length, used to connect to the  $100\Omega$  resistor. Although the proposed design theoretically yielded good result, but when combined with the phase shift section, it failed to give acceptable simulation response.

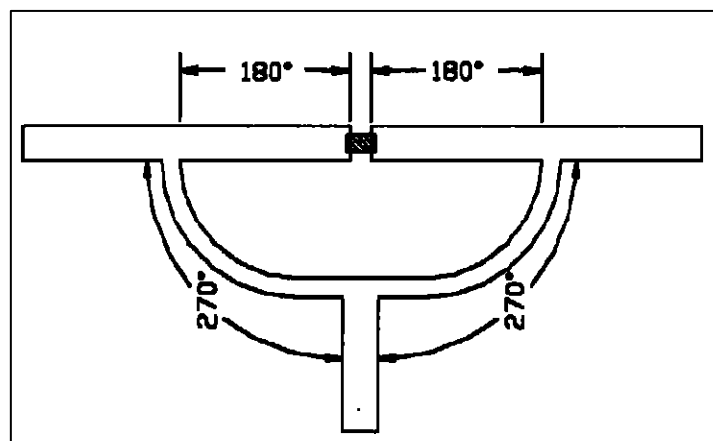


Figure3. 6 Microstrip Wilkinson power divider of Antsos, Crist and Sukamto [38]

The impedance bandwidth limitation of the Wilkinson power divider is improved by replacing the  $\lambda/4$  transformer with multi-section quarter wave transformers ( $n\lambda/4$ ). A Wilkinson power divider with three sections of quarter wave transformer is shown in Figure3. 7.

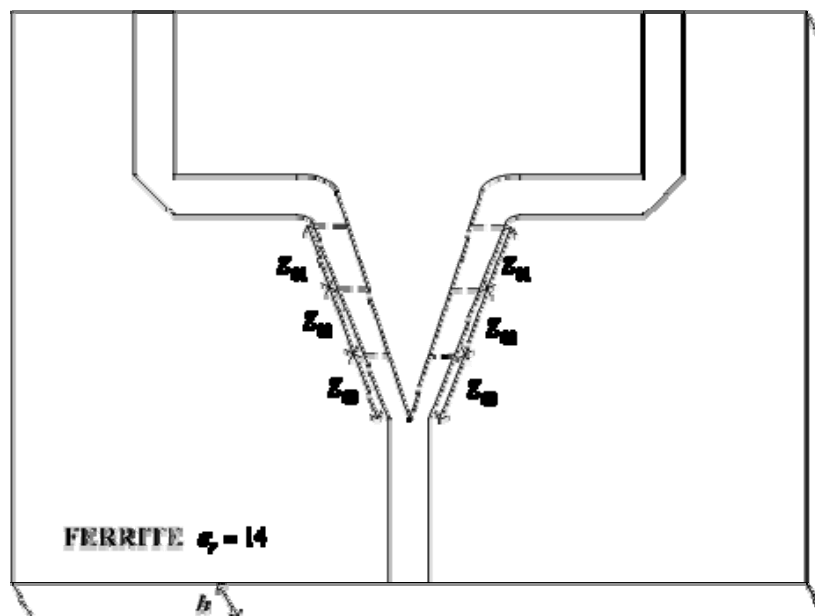


Figure3. 7 Two port power divider with multisection quarter wave transformer

This realization of the multisection quarter wave transformer can be done based on a couple of techniques. The most popular and widely used techniques are the Butterworth (or Binomial) method and the Tchebyscheff method. In the binomial method a resistive load  $R_L$  can be matched to an input line of characteristic impedance  $Z_0$  by using the following formula,

$$Z_{0k} = Z_0 \left( \frac{R_L}{Z_0} \right)^{M_k / 2^n} \quad k = 1, 2, \dots, n \quad (3.7)$$

And 
$$M_k = C_1 + C_2 + \dots + C_k \quad k = 1, 2, \dots, n \quad (3.8)$$

Where  $C_1, C_2, \dots, C_n$  are binomial coefficients given by

$$C_k = \frac{n!}{(n-k+1)!(k-1)!} \quad k = 1, 2, \dots, n \quad (3.9)$$

The Tchebyscheff transformers on the other hand utilize the theory of Tchebyscheff polynomials in order to calculate the individual impedances of the transformer sections. Based on the approximate analysis a relationship can be derived between bandwidth and maximum-in-band reflection coefficient  $|\Gamma|_m$ ,

$$|\Gamma|_m T_n \left( \frac{1}{\cos \phi_0} \right) = \left| \frac{R_L - Z_0}{R_L + Z_0} \right| \quad (3.10)$$

Where  $T_n$  is the Tchebyscheff polynomial given by

$$T_n(x) = 2xT_{n-1} - T_{n-2} \quad (3.11)$$

And  $\phi_0 (= \beta l)$  is the angle in radians for which the response of SWR remains maximally flat. Following this analysis a three section quarter wave transformer was designed as shown above. With impedances of individual quarter wave transformers being  $Z_{01}=54.25\Omega$ ,  $Z_{02}=70.71\Omega$ ,  $Z_{03}=91.7\Omega$  and their corresponding widths being  $W_{Z01}=0.74\text{mm}$ ,  $W_{Z02}=0.33\text{mm}$ ,  $W_{Z03}=0.12\text{mm}$  respectively. But all the quarter-wave transformers require

abrupt changes in characteristic impedance, resulting in discontinuity in transverse dimension, producing reactive effects. To compensate for this, the lengths of the transformers can be reduced slightly or tapered as required. Although this class of power divider illustrated good transmission and reflection characteristics, it cannot be adopted in the work due to the limitation of available ferrite dimensions. Using this approach when a four way power divider is designed, the physical height of the total power divider crossed the available width of the ferrite substrate. Thus, the conventional Wilkinson power divider with minor modification is designed and optimized in this study. The design process is discussed in the next section.

### **3.2.3 DESIGNED POWER DIVIDER FEED NETWORK**

The design of the power divider network is often restricted by the limitations imposed by the dimensions of the radiating patches. In our study, the patch elements were designed on a microstrip substrate (called Duroid) with dielectric constant,  $\epsilon_{r,duroid} = 2.2$ . Due to the large patch widths (to resonate in designed frequency) and the required patch separation 'd' (to avoid mutual coupling), the output arms of the two way power divider needed to be elongated without modifying the amplitude or phase behavior. In this design, the elongation process is exploited to achieve dual purpose; (a) to accommodating the patches and (b) to enable the integration of phase

shifter. Also to allow the integration of the phase shifter, a substrate similar to ferrite with dielectric constant of 14 is selected to design the power divider. The calculated dimensions for radiating patches and design process of the phase shifter are presented in the sections 4.2 of chapter 4, respectively.

Initially much effort is consumed for implementing a proper design for the power divider, which sustained all of the design criteria and overcome the limitations. In the designed two way power divider, shown in figure 3.8, the output arm lengths are selected to maintain the required differential phase difference  $360^\circ$  (in other words, almost same phase in each arm).

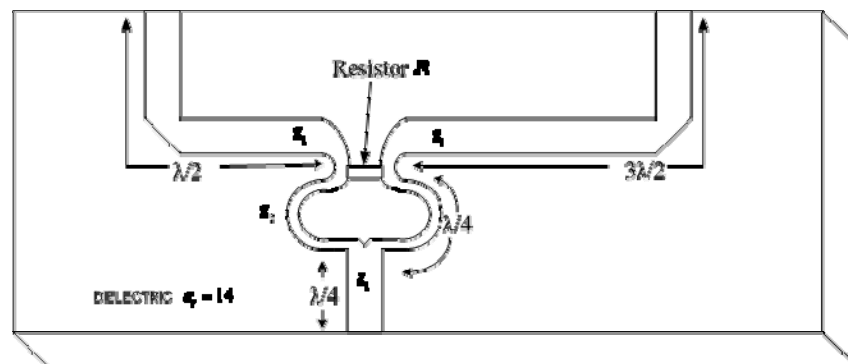


Figure3. 8 Design of Wilkinson two way power divider on dielectric

To avoid the anticipated mutual coupling and the reactive affects introduced by the sharp discontinues, optimum bends associated with the output arms of the microstrip is implemented. For  $Z_1 = 50\Omega$ ,  $Z_2 = 70.7\Omega$  and

$R=100\Omega$ , the amplitude and phases response of the above power divider is observed to be very similar for both the output signals. The output isolations are also observed to be acceptable, as expected in Wilkinson power dividers.

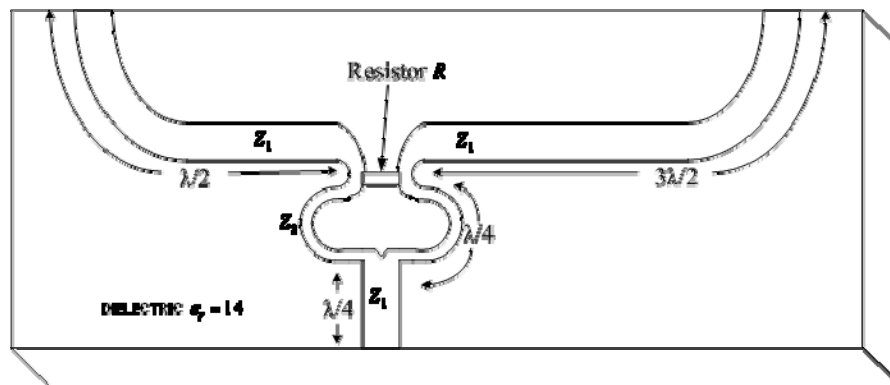


Figure3. 9 Design of modified Wilkinson two way power divider

To improve the response and reduce the dimension of the divider, the compensated bends and curves (that connects isolation resistance  $R$ ) are replaced with maximum affordable curvaceous and circular bends as shown in the above Figure3. 9. This modification also introduced the space required to optimize the position of isolation resistance ( $R$ ). Although the proper placement of ' $R$ ' has no affect on the impedance bandwidth, but it influenced the isolation characteristics of the divider, such as the S- parameter values of  $S_{23}$  and  $S_{32}$ . As this study involves the design of a four element linear array antenna, two more output ports are introduced by cascading the designed two

way power divider. To accommodate four patch elements, an additional length of  $\lambda$  is added to the feeder arms of the bottom power divider.

The individual response of the two power dividers are presented below. For the purpose of simulations a dielectric with permittivity of 14 is selected. This is because while integrating the phase shifter, this choice will aid the design process (as will be shown in later section)

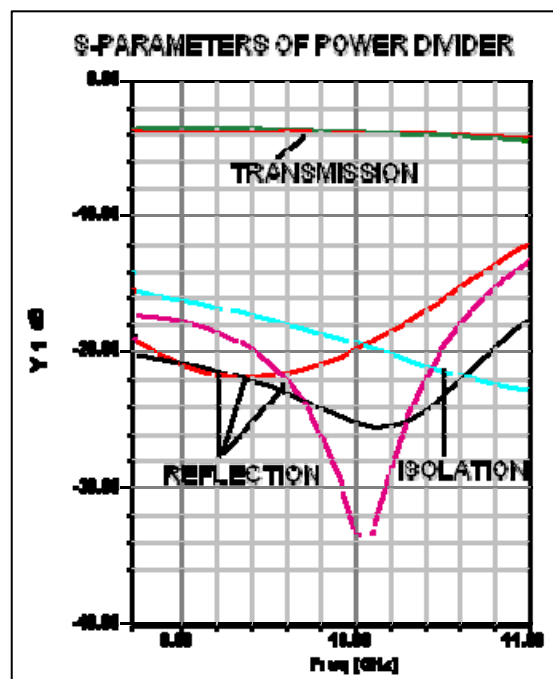


Figure3. 10 S-parameters of two-way Wilkinson power divider (top segment)

The simulated response of the top power divider is presented in Figure3. 10. It is evident from the figure that at or around the design frequency of 10 GHz, the reflection parameters ( $S_{11}$ ,  $S_{22}$  and  $S_{33}$ ) are below -

20dB and the isolation parameters ( $S_{32}$  and  $S_{23}$ ) are approximately around -18dB. The transmission parameters ( $S_{21}$  and  $S_{31}$ ) are also observed around -3dB line, as targeted by the designed process. The bottom power divider, which is implemented by adding additional lengths to the feed lines in order to accommodate four patches, demonstrated a similar transmission, reflection and isolation response. The figure below (Figure3. 11) shows the simulated S-parameters around at and around the design frequency of 10 GHz. of bottom power divider

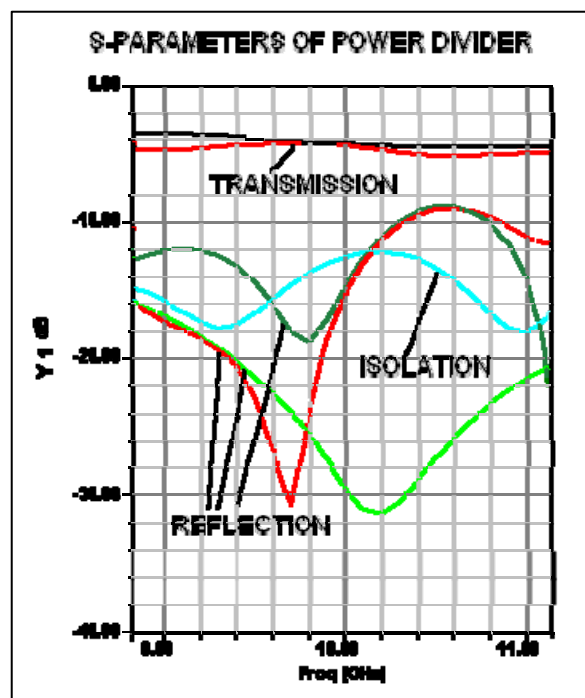


Figure3. 11 S-parameters of two-way Wilkinson power divider (bottom segment)

It is of note that the performance in the bottom divider is more acceptable at 9.8 GHz rather than 10 GHz. This design could have been optimized to improve the 10 GHz response, but since this response will be affected by the cascading of top and bottom divider sections to form the final array feeder, the optimization on the 4 way array feeder is planned to implement directly. The final design of the cascaded four way power dividers that form the array feeder is shown in Figure3. 12

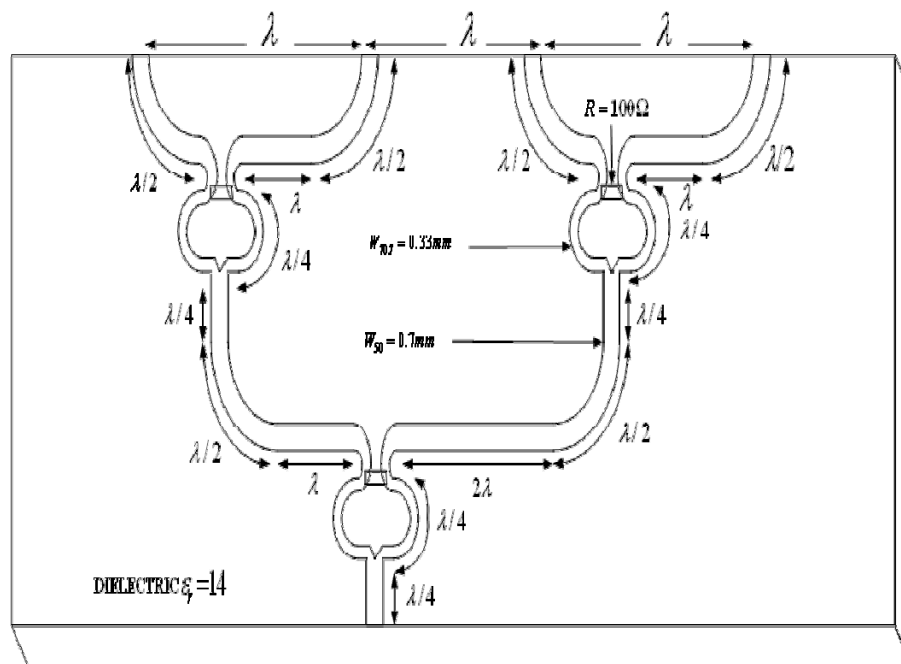


Figure3. 12 Modified Wilkinson four-way power divider network on dielectric

The related simulated S-parameters response is shown in Figure3. 13  
Note the transmission and reflection S-parameters demonstrate are very close

to the required responses as per design parameters mentioned in the objectives in Chapter 1. It will be shown that when this designed power divider is integrated with phase shifter (discussed in section 3.3); the response (in chapter 4) will be more close to the expected values.

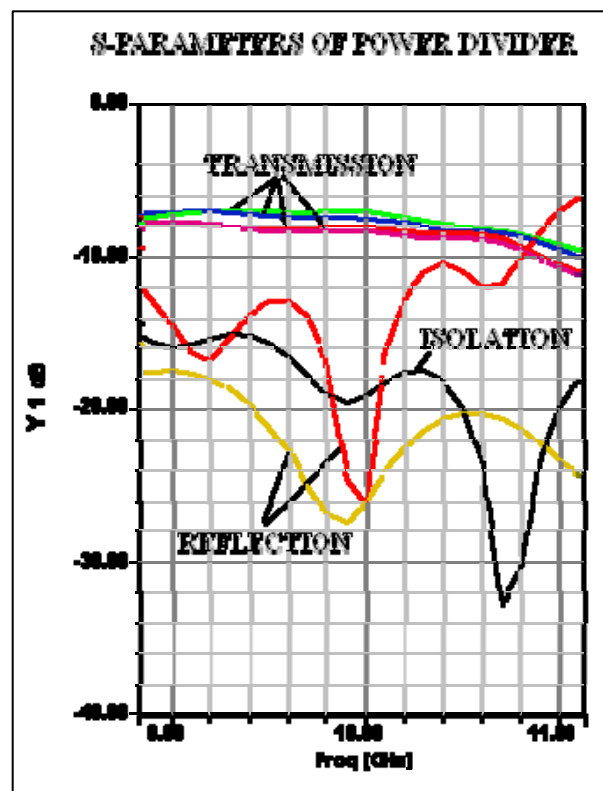


Figure3. 13 S-parameter response of four-way power divider on dielectric similar to ferrite

### 3.3. DESIGN OF PHASE SHIFTER USING FERRITE

Ferrite devices are widely used in communication systems to control and route microwave signals. In the present research, ferrite phase shifters are implemented using microstrip lines used by the array feeder. This is achieved by replacing the substrate of the microstrip feeder network with ferrite material. The high dielectric constant ( $\epsilon_r=14$ ) of the ferrite substrate helped in reducing the antenna dimensions. Also, in the presence external DC magnetic field, ferrite substrate exhibited a number of novel properties [46] like; tunable insertion phase, frequency agility and, generation of circular polarized wave etc. Thus, for the microstrip-lines printed on a ferrite substrate, a significant change in differential phase is achieved by changing the normally applied biasing magnetic field. In this study, an externally biased microstrip ferrite phase shifter is designed and integrated with the power divider section of the array antenna for beam scanning purpose. The variable length of the power divider output arms are utilized to introduce an initially slanted main beam. The beam is then steered by changing the external biasing magnetic fields.

If the ferrite substrate is biased by a static magnetic field, perpendicular to the direction of propagation and the ground plane, the tensor permeability of the given media is expressed as [42],

$$\mu_r = \begin{pmatrix} \mu & 0 & -j\kappa \\ 0 & 1 & 0 \\ -j\kappa & 0 & \mu \end{pmatrix} \quad (3.12)$$

Where the definition  $\mu_r$  is already been given in section 2.6 of previous Chapter 2. The frequency and biasing field dependence of the gyrotropic ferrite media is shown in Figure 3.14. The definition of effective permeability of ferrite material is already given in equation 2.15.

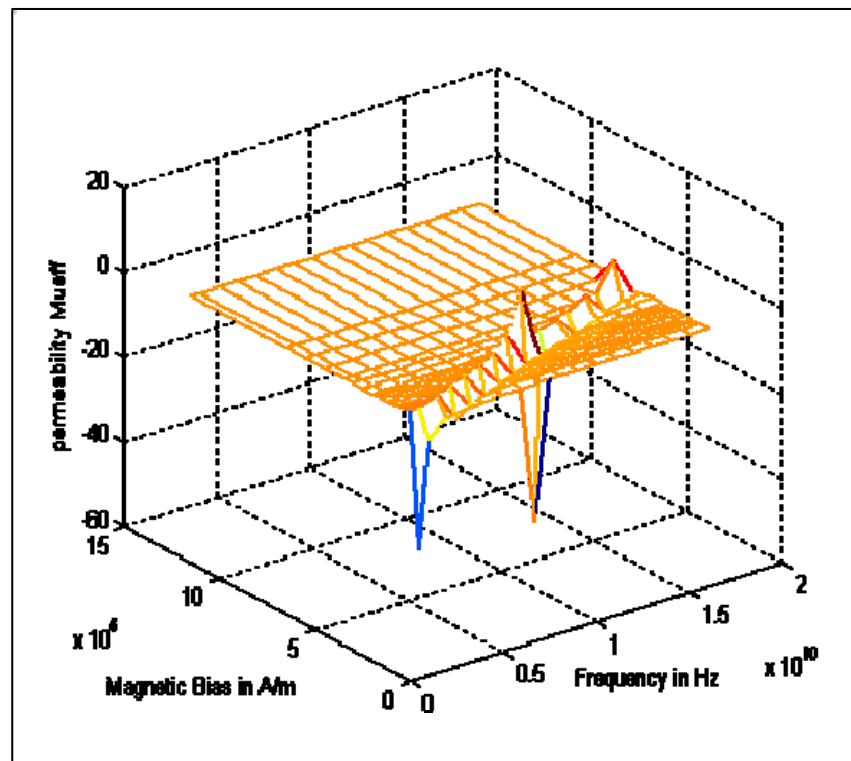


Figure3. 14 Behavior of effective permeability of ferrite media with magnetic bias and frequency

Note that dip in  $\mu_{eff}$  values represent lossy resonance region. While designing the phase shifter, this region of biasing is carefully avoided, as at resonance most of the power from the microwave signal is absorbed by the ferrite material. Brown et al [41] have used stripline on ferrite substrate to feed and steer the main beam of the antenna. Using FEM method, they calculated the effective phase constant ( $\beta_{eff}$ ) over the range for different bias

points. Assuming an infinite ferrite substrate, the expression of  $\beta_{eff}$  used in their paper was,

$$\beta_{eff} = \frac{2\pi}{\lambda_g} \quad (3.13)$$

This general expression approximated the phase response of the planar ferrite phase shifter with limited accuracy. The response can be improved by including boundary limitations into the derivation process. In this study, we will use parallel plate approximation with proper boundary conditions to calculate the insertion phase properties of the biased microstrip-line ferrite phase shifter.

### **CALCULATED PHASE RESPONSE:**

Electromagnetic wave propagation in a Parallel plate waveguide has long been used to study anisotropic microstrip structures [33, 34]. An externally magnetized ferrite filled parallel plate waveguide is shown in Figure 3.15. The characteristic equation related to the microwave signal propagation within this parallel plate structure is derived below.

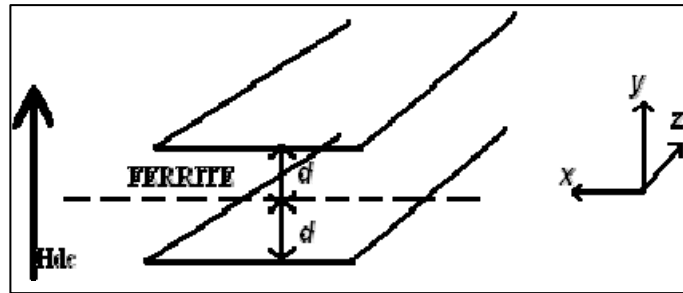


Figure3. 15 Parallel plate ferrite structure used for derivation of characteristic equation

Maxwell's curl equation, obtained from Faradays law of electromagnetic induction that states that the electromagnetic magnetic force in a closed circuit (curl of the electric field) is proportional to the rate of change of the magnetic flux threading the circuit, is expressed as,

$$\nabla \times E = -\frac{\partial B}{\partial t} \quad \text{or,} \quad \nabla \times E = -j\omega\mu_0\mu_r H \quad (3.14)$$

For a transversely (y-axis) magnetized ferrite media, substituting the tensor permeability ( $\mu_r$ ) from equation (3.12) gives,

$$\nabla \times E = -j\omega\mu_0 \begin{pmatrix} \mu & 0 & -j\kappa \\ 0 & 1 & 0 \\ -j\kappa & 0 & \mu \end{pmatrix} H \quad (3.15)$$

Since for the given structure, the EM wave propagates in  $-z$  direction,

substituting  $\frac{\partial Z}{\partial t} = -\gamma$  in above expression yields,

$$\frac{\partial E_z}{\partial y} + \gamma E_y = -j\omega\mu_0 [\mu H_x - j\kappa H_y] \quad (3.16)$$

$$\frac{\partial E_z}{\partial x} + \gamma E_x = -j\omega\mu_0 H_y \quad (3.17)$$

$$\frac{\partial E_y}{\partial x} - \frac{\partial E_x}{\partial y} = -j\omega\mu_0 [j\kappa H_x - \mu H_z] \quad (3.18)$$

Similarly, from the remaining Maxwell's curl equation,  $\nabla \times H = -j\omega\epsilon_0\epsilon_r E$ ,

we get;

$$\frac{\partial H_z}{\partial y} + \gamma H_y = -j\omega\epsilon_0\epsilon_r E_x \quad (3.19)$$

$$\frac{\partial H_z}{\partial x} + \gamma H_x = -j\omega\epsilon_0\epsilon_r E_y \quad (3.20)$$

$$\frac{\partial H_y}{\partial x} - \frac{\partial H_x}{\partial y} = -j\omega\epsilon_0\epsilon_r E_z \quad (3.21)$$

Writing these equations in vector form yields,

$$\begin{pmatrix} \frac{\partial E_z}{\partial x} \\ \frac{\partial E_z}{\partial y} \\ \frac{\partial H_z}{\partial x} \\ \frac{\partial H_z}{\partial y} \\ H_z \end{pmatrix} = \begin{pmatrix} E_x & H_x & E_y & H_y & H_z \\ -\gamma & 0 & 0 & j\omega\mu_0 & 0 \\ 0 & -j\omega\mu_0\mu & -\gamma & 0 & -\omega\mu_0\kappa \\ 0 & -\gamma & -j\omega\epsilon_0\epsilon_r & 0 & 0 \\ j\omega\epsilon_0\epsilon_r & 0 & 0 & -\gamma & 0 \\ 0 & 0 & 0 & 0 & 1 \end{pmatrix} \begin{pmatrix} E_x \\ H_x \\ E_y \\ H_y \\ H_z \end{pmatrix}$$

Using matrix manipulation, we can express above equation as,

$$\left. \begin{aligned} E_x &= \frac{-\gamma}{\gamma^2 + K_0^2 \epsilon_r} \left( \frac{\partial E_z}{\partial x} \right) - \frac{j\mu_0 \omega}{\gamma^2 + K_0^2 \epsilon_r} \left( \frac{\partial H_z}{\partial y} \right) \\ H_x &= \frac{-j\omega \epsilon_0 \epsilon_r}{\gamma^2 + K_0^2 \mu \epsilon_r} \left( \frac{\partial E_z}{\partial y} \right) - \frac{\gamma}{\gamma^2 + K_0^2 \mu \epsilon_r} \left( \frac{\partial H_z}{\partial x} \right) + \frac{j\kappa_0^2 \epsilon_r \kappa}{\gamma^2 + K_0^2 \mu \epsilon_r} (H_z) \\ E_y &= \frac{-\gamma}{\gamma^2 + K_0^2 \mu \epsilon_r} \left( \frac{\partial E_z}{\partial y} \right) + \frac{j\omega \mu_0 \mu}{\gamma^2 + K_0^2 \mu \epsilon_r} \left( \frac{\partial H_z}{\partial x} \right) - \frac{\omega \mu_0 \kappa \gamma}{\gamma^2 + K_0^2 \mu \epsilon_r} (H_z) \\ H_y &= \frac{-j\omega \epsilon_0 \epsilon_r}{\gamma^2 + K_0^2 \epsilon_r} \left( \frac{\partial E_z}{\partial x} \right) - \frac{\gamma}{\gamma^2 + K_0^2 \epsilon_r} \left( \frac{\partial H_z}{\partial y} \right) \\ H_z &= H_z \end{aligned} \right\} \quad (3.22)$$

$$\text{Where } K_0^2 = \omega^2 \epsilon_0 \mu_0 \quad (3.23)$$

Now considering the ferrite media as perfectly insulator with no stored charges, Maxwell's divergent equation can written as,

$$\nabla \cdot D = 0 \quad (3.24)$$

Substituting the material property,  $D = \mu_0 [\mu_r] H$  and  $\frac{\partial}{\partial Z} = -\gamma$  into the

expanded form of above equation yields,

$$\mu_0 \mu_r \frac{\partial H_x}{\partial x} - j\kappa \mu_0 \frac{\partial H_y}{\partial x} + \mu_0 \frac{\partial H_y}{\partial y} - j\kappa \gamma \mu_0 H_x - \gamma \mu_0 \mu_r H_z = 0 \quad (3.25)$$

Now assuming the parallel plate structure under consideration (shown in Figure3. 15) is a symmetrical structure extended infinitely along  $\pm x$ -axis, the field variation in x-axis can be neglected. Thus,

$$\frac{\partial}{\partial x} = 0$$

For quasi TE mode operation ( $E_z = 0$ ), substituting these conditions into equation 3.22, allows us to obtain modified expression for the field components of  $H_x$  and  $H_y$ . Now substituting the conditions and the modified expression of  $H_x$  and  $H_y$  in the equation 3.25 yields,

$$\frac{\gamma}{\gamma^2 + K_0^2 \epsilon_r} \cdot \frac{\partial^2 H_z}{\partial y^2} + \left\{ \frac{K_0^2 \epsilon_r \kappa^2 \gamma}{\gamma^2 + K_0^2 \mu \epsilon_r} - \mu \gamma \right\} H_z = 0 \quad (3.26)$$

The above equation can also be written as

$$\frac{\partial^2 H_z}{\partial y^2} + \left\{ \frac{\gamma^2 + K_0^2 \epsilon_r}{\gamma} * \left( \frac{K_0^2 \epsilon_r \kappa^2 \gamma}{\gamma^2 + K_0^2 \mu \epsilon_r} - \mu \gamma \right) \right\} H_z = 0 \quad (3.27)$$

Since for a general wave equation is expression as,

$$\frac{\delta^2 H_z}{\partial y^2} + K_e^2 H_z = 0,$$

Comparing this equation with above expression (3.27), we can say that for the parallel plate structure under consideration;

$$K_e^2 = \frac{-\beta^2 + K_0^2 \epsilon_r}{-\beta^2 + K_0^2 \mu \epsilon_r} \left\{ -\beta^2 \mu + K_0^2 \mu \epsilon_r \cdot \mu_{eff} \right\} \quad (3.28)$$

Again from the boundary conditions (see Figure3. 15) of the symmetrical parallel plate structure, it is evident that at  $y=\pm d$ , the parallel electric field component becomes zero ( $E_x=0$ ).

Now for a general expression,

$$E_x = C \cos(K_e y),$$

This condition is only valid for

$$K_e = (2m+1) \frac{\pi}{d}; \text{ With } m = 0, 1, 2, \dots$$

Now equating the two expression of the wave number,  $K_e$ , yields the characteristic equation related to the transversely biased (y-axis) ferrite filled parallel plate structures and is given by;

$$\frac{-\beta^2 + K_0^2 \epsilon_r}{-\beta^2 + K_0^2 \mu \epsilon_r} \left\{ -\beta^2 \mu + K_0^2 \mu \epsilon_r \cdot \mu_{eff} \right\} = \left\{ (2m+1) \frac{\pi}{d} \right\}^2 \quad (3. 29)$$

Solving this characteristic equation, we can calculate the insertion phase properties of the ferrite substrate and how they are affected by external biasing field ( $H_{dc}$ ). The variation of insertion phase ( $\beta$ ) per unit length as a function of the magnetic bias  $H_{dc}$ , is plotted in Figure3. 16. Note that abrupt change in insertion phase occurs as the ferrite nears the resonance regions (cut-off region).

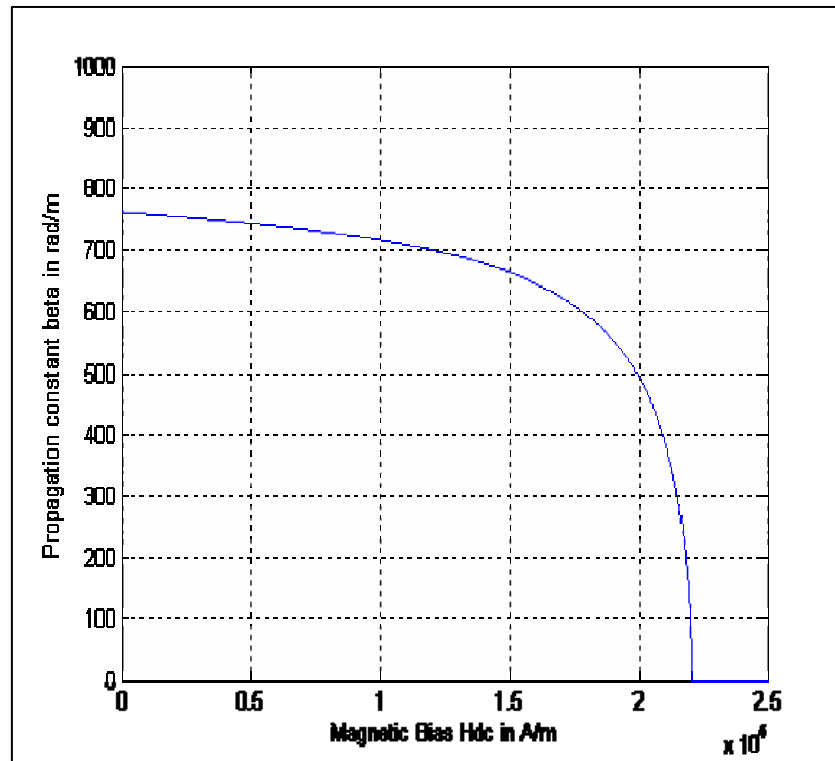


Figure3. 16 Theoretical plot of variation of propagation constant  $\beta$  with magnetic bias  $H_{dc}$

### **SIMULATED PHASE RESPONSE:**

The integrated power-divider/phase-shifter, designed in this study, is achieved by replacing the dielectric substrate of the four-way power divider with ferrite material. This can be easily achieved by replacing the dielectric substrate with an equivalent ferrite substrate of same height and permittivity. Keeping this theory, for designing the power divider in section 3.2.2, the dielectric substrate is selected to be equivalent to that ferrite (except the magnetic properties of ferrite). Thus due to the same dimensions ( $h=1.2\text{mm}$ )

and permittivity ( $\epsilon_{\text{dielectric}} = \epsilon_{\text{ferrite}} = 14$ ), the designed microstrip power divider can also be made to work as a phase shifter by introducing magnetized ferrite substrate. Because the permittivity of ferrite and dielectric used was similar, the structure remains the same as far as dimensions are concerned; only the intrinsic material properties change when ferrite is introduced. The next Chapter 4 talks about the integrated power divider/phase shifter and implemented by explaining the design process and also discusses the response of this feeder network.

Although, during the design of the power divider, the realization of variable output feed arm lengths was for the accommodation of the large patches. This realization also served the purpose of achieving a tunable-progressive-phase-shift and an initially-inclined-beam. The progressive phase shift achieved by utilizing unequal lengths between arms is  $360^{\circ}$  (in other words the phase of the electromagnetic wave coming out of individual arms was almost the same). Note that the external biasing field is realized by using powerful and miniaturized fixed magnets and the biasing techniques used in the experimental process is discussed in detail in chapter 5.

High Frequency Structural Simulator (Ansoft HFSS v9.0), a well known software for simulating microwave passive devices, is selected to simulate insertion phase response of the phase-shifter. Figure 3.17 shows the

final optimized design of the magnetized ferrite based integrated power-divider/phase-shifter geometry.

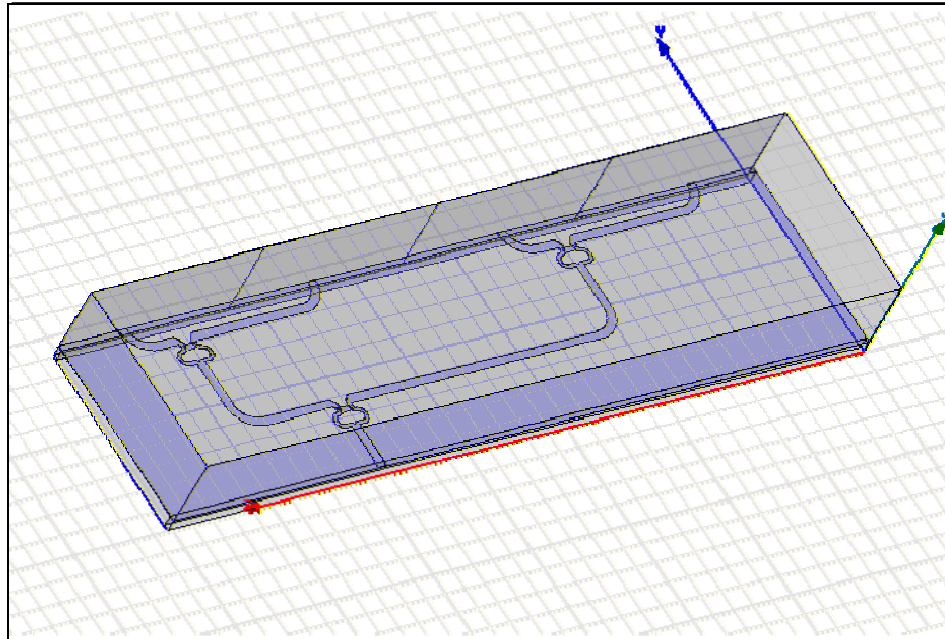


Figure3. 17 Four way power divider on ferrite substrate

Figure3. 18, compares the simulated phase response with the theoretically calculated phase response of the phase shifter. Though the characteristics of both the theoretical and simulated curves are very similar, but they slightly differ in magnitude as the theoretical calculation ignored the losses and full boundary conditions associated with ferrite microstrip structure.

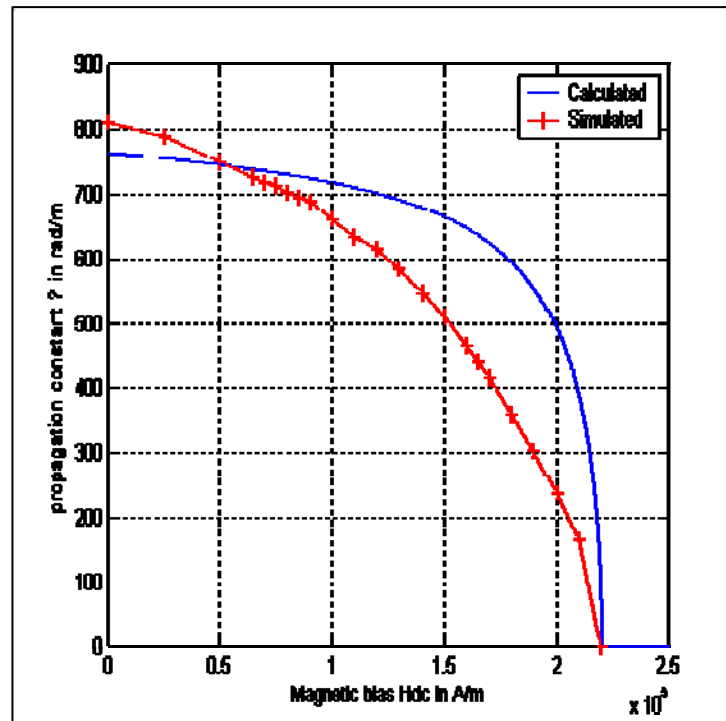


Figure3. 18 Variation of propagation constant  $\beta$  ( $\beta$ ) with magnetic bias for ferrite media

## **CHAPTER 4**

# **DESIGN OF MICROSTRIP LINEAR PHASED ARRAY ANTENNA**

### **4.1 INTRODUCTION**

Phased array antennas have broad applicability for both commercial and military applications, including military radars, cellular base stations, satellite communications and automotive anti-collision radars. Electronically scanned phased array antennas introduces many benefits, including fast scanning, wider operating bandwidth, the ability to host multiple antenna beams on the same array and eliminating mechanical complexity and reliability issues. The electronically scanning property of a phased array antenna is often achieved by ‘forced excitation’, where elements are excited with signals of constant amplitude but progressive phase, required for steering the antenna beam in desired direction. In this chapter, the essential design characteristics for this class of microstrip linear phase array antenna are calculated, and the design is simulated and optimized to achieve the required radiation pattern.

## 4.2 DESIGN CONSIDERATIONS

In a linear phased array antenna, the radiated beam is often manipulated using several controlling factors to achieve the desired radiation characteristics. These controlling factors include; selection of radiating microstrip elements and its array configuration, displacement between the elements, and excitation phase and amplitude of each element. In this section, the calculation processes associated with these design parameters are presented.

### 4.2.1 DIMENSIONS OF RADIATING ELEMENTS

In this study, four rectangular microstrip radiating elements are used to design the linear phased array antenna. A rectangular microstrip radiating patch shown in Figure 4.1 can be considered as an open-ended transmission line of length  $L$  and width  $W$ . Due to finite length of this antenna, electromagnetic fields at the edge of the patch undergo fringing. Thus, to account for the fields present in the air (fringing) and in the substrate, effective dielectric constant ( $\epsilon_{\text{eff}}$ ) is introduced.

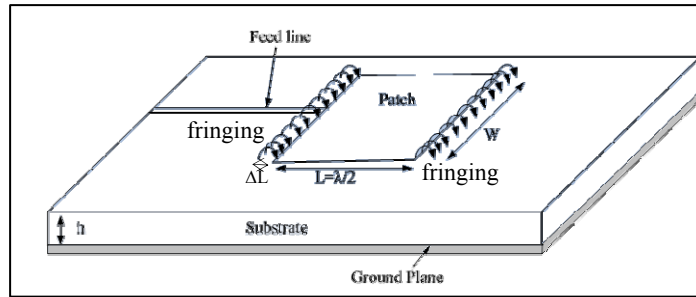


Figure4. 1 Radiation mechanism associated with microstrip patch [1]

At low frequencies,  $\epsilon_{eff}$  remains constant and can be expressed in terms of patch dimensions and substrate dielectric constant ( $\epsilon_r$ );

$$\epsilon_{re\text{ff}} = \frac{\epsilon_r + 1}{2} + \frac{\epsilon_r - 1}{2} \left[ 1 + 12 \frac{h}{W} \right]^{-1/2} \quad (4.1)$$

Also, due to the fringing effect, the electrical length of the patch increases by a distance of  $2\Delta L$ , as illustrated in Figure4. 1. In transmission line model,  $\Delta L$  is expressed as [1],

$$\Delta L = h * 0.412 \frac{(\epsilon_{re\text{ff}} + 0.3) \left( \frac{W}{h} + 0.264 \right)}{(\epsilon_{re\text{ff}} - 0.258) \left( \frac{W}{h} + 0.8 \right)} \quad (4.2)$$

and is used to compute the actual length ( $L$ ) of the patch;

$$L = \frac{1}{2f_r \sqrt{\epsilon_{re\text{ff}}} \sqrt{\mu_0 \epsilon_0}} - 2\Delta L \quad (4.3)$$

resonating at a frequency represented by ' $f_r$ '. Now, for a practical resonator, the patch width that leads to good radiation efficiencies is given by [1],

$$W = \frac{1}{2f_r \sqrt{\mu_0 \epsilon_0}} \sqrt{\frac{2}{\epsilon_r + 1}} = \frac{v_0}{2f_r} \sqrt{\frac{2}{\epsilon_r + 1}} \quad (4.4)$$

where,  $v_0$  is the free space velocity of light. Input impedance of a patch antenna is another important characteristic that plays an important role during excitation of the radiation element. For a rectangular patch, typical input impedances at the edge of a patch range from  $100\Omega$  to  $400\Omega$ , and can be approximated as follows [1],

$$R_{in} = 90 \frac{\epsilon_r^2}{\epsilon_r - 1} \left( \frac{L}{W} \right)^2 \Omega \quad (4.5)$$

Now, as operating frequency increases, effective dielectric constant ( $\epsilon_{eff}$ ) increases and eventually approaches the value of substrate dielectric constant ( $\epsilon_r$ ). As the design frequency used in the study is 10 GHz, the equations presented above needs to be modified to accurately model the high frequency response of the radiating patches. The modified equations are given by;

$$\epsilon_{r,eff} = \epsilon_r - \left[ \frac{\epsilon_r - \epsilon_{r,eff}(0)}{1 + \frac{\epsilon_{r,eff}(0)}{\epsilon_r} \left(\frac{f}{f_t}\right)^2} \right] \text{ where } f_t = \frac{Z_c(0)}{2\mu_0 h} \quad (4.6)$$

$$W_{eff}(f) = W + \frac{W_{eff}(0) - W}{1 + \left(\frac{f}{f_t}\right)^2} \quad (4.7)$$

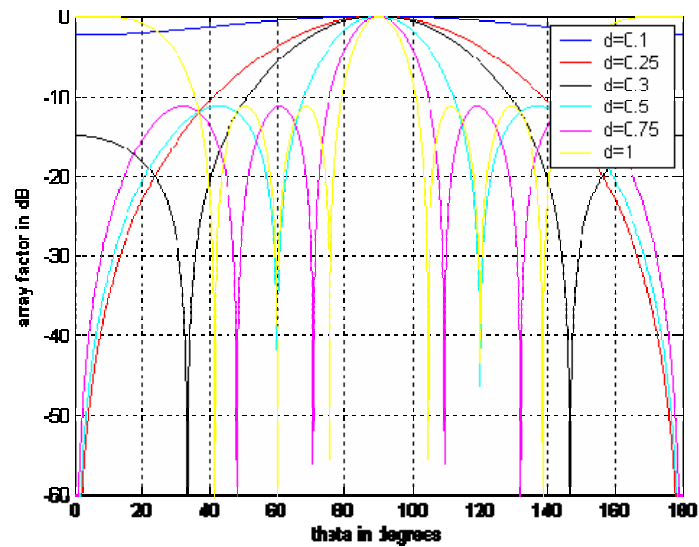
Above expressions are used here to calculate the rectangular patch dimensions required to resonate at and around the design frequencies of 9, 10 and 11 GHz. The related edge input impedance of the radiation element is also calculated and tabulated. It is clear from the calculated values listed in Table4. 1, that the patch characteristics drastically changes with changing resonant frequency.

Table4. 1 Dimension of rectangular microstrip patch calculated

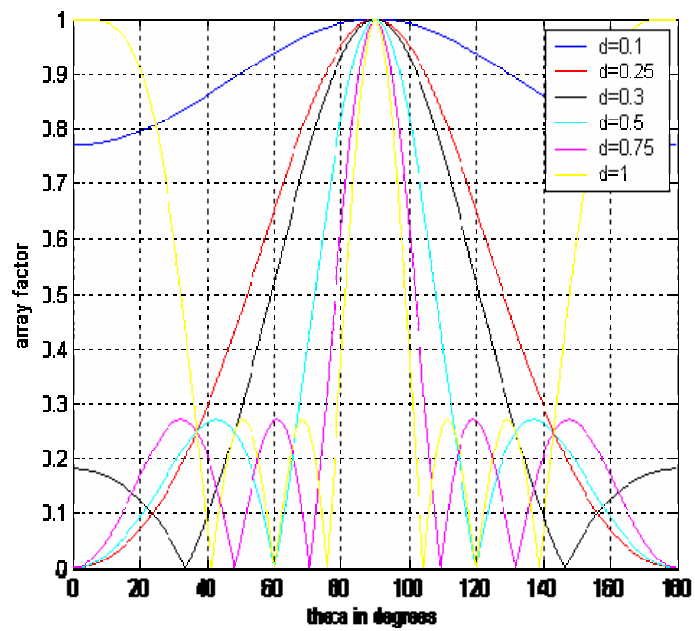
Frequency	$\epsilon_{reff}$	Width of patch (W) mm	Length of Patch (L) mm	Input Impedance ( $R_{in}$ ) $\Omega$
9GHz	2.14	13.2	10.09	212
<b>10GHz</b>	<b>1.94</b>	<b>11.86</b>	<b>9.3</b>	<b>223</b>
11GHz	1.92	10.78	8.80	241

## **4.2.2 RELATIVE DISPLACEMENT OF RADIATING ELEMENTS**

The relative spacing between elements are essential in shaping the radiation pattern of the array antenna. In this section, Matlab is used to obtain the optimum separation distance between elements, to achieve the desired radiation characteristics of the designed array antenna. Figure4. 2 shows radiation pattern with different distance of separation. It is clear from the figure that as the separation distance increases the response of the array becomes narrower and more directive, although sidelobes starts to appear. So selecting a lower separation distance that produces required directive pattern with relatively low sidelobe seems like a better choice. Also, when the separation distance increases to larger fractions of  $\lambda$ , undesired grating lobes start to appear. Since the design specification of the array antenna required minimum sidelobe level with no grating lobes present in the radiation pattern, a patch separation distance of  $0.3\lambda$  is selected for the designed antenna array.



(a)



(b)

Figure 4.2 Radiation pattern of the antenna array for varying distance in terms  $\lambda$  between elements, (a) dB scale, (b) normalized

### 4.2.3 EXCITATION AMPLITUDE AND PHASE OF ELEMENTS

The array factor for any N-element array, given in equation 2.13, is reproduced here,

$$AF = \sum_{n=1}^N a_n e^{j(n-1)\psi} \quad (4.8)$$

where, 
$$\psi = kd \cos \theta + \beta = \frac{2\pi d}{\lambda} \cos \theta + \beta$$

From this equation it is evident that the excitation phase ( $\approx \beta$ ), and the excitation amplitude ( $\approx a_n$ ) are important factors (among others) to influence the radiation characteristics of the designed array antenna. For example, if maximum radiation of the antenna array is to be oriented at an angle  $\theta_0$ , the phase excitation ( $\beta$ ) between the elements must be adjusted, so that  $\psi = 0$ . This yield,

$$\beta = -kd \cos \theta_0 \quad (4.9)$$

So by controlling the progressive phase difference ( $\beta$ ) between elements, the main beam can be scanned in any desired direction. In this study, since  $d=0.3\lambda$  and  $\theta=87^\circ$ , the required progressive phase shift required for a 4-element linear array is,  $\beta=-5.65^\circ$ . It is evident that another factor,  $a_n$ , can also

be used to affect the array factor. In section 2.4.1, several methods used to determine the array factors are introduced. In this section, Dolph-Tschebysheff method used to determine the array factor of the antenna, is briefly discussed,

**Dolph-Tschebysheff Design of Non-Uniform Array Antenna:**

Generally, Dolph-Tschebysheff method is implemented by set of polynomials called, Dolph-Tschebysheff polynomials, given by;

$$T_m(z) = \cos[m \cos^{-1}(z)] \quad -1 \leq z \leq 1$$

$$T_m(z) = \cos[m \cosh^{-1}(z)] \quad z < -1, z > +1$$

The array factor in this case is given by;

$$(AF)_{2M}(\text{even}) = \sum_{n=1}^M a_n \cos[(2n-1)u] \quad (4.10)$$

$$(AF)_{2M+1}(\text{odd}) = \sum_{n=1}^{M+1} a_n \cos[(2n-1)u] \quad (4.11)$$

$$\text{Where } u = \frac{\pi d}{\lambda} \cos \theta$$

Because of the tradeoffs between main lobe width and side lobe attenuation, the extra attenuation of the furthest side lobes will come at the expense of increased main lobe width. If the attenuation of these side lobes could be decreased (up to the level of the minimum side lobe level), then the main lobe width would become narrow. It follows that for a given minimum desired side lobe level, the narrowest main lobe width will be achieved by a

window whose side lobes are all equal to minimum desired side lobe level. Conversely, for a given maximum desired main lobe width, the largest side lobe attenuation will be achieved by a Dolph-Tschebysheff method with equal side lobe levels. Thus, the corresponding amplitudes are obtained by calculating and equating the coefficients, such as,

$$a_n = \left\{ \sum_{q=n}^M (-1)^{M-q} (z_0)^{2q-1} \frac{(q+M-2)!(2M-1)}{(q-n)!(q+n-1)!(M-q)!} \right. \quad (4.12)$$

for even  $2M$  elements  $n = 1, 2, \dots, M$

$$a_n = \left\{ \sum_{q=n}^{M+1} (-1)^{M-q+1} (z_0)^{2(q-1)} \frac{(q+M-2)!(2M)}{\varepsilon_n (q-n)!(q+n-2)!(M-q+1)!} \right. \quad (4.13)$$

for even  $2M + 1$  elements  $n = 1, 2, \dots, M + 1$

$$\text{where } \varepsilon_n = \begin{cases} 2 & (n=1) \\ 1 & (n \neq 1) \end{cases}$$

The above equations are used to find the amplitudes of an  $N = 4$  antenna array, which has microstrip radiating element with a relative element separation distance of  $0.3\lambda$ . The calculated values of the related coefficients are; **1, 1.0677, 1.0677** and **1**.

The corresponding array factor can be represented as,

$$(AF)_4 = \cos(u) + 1.0677 \cos(3u)$$

where  $u = [(\pi d / \lambda) \cos \theta]$  and  $d=0.3\lambda$  and  $\theta=87^\circ$ , as determined previously.

Figure4. 3 plots the related array factor of this non-uniform 4-element microstrip planar phased array antenna with sidelobe level, 12dB below the main lobe level.

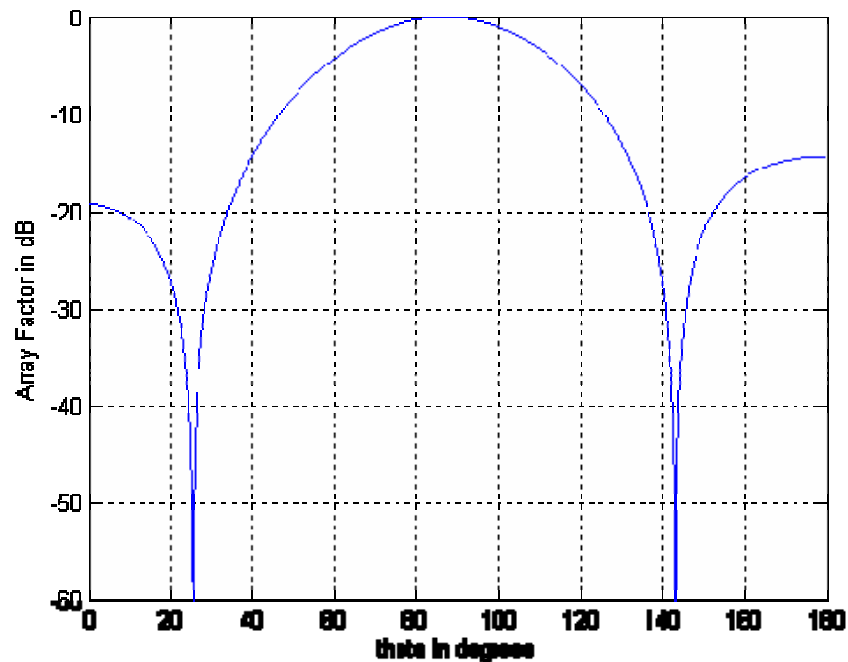


Figure4. 3 Array factor of 4-element non-uniform Dolph-Tschebeysheff array designing

Now, a 4-way array feeder is needed to be designed that will realize the calculated amplitude ratios, of the non-uniform microstrip linear phase array antenna. To achieve the normalized excitation amplitudes of **1, 1.0677, 1.0677, and 1**, among the patch elements (from outer to inner element), a power divider network that provides this required uneven power division

ratio is to be realized. Using microstrip technology, this type of power divider is designed by selecting appropriate impedance ratio between the output arms of the divider. Consequently, large variations in the width of the microstrip-line used in the output arms are resulted. Figure4. 4 illustrate such a 2-way uneven power divider that uses microstrip lines with different width. In our study, since the ultimate target is to fabricate this power divider on ferrite substrate with  $\epsilon_r=14$ , it seemed very difficult to realize the designed microstrip power divider using the fabrication facilities available in our lab

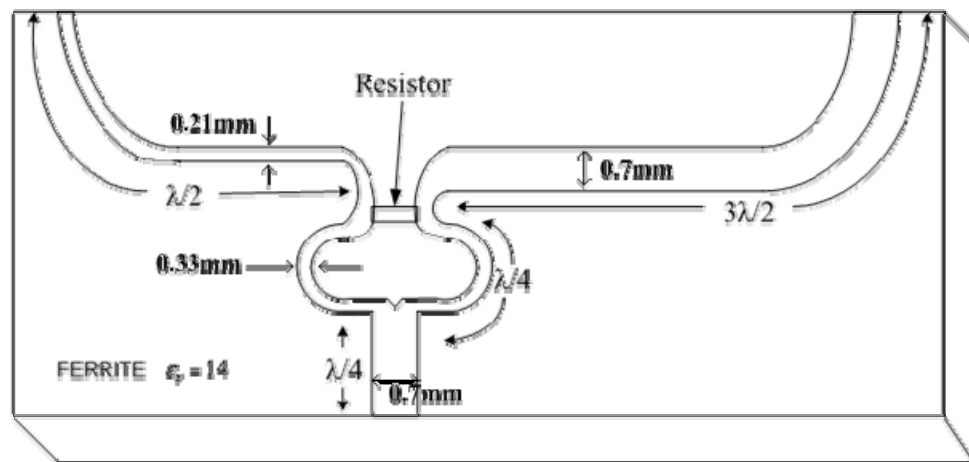


Figure4. 4 Unequal power divider implemented on ferrite substrate

To avoid this set-back, we decided to excite the radiating rectangular patches with equal amplitude but progressively phase shifted input signals. So, instead of the non-uniform array, we implemented a uniform four element

microstrip linear phased array antenna with the pre-calculated array characteristics but with a constant amplitude excitation. The radiation characteristics of the designed antenna are investigated in the following section.

#### **4.2.4 RADIATION CHARACTERISTICS**

The total field radiated from an array is the vector addition of all the fields radiated by the individual element. To provide a directive (high gain) pattern, fields from all the elements needs to interfere constructively in desired direction and cancel each other in remaining space. The radiated field expression for this microstrip antenna array is given by,

$$E'_\phi \cong +j \frac{hk_0WE_0e^{-jk_0r}}{\pi r} \left\{ \sin \theta \frac{\sin\left(\frac{k_0h}{2} \sin \theta \cos \phi\right) \sin\left(\frac{k_0W}{2} \cos \theta\right)}{\frac{k_0h}{2} \sin \theta \cos \phi \quad \frac{k_0W}{2} \cos \theta} \right\} X \cos\left(\frac{k_0L_e}{2} \sin \theta \sin \phi\right)$$

Since the antenna array designed here is made up of microstrip patches as elements, the corresponding E-plane of single microstrip patch antenna positioned in the x-z plane, and so the radiated field expression reduces to,

$$E'_\phi \cong +j \frac{hk_0WE_0e^{-jk_0r}}{\pi r} \left\{ \frac{\sin\left(\frac{k_0h}{2} \cos \phi\right)}{\frac{k_0h}{2} \cos \phi} \right\} \cos\left(\frac{k_0L_e}{2} \sin \phi\right) \quad (4.14)$$

Where  $\theta = 90^\circ$  and  $-90^\circ < \phi < 90^\circ$

The H-plane of the microstrip antenna is the x-y plane, and so the radiated field expression reduces to,

$$E_{\phi}^r \cong +j \frac{hk_0 W E_0 e^{-jk_0 r}}{\pi r} \left\{ \sin \theta \frac{\sin\left(\frac{k_0 h}{2} \sin \theta\right) \sin\left(\frac{k_0 W}{2} \cos \theta\right)}{\frac{k_0 h}{2} \sin \theta \frac{k_0 W}{2} \cos \theta} \right\} \quad (4.15)$$

Where  $\phi = 0^\circ$  and  $0^\circ \leq \theta \leq 180^\circ$

This radiation characteristic is plotted in Figure4.6. It is clear from the figure that the beam width is very large and the antenna is not very directive. This point is also evident from Figure4. 7, it shows the related polar form of the same radiation pattern. Figure4. 8 shows the related H field pattern of the radiating patch.

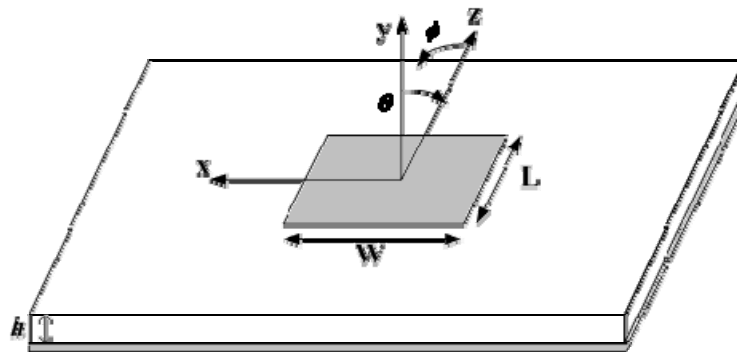


Figure4. 5 Rectangular microstrip patch and its orientation with respect to azimuthal & elevation angles

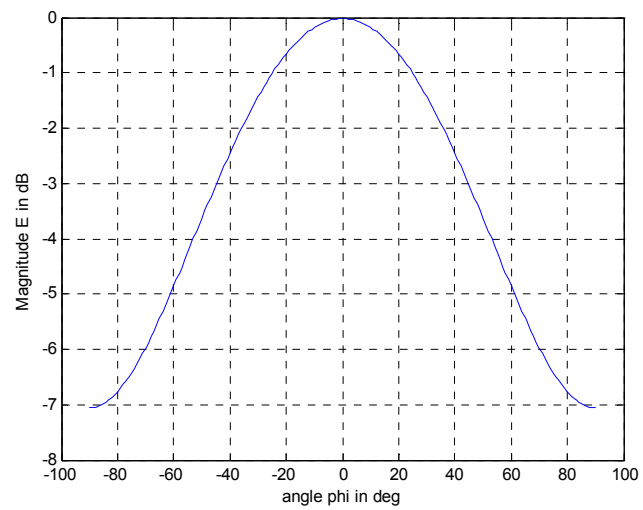


Figure4. 6 Radiation pattern of single microstrip antenna in dB

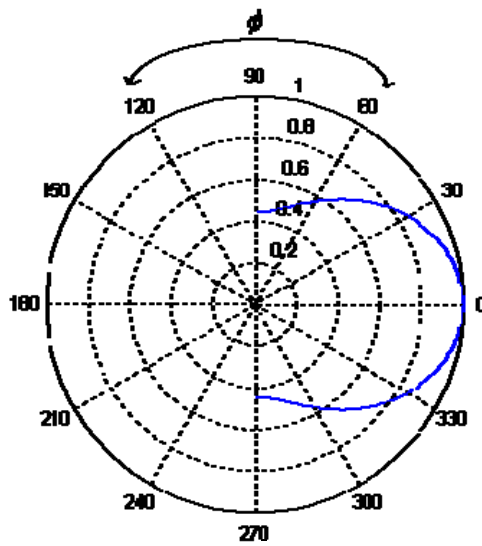


Figure4. 7 Radiation pattern of single microstrip patch in polar plot

Now, if uniform linear phased array antenna is designed using four patch elements, the corresponding radiation pattern is obtained by multiplying the above single patch patterns with the related array factor.

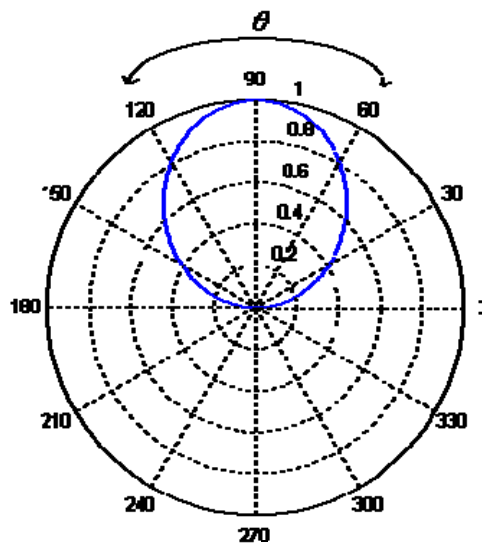


Figure4. 8 H-plane radiation pattern of the single microstrip patch in polar plot

This is pattern multiplication is already discussed in detail in chapter2. The resulting radiation pattern of the E-plane and the H-plane of the four element antenna array is shown Figure4. 9 and Figure4. 10 respectively. It is clear from these figures that the array antenna demonstrates a more directive pattern with lower half power beamwidth compared to that of individual patch

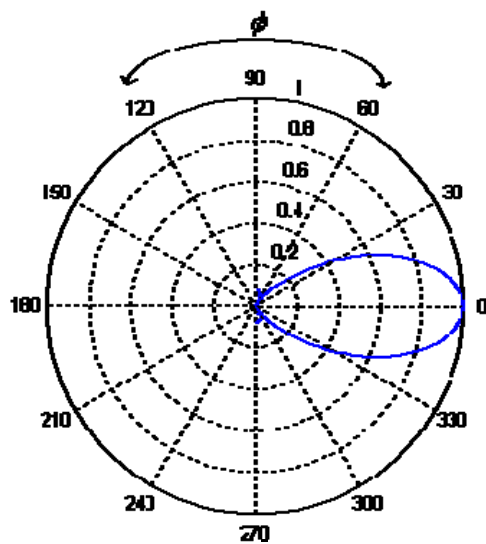


Figure4. 9 E-plane radiation pattern of the 4-element microstrip linear antenna array

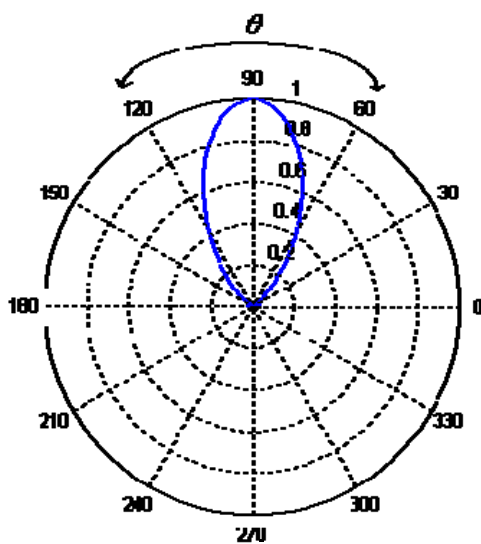


Figure4. 10 H-plane radiation pattern of the 4-element microstrip linear antenna array

After successfully characterizing the array antenna, the design process of required array feeder is presented below.

Amongst the important antenna characteristics are the antenna half-power beamwidth, antenna directivity and antenna gain. Theoretically for this antenna they are calculated to be as follows, the half power beamwidth of this antenna is calculated to be equal to  $45.3^\circ$ , and the antenna directivity is obtained to be 8.17dB, and the corresponding gain assuming the antenna to be lossless ( $\epsilon_{cd}=1$ ) we get the antenna gain also to be 8.17dB.

#### **4.2.5 INTEGRATED ARRAY FEEDER**

In this study, the array feeder is designed to be an integrated structure combining modified Wilkinson's four-way power divider with planar ferrite phase shifters. The design processes of each of these components were presented in chapter 3. Figure 4. 11 shows the integrated structure based on ferrite substrate. The related microstrip dimensions are tabulated in Table 4. 2

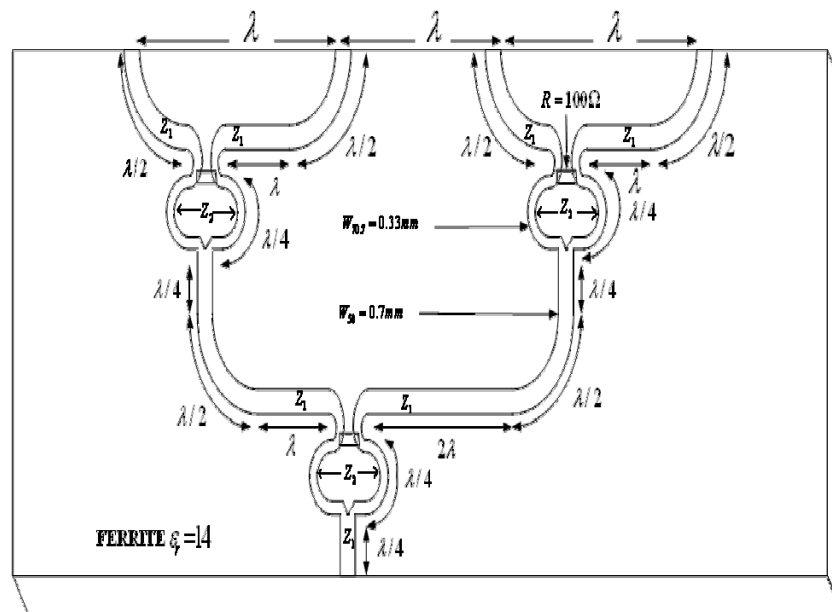


Figure4. 11 Integrated ferrite based modified Wilkinson power divider/phase shifter

Table4. 2 Power Divider Phase Shifter Parameters

S.No	Impedance	$\epsilon_{eff}$	Width (in mm)
1	50Ω	10.19	0.7
2	70.7Ω	9.26	0.33

The reason for the asymmetrical design is to achieve an initially slanted beam, pointing at  $87^{\circ}$  and then using external biasing steer that beam to achieve a maximum scan angle of  $20^{\circ}$ . The transmission, isolation and reflection response of this integrated power-divider and phase shifter

structure is simulated and optimized here using a commercial software HFSS. The simulated transmission and reflection (S-parameter) responses are presented in Figure4. 12 and Figure4. 14. The main reflection response ( $S_{11}$ ) of below -25 dB is more than what is expected in the design objective. But the transmission responses of this integrated array feeder are little off from the desired values, although they are correctly achieved in the original dielectric based power divider, presented in Figure3. 13 of Chapter 3. So, although ferrite and dielectric substrates in have same dielectric constant of 14, it is the magnetic properties of the ferrite substrate used in the final design that caused this deterioration of the transmission properties.

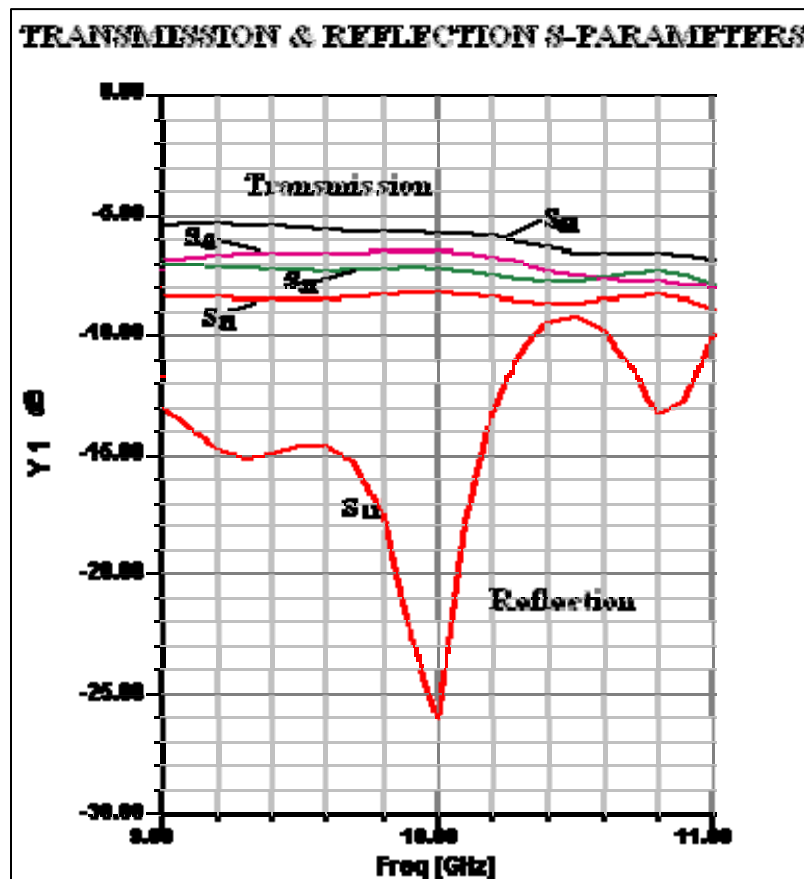


Figure4. 12 Transmission and reflection S-parameter curves for four port power divider.

The isolation curves ( $S_{32}$ ,  $S_{23}$ ,  $S_{54}$ , and  $S_{45}$ ) for the designed four port integrated array feeder are shown in Figure4. 13. It is clear from this figure that the isolation response at the operating frequency of 10 GHz is approximately below -20dB, which satisfies the design objective related to port isolation of the array feeder network.

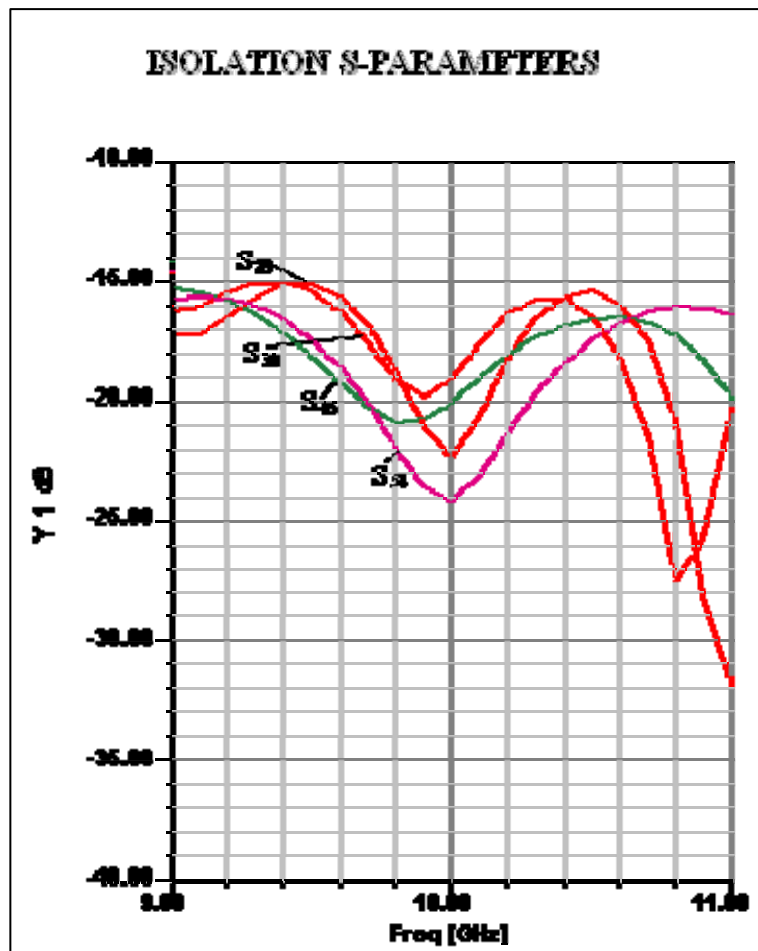


Figure4. 13 Isolation S-parameters for the four port power divider

The reflection S-parameters ( $S_{11}$ ,  $S_{22}$ ,  $S_{33}$ , and  $S_{44}$ ) for the four port power divider are shown below in the Figure4. 14. These curves demonstrate that around 10 GHz the integrated power-divider/phase-shifter network also exhibit acceptable reflection response as per design objective.

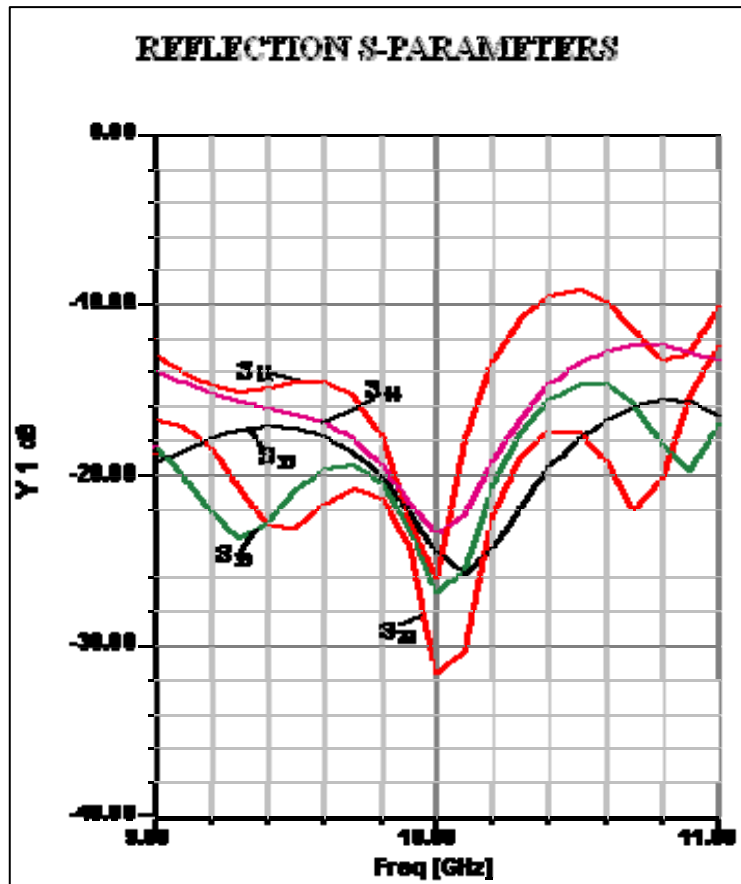


Figure4. 14 Reflection S-parameters for the four port power divider

### 4.3 DESIGN OF MICROSTRIPLINE FED LINEAR PHASED ANTENNA ARRAY

Based on the calculation of the previous sections, the designed microstrip line feed uniform 4-element linear phase array antenna is analyzed in this section. The schematic diagram of the array antenna with integrated power-divider/phase-shifter is shown in Figure4. 15.

Note that separate substrates are used for the array feeder and the radiating patch. This is done to improve the radiating characteristics of the antenna, at the cost of substrate un-uniformity associated with device. The input impedance at the edge of the patch, calculated using equation 2.5 (of chapter 2) resulted in a  $R_{in} = 267.35\Omega$ . To match this input impedance with the  $50\Omega$  feedline impedance, an  $116\Omega$  quarter-wave ( $\lambda/4$ ) transformer is used. The impedance mismatch in the feed line, resulted from the different dielectric constants of the two substrates, is minimized by utilizing appropriate sized (width) microstrip line.

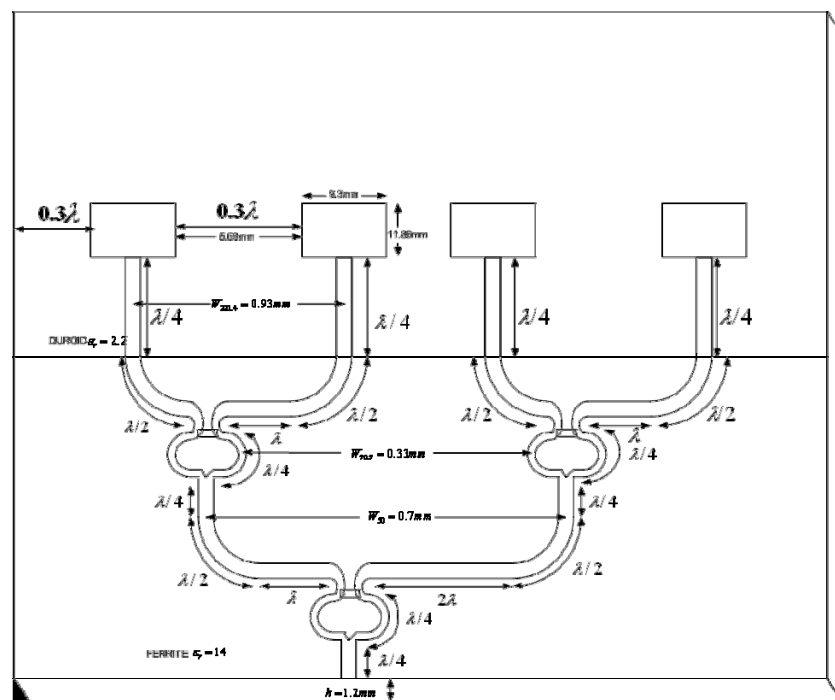


Figure4. 15 Four-Element microstrip antenna array structure line-fed.

The geometrical and material characteristics associated with the final design of the microstrip antenna array are tabulated in Table4. 3. The radiation characteristics are already specified in individual design sections. The next Table4. 4 shows the antenna characteristics obtained theoretically from simulations performed on Matlab.

Table4. 3 Geometrical and material Parameters of Microstrip line fed Antenna Array

<b>Antenna element</b>	<b>Dimensions/ Parameters</b>
Patch	Length of Patch $L_p=9.3\text{mm}$ , Width of Patch $W_p=11.86\text{mm}$
Distance between elements	$d = 6.2\text{mm} (0.3\lambda)$
Substrate	Thickness $h=1.2\text{mm}$ , relative dielectric constant of substrate $\epsilon_r=2.2$ , relative dielectric constant of ferrite substrate $\epsilon_r=14$
Feed-line widths	Width of feedline $W_{50}=0.7\text{mm}$ & $W_{70.7}=0.33\text{mm}$ Width of quarter wave transformer feedline $W_{116}=0.93\text{mm}$
Magnitude of resistors	$R=100\Omega$

Table4. 4 Antenna Characteristics as obtained from Matlab (Theoretical)

<b>S.No</b>	<b>Antenna Characteristics</b>	<b>Magnitude</b>
1	Main Beam Angle ( $\theta$ )	$87^{\circ}$
2	Progressive Phase Shift ( $\beta$ )	$-5.64^{\circ}$
3	Half-Power Beamwidth	$45.3^{\circ}$
4	Main Lobe to side lobe Ratio	-12dB
5	Antenna Gain(dB)	8.17 (assuming lossless)

Commercial simulation software, HFSS, is used to simulate and optimize the designed antenna to achieve the required radiation characteristics. Since this software allows the application of external magnetic field, ferrite substrate is easily biased using any amount of external biasing. It is of note that, among various commercial software, Ansoft HFSS (version 8.0 or above) is the only software that allows the simulation of anisotropic material used in passive devices. In order to calculate the full three-dimensional electromagnetic field inside a structure and the corresponding S-parameters, HFSS employs the finite element method (FEM) [47]. FEM is a powerful tool for solving complex engineering problems, the mathematical formulation of which is not only challenging but also tedious. The basic approach is to divide a complex structure into smaller

sections of finite dimensions known as elements. These elements are connected to each other via joints called nodes. Each unique element is then solved independently of the others thereby drastically reducing the solution complexity. The final solution is then computed by reconnecting all the elements and combining their solutions. A detailed description of how HFSS software functions are given in Appendix A.

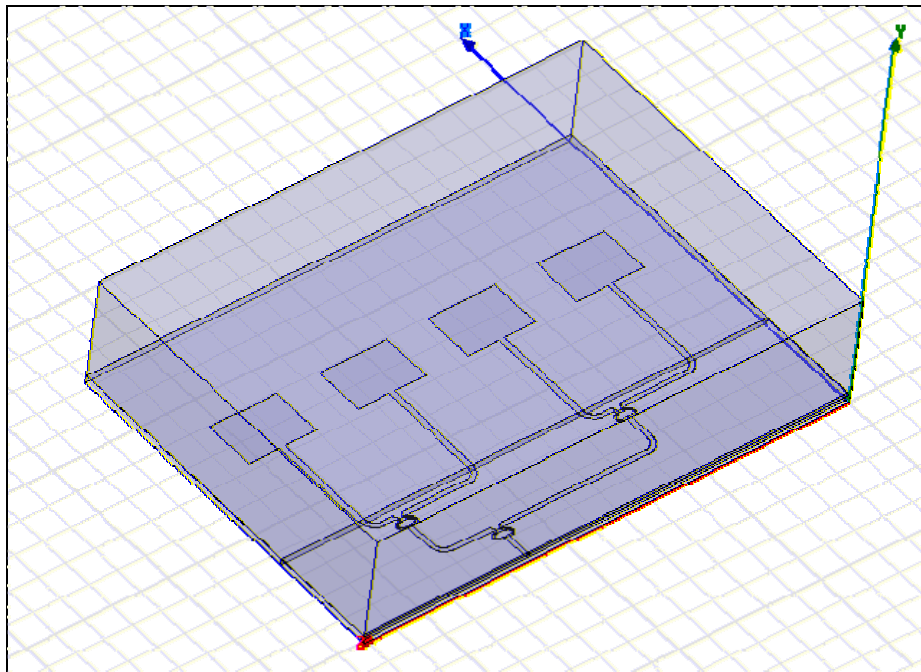


Figure4. 16 HFSS Schematic of implementation of microstrip line fed patch antenna array

The simulated antenna using HFSS software is shown in Figure4. 16. Note, the software also allowed the inclusion of the isolation resistors used in the Wilkinson power divider, although compromise had to be made in the total

allowable antenna dimension to minimize the hardware and simulation time requirements. The reflection parameter response ( $S_{11}$ ) of this antenna array is shown in Figure 4.17. This figure illustrates the resonance characteristic of the antenna array and the impedance bandwidth. It is clear from this figure that an antenna resonates at a frequency of 9.93 GHz and has an impedance bandwidth of 10%. These values are very close to the desired design characteristics mentioned in the objective section. The narrow band characteristic of this array antenna is due to the inhibit property of the microstrip antennas. In the next section, the feed techniques will be changed in an attempt to improve the impedance bandwidth of the antenna.

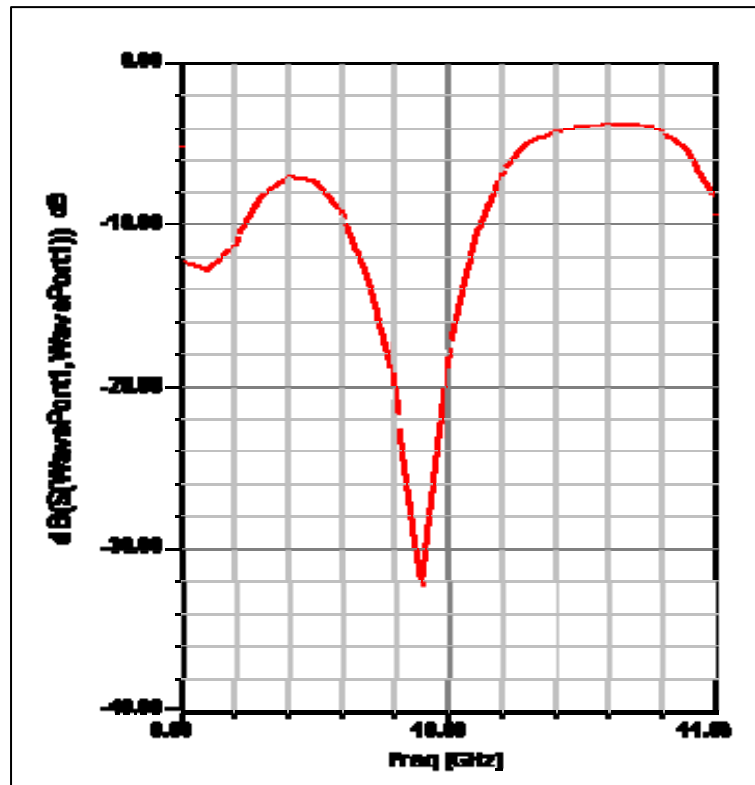


Figure4. 17 Reflection curve ( $S_{11}$ ) of four element microstrip antenna array

The radiation pattern for the four element microstrip antenna array is shown in Figure4. 18. Note the side lobe level is below -10 dB and the patten is more directive compared to that of single patch. Also the radiation response of this figure represents the un-biased case, meaning no external biasing field applied to the microstrip ferrite phase shifter sections.

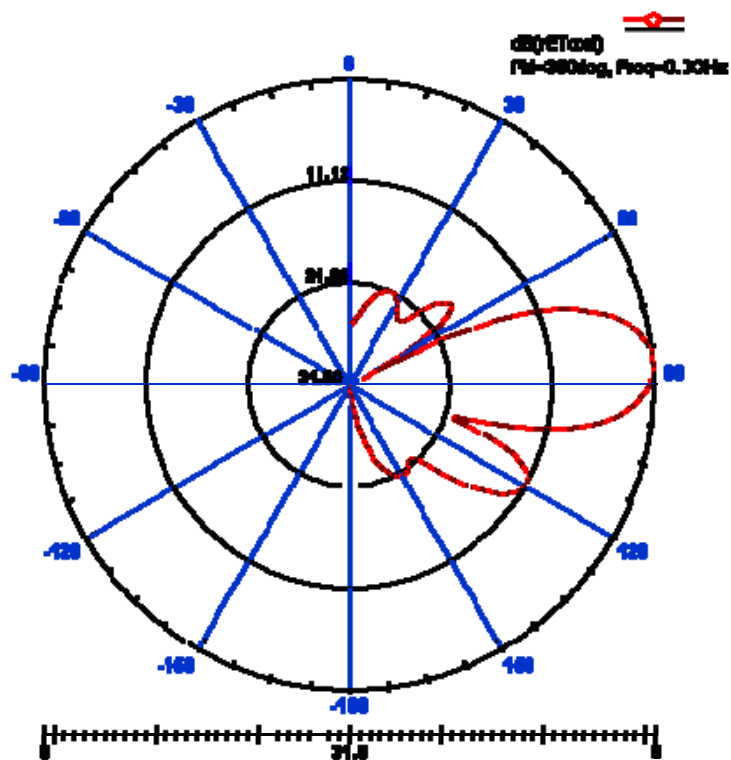


Figure4. 18 Radiation pattern (E-plane) of the four element antenna array

To observe the tunable insertion phase characteristics of the ferrite phase shifters, external magnetic biasing field is transversely (y-axis direction) applied to the integrated array feeder. The strength of the magnetic field was selected to at least saturate the ferrite material to avoid partial saturation. Also, care is taken so that the ferrite material is not driven into lossy saturation region.

Table4. 5 Antenna Characteristics as obtained from Simulation (Practical)

S.No	Antenna Characteristics	Magnitude (Practical)
1	Main Beam Angle ( $\theta$ )	$87^0$
2	Progressive Phase Shift ( $\beta$ )	$-4.86^0$
3	Half-Power Beamwidth	$26^0$
4	Main Lobe to side lobe Ratio	-12dB
5	Antenna Gain (dB)	13.12
6	Impedance Bandwidth	10%

As the above Table4. 5 shows the antenna characteristics we can conclude that the simulated structure of the antenna is narrow band and has a half-power beamwidth which is equal to approximately  $26^0$ , also the directivity of the antenna is more than the theoretical which is 13.12dB, the main beam in this simulation also showed a squint to  $87^0$ , and the gain of the antenna is also high compared to the theoretical calculation being 13.12dB. After having achieved the successful implementation of the designed antenna array structure, a magnetic bias normal to the array feed was applied to the ferrite substrate. The results of which are discussed below.

For different biasing field the antenna demonstrated beam scanning properties. The angle related to the squinted beams and the related external biasing field is shown in Figure4. 19. It is clear from this figure that for

smaller magnetic biases of 150 KA/m, the main beam of the antenna got steered to very small angles from approximately  $87^{\circ}$  to  $84^{\circ}$ . But, as the bias is increased from 200KA/m to 235KA/m, the scan angle got shifted by a considerable amount. This can be attributed to the theory which has already been mentioned and explained in the earlier chapters that when ferrite is operated in the region closed to its cut-off, slight change in the magnetic bias produces considerable changes in the insertion phase. In the present work, by magnetizing the ferrite close to the saturation region [42], a beam squint of approximately  $15^{\circ}$  ( $235^{\circ}$ - $200^{\circ}$ ) is achieved for 35 KA/m (200-235 KA/m) change in biasing field. It is also observed that as ferrite enters into saturation region with biasing field more than 240 KA/m, increasing the magnetic bias beyond this point do not increase the insertion phase of the ferrite

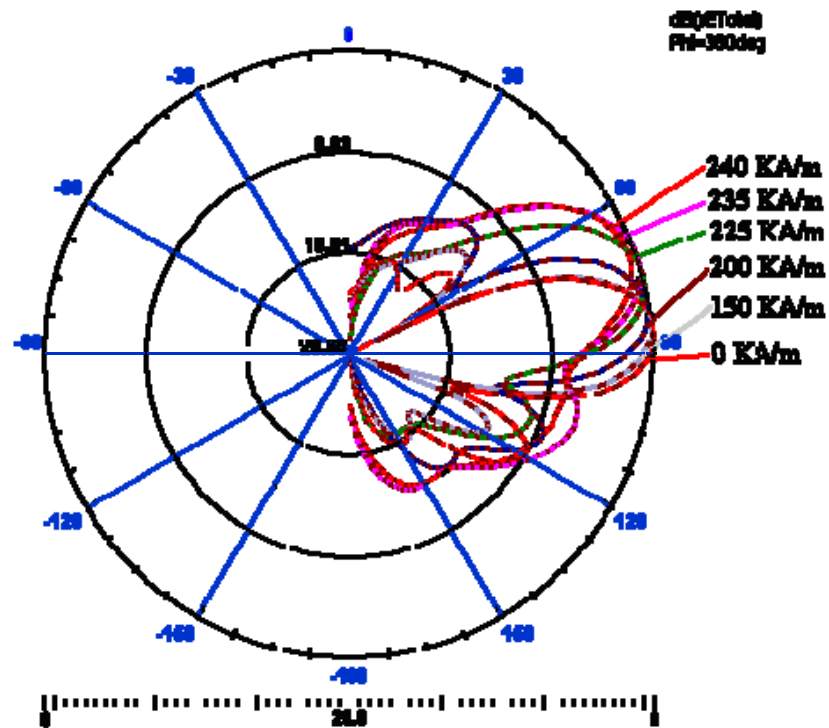


Figure4. 19 Radiation pattern showing the main beam of the antenna scanned for different magnetic biases.

This point is also demonstrated from the final two responses of the Table4. 6. Also, since the ferrite material becomes very lossy at resonance, operating at resonance region do not produce correct response. The magnetic bias and the main beam steering angle can be tabulated as follows,

Table4. 6 Main beam angle scanning at different magnetic bias

<b>S.No</b>	<b>Magnetic Bias</b>	<b>Main Beam angle</b>
1	0KA/m	87 <sup>0</sup>
2	150KA/m	85 <sup>0</sup>
3	200KA/m	83 <sup>0</sup>
4	225KA/m	75 <sup>0</sup>
5	235KA/m	69 <sup>0</sup>
6	240KA/m	67 <sup>0</sup>

It is clear from the above simulation data that the designed antenna has a very low impedance bandwidth. To improve the bandwidth requirements, aperture coupling technique is utilized. Next section presents the design process of an aperture coupled uniform 4-element microstrip phase array antenna.

## **CHAPTER 5**

### **EXPERIMENTAL RESULTS & DISCUSSIONS**

#### **5.1 INTRODUCTION**

The fabrication process to realize the designed four element microstrip linear phased array antenna is discussed in the first half of this chapter. The tools used to perform the experimentation and the experimental response is presented in the second half of the chapter. The simulated reflection response ( $S_{11}$ ) and beam scanning properties of the array antenna are corroborated with the related experimental results.

#### **5.2. CAD/CAM TOOLS DESCRIPTION**

The designed four element array antenna is fabricated using PCB plotter. To begin with, the PCB diagram of the array antenna is transferred to the 'CircuitCAM' software. 'LPKF CircuitCAM' is as user friendly program offering powerful editing options for data or structure creation and/or modification. Its core is the intelligent insulation process used to produce the milling paths for LPKF circuit board plotter. Due to the individually adjusted diverse insulation, milling and drilling options, CircuitCAM is considered to be one of popular software used of RF and microwave circuit layouts. Even

lines with millimeter to micrometer widths and complicated bends and curves can be easily realized using this software [56].

After finalizing the PCB layout in the CircuitCAM software and performing required insulation, it is exported to LPKF software called 'BoardMaster'. BoardMaster is machine control software that also allows the user to analyze the actual design before implementing the printed circuit on the substrate. It has intelligent tool management, specifying the user when to change a worn out tool and can automatically assign the tools associated with the processing phases using the information provide by the CircuitCAM software. BoardMaster is also used to determine the PCB location, drilling depth, milling depth, hole size and location related to the circuit [56].

Once the BoardMaster layout is completed and the Copper coated board is placed in the correct place, the plotter (LPKF Protomate C60) is used to realize the microstrip array antenna. A picture of the plotter is shown in Figure5. 1. LPKF ProtoMat C60 is a circuit board plotter, ideal for single or double sided medium density boards for analog, digital or RF circuits. The minimum width or gap that can be etched by this plotter is approximately 0.2mm and diameters as small as 0.25mm, where different drills are used for milling and drilling purposes [56].

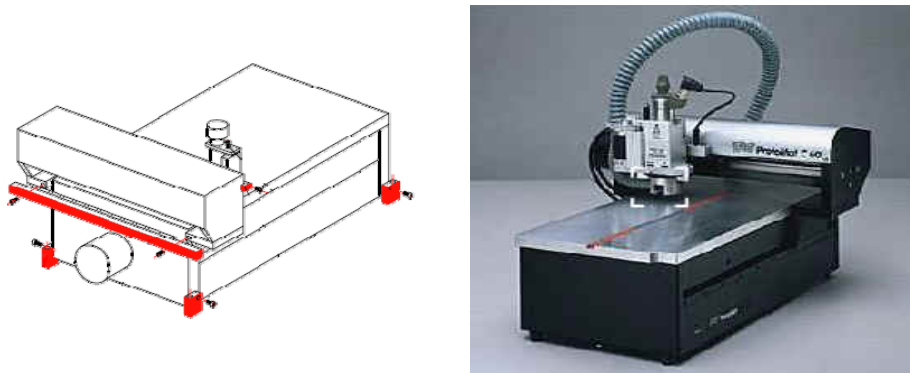


Figure5. 1 PCB plotter used to fabricated the designed microstrip array antenna

### 5.3 ANTENNA MEASUREMENT TOOLS

The reflection measurements are perhaps the only tool available to analyze the frequency response of a single port device, such as, a linear array antenna. Since HP 8510 Vector Network Analyzer allows the measurement of reflection and transmission relate S-parameter, it a very popular tool in measuring active and passive microwave devices [54]. Network analyzer is used in this study to measure the scattering parameters of the designed array antenna. In the following section, brief description of how the network analyzer is used to perform the S-parameter measurements is presented.

The vector network analyzer available in the EE lab (HP-8510C) is capable of measuring both the magnitude and phase of a sinusoidal voltage signal. It uses complex RF circuitry to make the analyzer much more accurate; with a typical dynamic range of 70-110 dB and frequency range of

0.4GHz to 40 GHz. Figure5. 2 shows the picture of the analyzer. It is clear from the picture that the analyzer consists of three parts; RF sweep generator, S-parameter test set, and a network analyzer. Brief descriptions of these components are presented as follows.

**Signal sweep generator:** The source provides the RF signal. An Agilent 8360 Series synthesized sweeper, or an 834x Series synthesized sweeper, or an 835x-Series sweep oscillator with an appropriate Agilent 835xx Series plug-in, may be used.

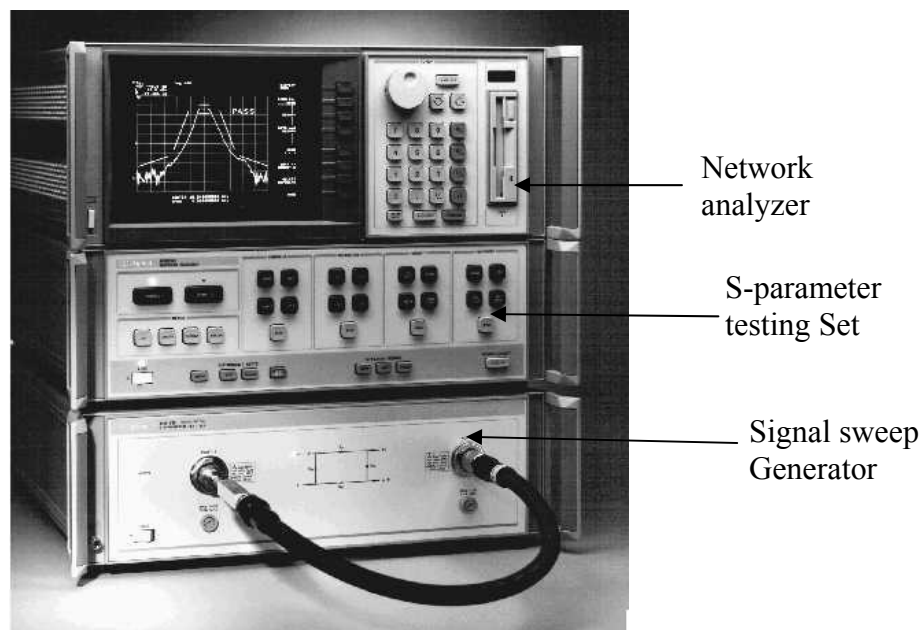


Figure5. 2 Network Analyzer [ 54]

**S-parameter testing Set:** The test set separates the signal produced by the source into an incident signal, sent to the device-under-test (DUT), and a reference signal against which the transmitted and reflected signals are later compared. The test set also routes the transmitted and reflected signals from the DUT to the receiver (IF/detector). Any 851x Series test set may be used.

**Network analyzer:** An 8510C network analyzer, which includes the Agilent 85101 Analyzer Display/Processor and the 85102 IF/Detector (Receiver). The receiver, together with the display/processor, processes the signals. Using its integral microprocessor, it performs accuracy enhancement and displays the results in a variety of formats.

The process used in network analyzer to measure the reflection parameters are schematically shown in Figure5. 3. The swept signal source is used to introduce a microwave signal sweep from 8 to 10 GHz into the test set. The RF signal is divided into *test* and *reference* signals. The reference signal is passed directly to the first mixer stage.

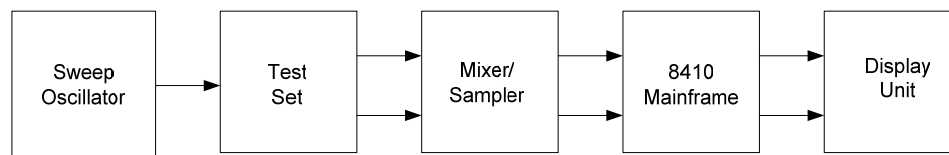


Figure5. 3 Block diagram of the Network Analyzer 8410 (Internal view)

The test signal goes through the unit under test and then to the mixer. Most test sets permit the selection of a particular S-parameter set-up by engaging the RF relays inside the set. The mainframe tries to maintain phase lock between the sampler and the sweep oscillator. It also down converts the input signal to 278 KHz IF. This is given to the display unit(s) [54]. This display is of two types one is the rectangular display for magnitude and phase of the s-parameters ( $S_{11}$ ,  $S_{12}$ ,  $S_{21}$  or  $S_{22}$ ) and other one is the polar display for Smith Chart.

But, reflection measurements are taken, calibrating the network analyzer is essential to ensure correct results. Calibration is a technique used to compensate for the frequency dependent phase and amplitude characteristics of the cables and receiving system of the analyzer and is performed using the known responses of standard loads (open, short, and 50  $\Omega$  terminations). This procedure is an important part of network analysis, and should be done each time a new measurement is taken with different frequency range. Since the device under consideration is a one port microstrip array antenna, the network analyzer is required to be calibrated for one port measurements. It is performed by initiating the calibration process and terminating port1 with required loads of short circuit, open circuit and broadband load.

## **5.4 FABRICATION & BIASING TECHNIQUES OF THE DESIGNED ANTENNA ARRAY**

The fabrication process of the designed microstrip array antenna was a rather difficult task, as it involved the realization of very small Wilkinson power divider circuit on the ferrite substrate. Since, metallic ferrite substrate was not available, copper strips were used to realize the integrated power-divider/phase-shifter network and pasted on the ferrite substrate. This was an arduous task, as the width of the microstrip lines involved with the 4-way array feeder was very small and could not be realized by hand with the help of a scissor. So, copper strips stuck were glued on temporary substrate and the PCB plotter was used to accurately transfer the array antenna on the copper strips. Once the printed circuit of the array feeder was completed, it was discovered that the available ferrite substrate were too small in width to host the feeder circuit. So, the ferrite was cut in halves and bound together (horizontally) to increase its width. Due to the lack of facilities available to cut the delicate ferrite substrate, a lot of ferrite samples were destroyed until a machine in Mechanical Engineering successfully performed the dissection. Once the ferrite substrate was ready, the printed copper strips were stuck on them to realize the array feeder on ferrite substrate. Using the same copper

strips, ground plane of the ferrite substrate was implemented. The figure of the array feeder on the ferrite substrate is show in Figure 5.4

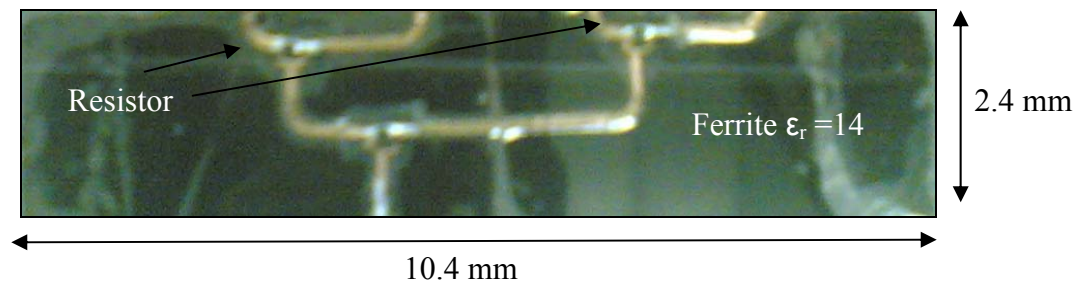


Figure5. 4 Feed Network implemented on Ferrite

Fabricating the linear array of radiating elements was relatively easy task, as required substrate with  $\epsilon_r=2.2$  were available on the EE store. So PCB plotter was used to construct this part of the device directly on the substrate.

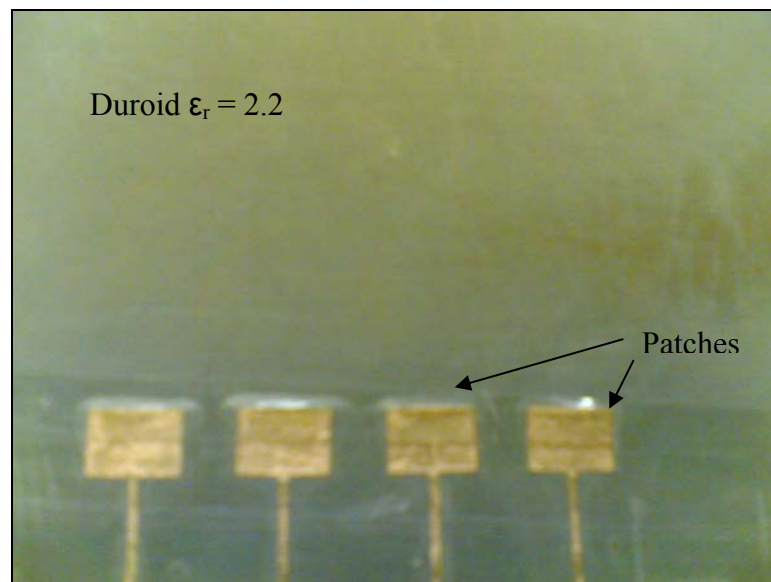


Figure5. 5 Microstrip Patches implemented on Duroid

While combining the two parts of the array antenna, it was found to be difficult to inter-connect the small feed lines of the patches and that of the array feeder network. So the fabrication process was repeated and the whole circuit was plotted on the copper strip. Then the array antenna printed on copper strips was glued on the composite dielectric-ferrite substrate to realize the designed 4-element microstrip linear phase array antenna. Figure 5.6 shows the fabricated array antenna. Note the composite substrate is visible in the figure. Also note the isolation resistors, soldered on the divider junctions.

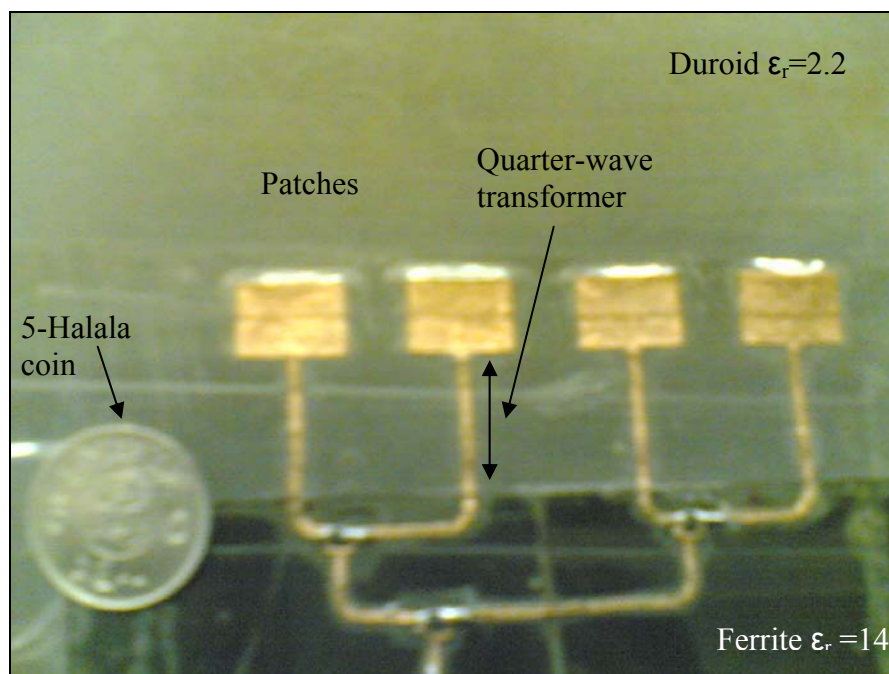


Figure 5.6 Linear Microstrip Antenna array against a metallic coin for comparison

## 5.5 EXPERIMENTAL RESULTS & ANALYSIS

The experimentation started with the measurement of the antenna reflection response ( $S_{11}$ ) using the network analyzer. The need, method of calibration and working principle of the network analyzer is presented in section 5.3. Since the antenna array is designed to operate at a frequency of 10 GHz, the reflection response of the device was observed for a frequency range of 8 to 12 GHz (X-band). Figure 5.4 plots the reflection response ( $S_{11}$ ) of the designed antenna array. From the figure, it is evident that the antenna is resonating at 9.75 GHz, which is very close to out operating frequency. Also the  $|S_{11}| = -35$  dB value, illustrated in the figure, demonstrate a good impedance at the resonant frequency. The impedance bandwidth of this device is calculated to be approximately 7%. The resulted narrow bandwidth is due to the inherent microstrip antennas properties and can be increased by using aperture coupling and several other methods mentioned in chapter 2. In order to corroborate the simulated results, the experimentally obtained reflection response of the antenna array is superimposed with that of simulated response and is presented in Figure 5.5.

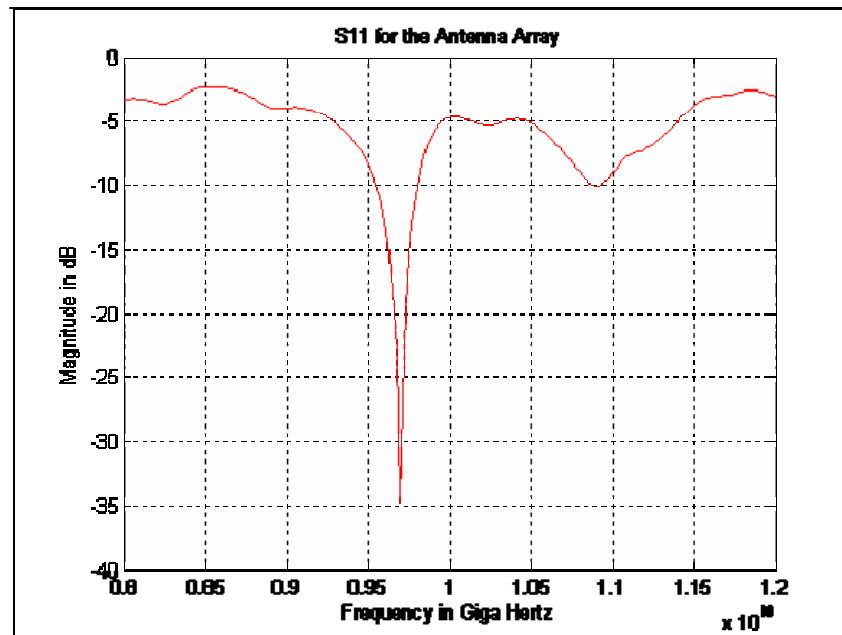


Figure5. 7 Reflection  $S_{11}$  for practically designed microstrip antenna array

Note that the simulated response has predicted a slightly wider impedance bandwidth with a slightly different resonance frequency. One of the reasons of this difference could be from human error while fabricating the antenna prototype, especially when connecting the SMA connector to the array feeder input. This was particularly difficult as the array feeder was designed on a copper strip and loosely placed on the ferrite substrate. Some of the other reasons could be; the use of relatively high error margin in the simulation process due to RAM or speed limitations of the computer; the errors during the experimental process as the network analyzer was calibrated using N-type connectors.

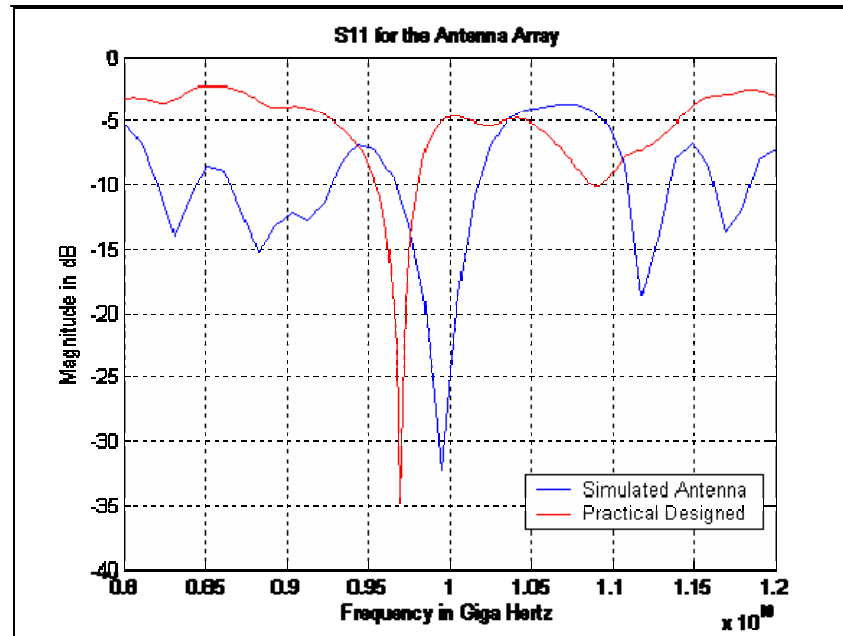


Figure 5.8 Comparison of simulated and experimental  $S_{11}$  response of antenna array.

The radiation characteristics of the antenna array were measured using the antenna training and measurement system (ATMS) available in the laboratory. Figure 5.9 shows the setup used for this purpose,

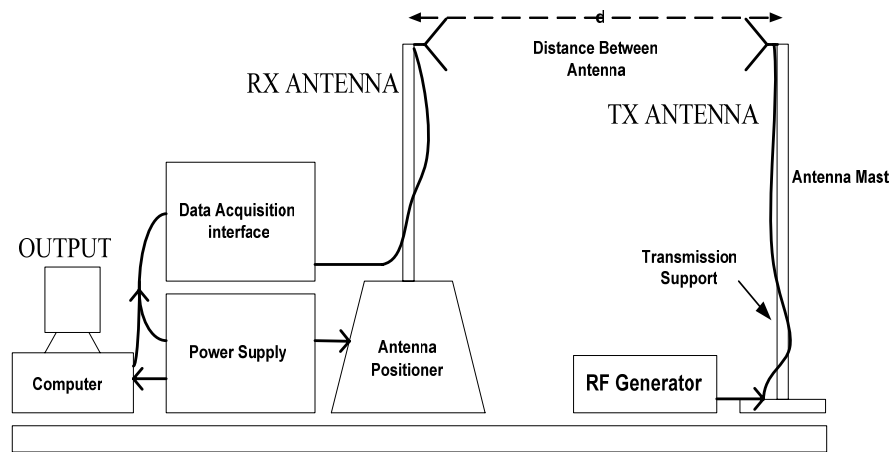


Figure5. 9 Block diagram of Antenna Training and Measuring Systems (ATMS)

Where the “RF generator” is used to transmit the 10GHz signal and data acquisition unit is used to analyze the received radiation pattern. The E and H-plane related to the designed antenna array is plotted in Figure 5.7 The loss associated with the peak of this radiation patter is mainly due to the badly connected SMA connector at the input of the antenna array. Next the beam scanning characteristics of the designed 4-element microstrip phased array antenna was observed. To excite the radiating elements with tunable progressive phase shifts, four small yet powerful permanent biasing magnets were used to tune the insertion phase of the microstrip ferrite phase shifter. Using the Tesla meter available in the lab, the maximum magnetic field produced by the permanent biasing magnets were found to be  $H_0 = 75 \text{ KA/m}$ .

Figure 5.8 shows the beam scanning behavior of the antenna array with respect to externally applied magnetic biasing field ( $H_0$ ).

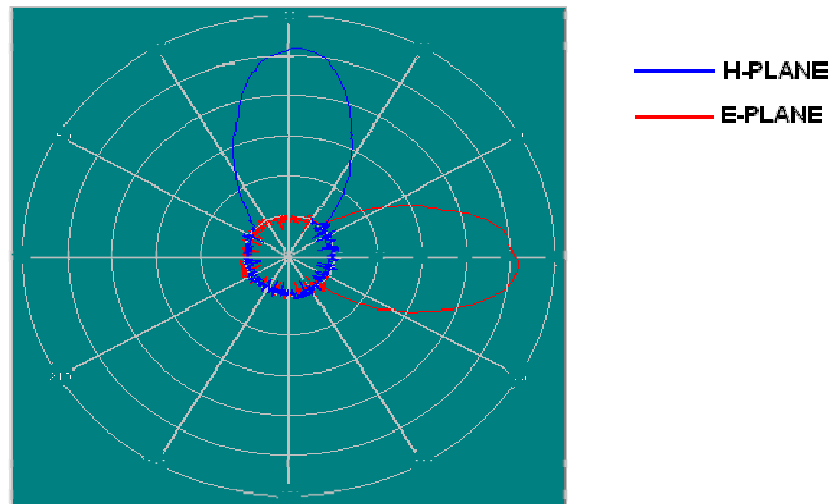


Figure5. 10 E-plane H-plane of the microstrip antenna array tested experimentally

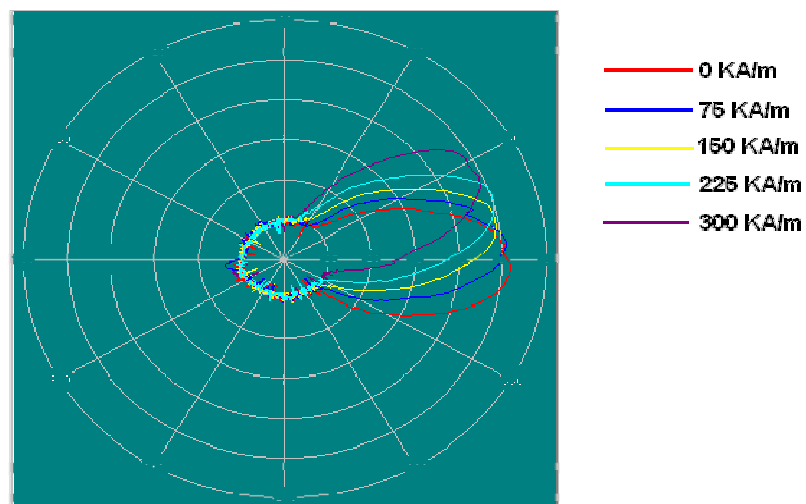


Figure5. 11 Main beam scan of fabricated microstrip antenna array for different magnetic bias

## **EXPERIMENTAL PROCEDURE ADOPTED FOR BEAM**

### **SCANNING:**

Initially, only one single magnet with bias magnitude  $H_0=75\text{KA/m}$  was placed to generate magnetic field. Later the number was gradually increased to vary the biasing field. The placements of the magnets were also optimized to ensure uniform biasing of the ferrite phase shifter. Note that the main beam is scanned from  $0^\circ$  to  $30^\circ$  by changing the biasing field from 75 to 300 KA/m (i.e., by changing the number of magnets from one to four respectively). It is clear from Figure 5.11 that the biasing magnetic fields less than 150 KA/m causes very less squint of the main beam. But when the biasing field is increased up to 225KA/m by using three permanent magnets, the main beam's shift was approximately  $20^\circ$ . Finally, when all four available magnets were used to generate the external DC magnetic biasing field, the main beam was steered by another  $8^\circ$ , making the total shift to  $28^\circ$ . The beam squint observed in the experimental process (Figure 5.11) is also tabulated in Table 5.1. (Here the optimized positions of the magnets are not mentioned). Thus, the whole antenna radiation characteristics match well with that of the simulated result presented in Figure 4.18 in the previous chapter.

Table5. 1 Main beam scan of the antenna array with different magnetic biases

<b>Number of Magnets used</b>	<b>Total Magnetic Bias applied to Ferrite</b>	<b>Main Beam Angle (Experimental)</b>	<b>Main Beam Angle (Simulated)</b>
1	75KA/m	0 <sup>0</sup>	3 <sup>0</sup>
2	150KA/m	5 <sup>0</sup>	5 <sup>0</sup>
3	225KA/m	22 <sup>0</sup>	15 <sup>0</sup>
4	300KA/m	30 <sup>0</sup>	21 <sup>0</sup>

## CHAPTER 6

### CONCLUSION & FUTURE WORK

#### 6.1 CONCLUSIONS

In this study, a 4-element microstrip linear phased array antenna is designed, simulated and tested. A brief summary of the simulated and experimentally observed results is presented below:

- The achieved characteristics of the designed antenna array are as following:
  - The antenna array was observed to be operating at a center frequency of 9.96 GHz with an impedance bandwidth of 8%. These values are very close to the desired design frequency of 10GHz and impedance bandwidth of 10%.
  - The array antenna gain of 13 dB was observed, whereas the designed antenna was required to have gain of 15 dB. This difference was due to the poorly soldered isolation registers and SMA connectors. The way to minimize this loss is to print the antenna feeder directly on

copper plated ferrite substrates, instead of printed it on copper strips and pasting it to ferrite substrate.

- For the designed antenna array, the half power beam-width of  $26^\circ$  was observed from both simulated and experimented radiation responses. Though these results were slightly lower than the required beam-width of  $30^\circ$ , it can easily be improved by increasing the fabrication accuracy of the designed antenna array.
- The main beam scan of the antenna array was experimentally observed to be  $30^\circ$ , whereas the desired maximum beam squint was  $35^\circ$ . This was due to the limitations in uniformly applying the biasing magnetic fields. The number of the magnets available was not sufficient to achieve uniform magnetization of the entire ferrite substrate.
- The characteristics obtained from the integrated array feeder, which was constructed by combining the Wilkinson power divider and microstrip ferrite phase shifters, are as follows:
  - The simulated reflection and isolation coefficient's ( $S_{11}$ ,  $S_{22}$ ,  $S_{33}$  and  $S_{23}$ ,  $S_{32}$ ,  $S_{45}$ ,  $S_{54}$  respectively) were observed to be of less than -20 dB in magnitude, which can be considered good as per design requirements.

- The transmission coefficients ( $S_{21}$ ,  $S_{31}$ ,  $S_{41}$ ,  $S_{51}$ ) of -6.2 dB in magnitude was observed. These values are also acceptable as per design requirements
  - Losses introduced by ferrite substrate were minimal although they caused slight variation between different transmission coefficients.
- 
- Electronic beam scanning of the designed array antenna was realized using a transversely (*perpendicular to GND plane*) applied external biasing magnetic field ( $H_0$ ). This biasing field changed the insertion phase of the ferrite phase shifter to produce the required progressive phase shift. When biased near saturation region, ferrite phase shifters exhibited maximum tunable insertion phase characteristics, although caution was taken not to over bias the ferrite material and drive it into saturation. It was observed that loss mechanism of ferrite material is a major disadvantage of this class of device.
  - While designing the power divider, incorporating the isolation resistor in the simulation software (HFSS) was a challenging task. It was observed that the calculation of the impedance transformers, proper placement of the isolation resistor, input phase requirements etc were vital issues in the successfully operation of the power divider. Another problem was

computer hardware (RAM) limitation, which caused problems to achieve accurate simulated responses.

- Some of the conclusions related to the difficulties encountered during the experimental design process, mainly due to the lack of resources, are presented here.
  - The first difficulty was faced at the time of integrating the antenna substrate. Because of the scarcity of the ferrite material, it had to be carefully handled while cutting into two equal pieces. Also this ferrite being very delicate, only high precision machine was used to successfully cut through it, without breaking or damaging the sample. The unavailability of this type of machine in KFUPM was the reason of several damaged ferrite samples. Finally a relatively low precision machine from mechanical engineering department was used for the purpose.
  - Next difficulty was faced during the printing the array feeder circuit on an the ferrite substrate. Due to the absence of copper coated ferrite material, the array feeder was printed on adhesive copper strips. Then with great difficulty and lot of careful trial, the copper strips were removed from the temporary substrate and glued on the ferrite

substrate. This job was very delicate, as microstrip lines with very small widths were involved in the layout.

- Another problem faced during the fabrication process was to incorporate the insulation resistors on the printed circuit. This also involved very delicate placement and soldering to achieve optimum performance.
- Finally, the 4-element linear phased array antenna was successfully assembled by combining the ‘array feeder on the ferrite substrate ( $\epsilon_r=14$ )’ with the ‘radiating elements on the dielectric substrate ( $\epsilon_r=2.2$ )’. The difference in substrate material was one of the major region of unwanted surface waves generation that compromised the efficiency of the antenna.

## 6.2 COMPARISON WITH LITERATURE

Finally the reference utilized for obtaining the goals of this research are compared with the results. Brown et al [41] performed a similar research with ferrite substrate for producing beam scanning. They designed a linear 4-element array on a composite substrate made of Duroid ( $\epsilon_r=2.2$ ), ferrite ( $\epsilon_r=14$ , saturation magnetization 140KA/m) and another dielectric ( $\epsilon_r=14$ ). They applied magnetic bias normal to the ferrite substrate of magnitude

around 400KA/m and managed to get beam scan of nearly  $40^0$  on experimental design. And in simulation they managed to get  $20^0$  in simulation. In other paper, Batchelor & Langley [46], designed a circular two element microstrip line fed linear array. They managed to get a beam scan of approximately  $40^0$  in experimental and simulation also closely followed. They utilized composite substrate of ferrite ( $\epsilon_r=14$ , saturation magnetization of 28KA/m) and a high permittivity substrate of dielectric ( $\epsilon_r=10.2$ ). And in contrast we managed to achieve a beam scan of approximately  $20^0$  in simulation and  $30^0$  in experimental with a linear 4-element microstrip line fed antenna array designed on composite substrate of ferrite ( $\epsilon_r=14$ , saturation magnetization of 64KA/m) and Duroid ( $\epsilon_r=2.2$ ).

### 6.3 FUTURE RECOMMENDATIONS

- The bandwidth limitations of the designed antenna can be improved by employing aperture coupled feeding technique or stacked patch configuration.
- Surface waves responsible for reducing the performance of the designed antenna can be improved by using substrates or ground planes with photonic bandgaps.
- Other types of array feeder, such as, the non-uniform feeder network discussed in chapter 3 can be implemented using similar ferrite substrate.

In this case the losses produced by the ferrite material will be use to produce the difference in amplitude of the excited signals.

- Due to resource limitations the experimental design could not be optimized and recommendations can be made in this regards.
- For the phase shifter, the lack of large and strong magnets that generates uniform magnetic bias for the whole ferrite substrate can be used to maximize radiation response.
- When coming to experimental setup, the recommendation is to use copper plated ferrite substrate or a single copper strip with large width. This will ease the printing (milling) process of the array feeder circuit.
- Lastly, the measurements can also be done inside an anechoic chamber to avoid external noises or disturbance. Although this facility is present in the antenna lab, we could not able to use it because of the lack of coaxial SMA cables needed to connect the experimental equipments with the chamber

## APPENDIX A

The software used for the designing and simulating the antenna model is High Frequency Simulation Software (HFSS v9.0). This part of the chapter provides a general insight into the various aspects involved in the process of setting up and running a simulation in HFSS. The version used is Ansoft version 9.0. HFSS is a software package for electromagnetic modeling and analysis of passive, three dimensional structures. In order to calculate the full three-dimensional electromagnetic field inside a structure and the corresponding S-parameters, HFSS employs the finite element method (FEM) [47]. FEM is a powerful tool for solving complex engineering problems, the mathematical formulation of which is not only challenging but also tedious. The basic approach is to divide a complex structure into smaller sections of finite dimensions known as elements. These elements are connected to each other via joints called nodes. Each unique element is then solved independently of the others thereby drastically reducing the solution complexity. The final solution is then computed by reconnecting all the elements and combining their solutions. These processes are named assembly and solution, respectively in the FEM [57]. FEM finds applications not only in electromagnetics but also in other branches of

engineering such as plane stress problems in mechanical engineering, vehicle aerodynamics and heat transfer.

FEM is the basis of simulation in HFSS. HFSS divides the geometric model into a large number of tetrahedral elements. Each tetrahedron is composed of four equilateral triangles and the collection of tetrahedron forms what is known as the finite element mesh. Each vertex of the tetrahedron is the place where components of the field tangential to the three edges meeting at the vertex are stored. The stored component is the vector field at the midpoint of the selected edges, which is also tangential to a face and normal to the edge. Using these stored values, the vector field quantity such as the H-field or the E-field inside each tetrahedron is estimated. A first-order tangential element basis function is used for performing the interpolation. Maxwell's equations are then formulated from the field quantities and are later transformed into matrix equations that can be solved using the traditional numerical techniques [ 57].

### **PROCESS OVERVIEW**

The first step is to draw the geometric model of the structure that is to be realized. The next step is to select the materials that the various drawn objects are made of. An accurate definition of boundaries for the structure, such as perfect electric, radiation etc, follows next. In HFSS, a port or a voltage source needs to be defined to excite the structure. This is done as part

of the excitation definition. Once the structure is completely modeled the solution is set up. This includes definition of various parameters such as the frequency at which the adaptive mesh refinement takes place and the convergence criterion. Finally, after the completion of the simulation, the solution data is post processed which may include display of far-field plots, plots and tables of S-parameters, smith chart graphs etc. the figure below is summarized flow-chart depiction of the above mentioned theory.

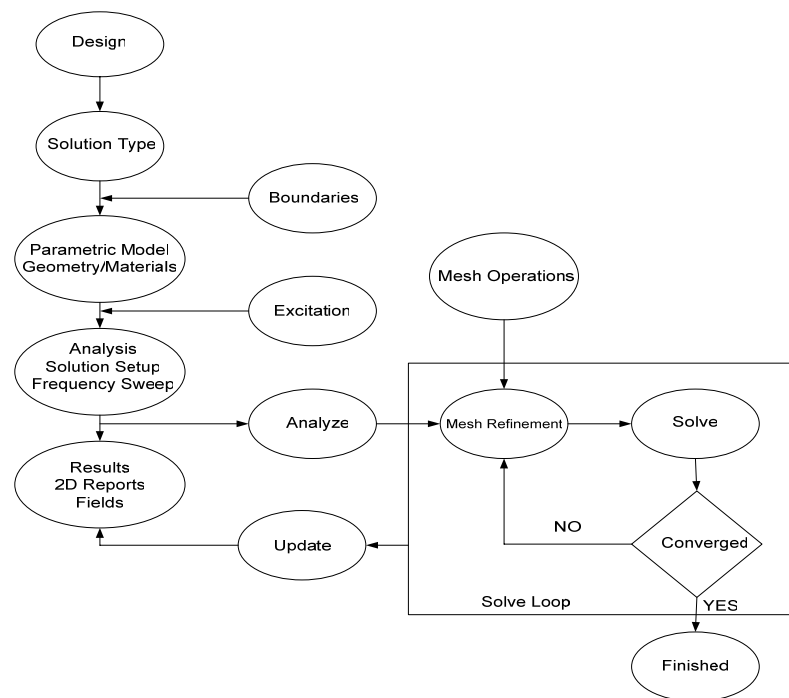


Figure 1. Process overview flow chart of the HFSS v9.0 Simulation module [47].

**REFERENCE:**

1. Balanis, Constantine, “ Antenna theory-Analysis and Design”, John Wiley & Sons Ltd, Reprinted 1997.
2. Saunders, Simon R., “Antennas and Propagation for Wireless Communication Systems”, John Wiley & Sons Ltd., October 2003.
3. Mailloux, R.J., et al, “microstrip antenna technology”, IEEE Trans. Antennas and Propagation, Vol. AP-29, January 1981, pp.2-24.
4. James, R.J., et al, “Some recent developments in microstrip antenna design”, IEEE Trans. Antennas and Propagation, Vol.AP-29, January 1981, pp.124-128.
5. Kumar, Girish & Ray, K.P., “ Broadband Microstrip Antennas”, Artech House Inc., MA, England, 2003.
6. Garg, R, Bhartia, P., Bahl, I., Ittipioon, A., “ Microstrip antenna design handbook”, Artech House Inc., MA, England, 2001.
7. Pozar, D.M., “A Review of Aperture Coupled microstrip Antennas: History, operation, Development, and Applications”, IEEE Letters, May, 1996.
8. Targonski, S.D., Waterhouse, R.B., Pozar, D.M., “Design of Wide band Aperture coupled Stacked microstrip antennas,” IEEE Trans. Antennas and Propagation, Vol. AP-46, pp1245-1251, 1998.

9. Kumar, G., Gupta, K.C., "Nonradiating Edges and four edges Gap coupled multiple resonator broadband microstrip antennas," IEEE Trans. Antennas and Propagation, Vol.AP-33, pp173-178, 1985.
10. Elboni E, Cerretelli M, "Microstrip Antennas for GPS Applications",
11. Hong, S.C., "Gain Enhanced Broadband Microstrip antenna", Proc. National Science Council, ROC(A), Vol.23, No.5, pp 601-611, 1999.
12. Reddy, V.S, Kalghatgi, A.T., "Cavity Backed Compact Microstrip Antenna", Central research Laboratory, Bharat Electronics,
13. Qian, Y., et al., "Microstrip Patch Antenna using Novel photonic bandgap structures," Microwave Journal, Vol. 42, pp 66-76, Jan.1999.
14. Croq, F., Kossiavas, G., Papiernik, A., "Stacked resonators for Bandwidth Enhancement: A comparison of two feeding techniques," IEEE Proc., Vol. 140, pp 303-308, 1993.
15. The Microwave encyclopedia online, <http://www.microwaves101.com/encyclopedia/couplers.cfm>.
16. S. J. Orfanidis, "Electromagnetic Waves & Antennas", Rutgers University: 2004
17. Deschamps, G.A., "Microstrip microwave Antennas", Proc. 3<sup>rd</sup> USAF Symposium on Antennas, 1953.

18. Munson, R.E., "Single Slot Cavity Antennas Assembly", US Patent No. 3713162. January 23, 1973.
19. Carver, K. R., Mink, J. W., "Microstrip Antenna Technology", IEEE Trans. Antennas propagation, Vol.AP-29, January 1981, pp.2-24.
20. Gao, S, C., Li, L, W., Yeo, T, S., Leong, M, S., "A dual frequency Compact Microstrip patch Antenna", Radio Science, Volume 36, Number 6, pp 1669-1682, Nov-Dec, 2001.
21. James, J.R., and P.S. Hall, Handbook of Microstrip Antennas, Vol. 1, London: Peter Peregrines Ltd., 1989.
22. Dubost, G., and G. Beauquet, "Linear Transmission line Model Analysis of Circular Patch Antennas," Electronics Letter, Vol. 22, October 1986, pp. 1174-1176.
23. Lo, Y.T., Solomon, D., and Richards, W.F., "Theory and Experiment on Microstrip Antennas," IEEE Trans. Antennas propagation, Vol.AP-27, March 1979, pp 137-145.
24. Newman, E.H., and Tulyathan, "Analysis of Microstrip Antennas Using Method of Moments," IEEE Trans. Antennas Propagation, Vol. AP-29, January 1981, pp.47-53.
25. Silvester, P., "Finite Element Analysis of Planar Microwave Network," IEEE Trans. Microwave Theory Tech., Vol. MTT-21, 1973, pp. 104-108.

26. Pozar, M. and S.D. Targonski, "Improved Coupling for Aperture Coupled Microstrip Antennas," *Electronics Letters*, Vol.27, No.13, 1991, pp.1129-1131.
27. Rathi, V. G. Kumar, and K.P. Ray, "Improved Coupling for Aperture Coupled Microstrip Antennas," *IEEE Trans. Antennas propagation*, Vol. AP-44, No.8, 1996, pp.1196-1198.
28. Lee, H. F., Chen, W., "Advances in Microstrip and Printed Antennas, New York", John Wiley & Sons, 1997.
29. Pozar, D.M. and Kauffman, B., "Increasing the bandwidth of microstrip antenna by proximity coupling," *Electronics Letters*, Vol. 23, No.8, 1987 , pp. 368-369.
30. Brookner, Eli., "Phased array around the world-Progress and Future trends," *IEEE Internat. Symp. On Phased Array Systems and technology*, MA., Oct 14-17, 2003.
31. Alexander Kuchar, Aperture Coupled Microstrip Patch Antenna Array, Report, Diplomarbeit, Technische Universitat Wien, 1996.
32. Oestergaard, A., M. Dich, and U. Gothelf, "A Network Model for the aperture coupled Microstrip patch," *International Journal of Microwave and Millimeter-wave Computer aided engineering*. Vol.3, No.4, 1993, pp.326-339.

33. Esa, M., Noor., N., A., M., Hamid, m., R., Subahir, S., Faisal, N., and Yusof, S., K., "Aperture coupled perturbed antenna with a parasitic element for rapidly deployable wireless ATM network,"
34. Pozar, D.M., "A reciprocity Method of Analysis for Printed Slot and Slot Coupled Microstrip Antennas," IEEE Trans. Antennas propagation, Vol.AP-34, No.12, December 1986, 1439-1446.
35. Sullivan, P.L., and Schaubert, D.H., "Analysis of an aperture coupled Microstrip antenna," IEEE Trans. Antennas propagation, Vol.AP-34, No.8, August 1986, 977-984.
36. Pozar, D.M., "Microstrip Antenna Aperture Coupled to a Microstrip Line," Electronic Letters, Vol. 21, No.2, 1985, p. 49-50.
37. Lee, R.Q., et al., "Characteristics of Two Layer Electromagnetically Coupled Rectangular patch Antenna," Electron.Lett., Vol.23, 1987, pp.1070-1072.
38. Antsos, D., Crist, R., Sukamto, L, "A Novel Wilkinson power divider with predictable performance at K and Ka band", IEEE MTT-S Digest, 1994.
39. Watson, T., "Affordable phase shifters for electronically scanned phased array antennas", article RFDesign Magazine, Oct. 1, 2003. ([http://rfdesign.com/mag/radio\\_affordable\\_phase\\_shifters/index.html](http://rfdesign.com/mag/radio_affordable_phase_shifters/index.html) ).

40. Adam, J., D., Davis, L., E., Dionne, G., F., Schloeman, E., F., Stitzer, S., N., "Ferrite Devices and Materials", IEEE Transaction on Microwave Theory and Techniques, Vol.50, No. 3, March 2002.
41. Brown, A.D., Kempel, L.C., and Volakis, J.L., "Design method for antenna arrays employing ferrite printed transmission line phase shifters," IEE Proc-Microw. Antennas Propag. Vol. 149, No.1, February 2002.
42. Batchelor J.C., *et all*, "Scanned Microstrip Arrays Using Simple Integrated Ferrite Phase Shifters", IEE Proc. Microwave Antennas Propagation, Vol. 147, No.3, PP 237-241, June 2000.
43. Stouten, P., "Equivalent capacitances of T junctions," Electronic Letters, vol.9, pp552-553, Nov. 1973.
44. Thompson, A., and Gopinath, A., "Calculation of microstrip discontinuity inductance," IEEE Trans. Microwave Theory Tech., vol. MTT-23, pp.648-655, Aug. 1975.
45. Menzel, W., & Wolff, I., "A method for calculating the frequency dependent properties of microstrip discontinuities," IEEE Trans. Microwave Theory and Tech., vol. MTT-25, No.2, Feb. 1977.
46. Batchelor, J.C., and Langley, R.J., "Beam scanning using microstrip line on biased ferrite," IEE Electronic letters, Vol.33, No.8, April 1997.

47. Ansoft HFSS version 9: Overview, 2003.
48. Pozar, D.M., "A Review of aperture coupled microstrip antennas: History Operation, Developments and Applications", on the Web,<http://www.ecs.umass.edu/ece/labs/antlab.html>.
49. Daniel, J.P., Dubost, G., Terrett, C., Citerne, J., Drissi, M., "Research on Planar Antenna Arrays: Structure Rayonnites", IEEE Antennas and Prop. Magazine, Vol. 35, No. 1, pp 14-38, February 1993.
50. Pozar, D. M., Schaubert, D, H., "Microstrip Antennas: The Design and Analysis of Microstrip Antennas and Arrays", IEEE Press, New York, 1995.
51. Esa, M., Noor., N., A., M., Hamid, m., R., Subahir, S., Faisal, N., and Yusof, S., K., "Aperture coupled perturbed antenna with a parasitic element for rapidly deployable wireless ATM network,"
52. Pozar, D.M., "A reciprocity Method of Analysis for Printed Slot and Slot Coupled Microstrip Antennas," IEEE Trans. Antennas propagation, Vol.AP-34, No.12, December 1986, 1439-1446.
53. Sullivan, P.L., and Schaubert, D.H., "Analysis of an aperture coupled Microstrip antenna," IEEE Trans. Antennas propagation, Vol.AP-34, No.8, August 1986, 977-984.

54. Hercovici, N., "CAD of aperture coupled microstrip transmission lines and antennas: software and user's manual," Artech House, 1996.
55. Kyriacou, G. A., Brienbjerg, O., Sahalo, J.N., "Aperture Coupled Microstrip Antennas: A Design approach", International Conference on Advances in Communication and Control: Telecommunications/Signal Processing, Athens, Greece, June 28-July 2, 1999.
56. LPKF ProtoMat- Rapid PCB Prototyping, Product Catalog, 2003.
57. Felippa, C., A., "Introduction to finite element method," available online at <http://caswww.colorado.edu.sa/courses.d/IFEM.d/IFEM.Ch01.d/IFEM.Ch01.pdf>
58. Park, J, Y., Wang, Y., Itoh, T., "A 60 GHz Integrated Antenna Array for High-Speed Digital Beamforming Applications", IEEE MTT-S International Microwave Symposium. Philadelphia, PA. June 7-13, 2003. pp. 1677-1680.

## VITAE

NAME: Mir Riyaz Ali

BIRTH: 24<sup>th</sup> SEPTEMBER, HYDERABAD, INDIA

EDUCATION: *BACHELOR OF TECHNOLOGY (B.Tech)*  
Electronics & Communication Engineering,  
Jawaharlal Nehru Technological University,  
A.P., India.

*MASTER OF SCIENCE IN TELECOMMUNICATION*  
Department of Electrical Engineering  
King Fahd University of Petroleum & Minerals  
Dhahran, K.S.A.

CONTACT: mirriyazali@gmail.com.